STRUCTURAL INTEGRITY INVESTIGATION

OF THE AN/FPS-117 RADAR AND

RADAR TOWER

by

David Parel Parker

A thesis submitted to the faculty of
The University of Utah
in partial fulfillment of the requirements for the degree of

Master of Science

Department of Mechanical Engineering

The University of Utah

August 2014

The University of Utah Graduate School

STATEMENT OF THESIS APPROVAL

The thesis of **David Parel Parker**

has been approved by the following supervisory committee members:

David W. Hoeppner	, Chair	**03/05/2014** Date Approved
K. Larry DeVries	, Member	**03/05/2014** Date Approved
Michael P. Blinn	, Member	**03/05/2014** Date Approved

and by **Tim Ameel**, Chair of

the Department of **Mechanical Engineering**

and by David B. Kieda, Dean of The Graduate School.

ABSTRACT

The purpose of this research is to verify the structural integrity of the AN/FPS-117 Long Range Radar and radar tower. An investigation is performed to understand how the fluctuating loads have an impact on the nucleation of crack-like discontinuities and the service life of the components and what steps should be taken as a result of the analysis. It is hypothesized that the rotation of the radar, in conjunction with the variation in level of the platform, creates fluctuating loads in support members that will decrease the life and reliability of these and other radar components.

An analysis is conducted of the changes in stress and strain amplitudes on the structure due to the rotation of the radar. Based on the material type, fatigue properties were determined and a strain-life curve was constructed to approximate the number of cycles to failure.

The resulting strain amplitude from the fluctuation of loads was found to be relatively small compared to the strain-life curve. The change in radar level did not have a significant impact on the strain amplitude and calculated cycles to failure based on strain gage measurements.

A damage tolerance assessment was completed to estimate the crack growth rate of the cracks found in the radar support plate. The results from this analysis were compared with a failure analysis that was performed on the radar support plate.

A nondestructive inspection of the structure was performed and multiple crack-like indications were found. The results from these inspections are shown. They document a representative sampling of the cracks that were found on the radar and tower structure. A holistic, damage-tolerant type approach will be taken to determine the residual life of the radar system.

The results from the fatigue analyses will provide inspection recommendations to be implemented to limit the probability of failure to within an allowable amount. It is recommended that the structure be continually inspected for fatigue cracks and a holistic approach be implemented in order to evaluate additional potential failure modes and mitigate the risk of a catastrophic structural failure.

I dedicate this thesis to my amazing wife, Julia, and my two angels, Stella and Delia. Thank you Julia for supporting me every step of the way and for the many reminders to stay focused. I love you Julia. Thanks girls for being patient and understanding. To all my family and friends, thank you for pushing me to dream big and achieve my goals.

TABLE OF CONTENTS

LIST OF TABLES

ACKNOWLEDGMENTS

I would like to thank my graduate committee, Dr. David Hoeppner, Dr. Larry DeVries, and Dr. Micheal Blinn, for your valuable time and energies spent in guiding me. I sincerely appreciate your support and the insights you have given me along the way.

Thank you to all my many friends on the AEWS team who have supported me and provided a great deal of critical resources during this work. Thanks Tim Perkins for your guidance, direction, and motivation. Thanks to the E-FAC team for the hands-on work on the system.

Thanks go to Dave Lindquist and the TSRT team, who provided the use of their equipment, sensors, and contracting means to accomplish this work. Thanks to Shane at SES for the collaboration with the tower studies and material testing. First Lieutenant Rollor, thanks for the jump start in creating the solid models.

Thanks go to Ward Fong for so willingly flying to Alaska with me to look for cracks. Thanks, Dave and Chuck, for picking up the tab. Thanks to my friends at Arctec in Alaska who make big things happen. Thank you Terry Herman, Doug Tucker, and Rita Allushi for the support from Canada. I appreciate the dedicated concern and interest in maintaining the integrity of the system. To the diligent radar maintainers in Alaska, Canada, Puerto Rico, and Hawaii, thank you.

Many thanks go to Dr. Mike Blinn and Josh Hodges, who helped immensely with the DTA. Thank you for your experience and insights. I appreciate the failure analysis lab at Hill Air Force Base, who provided the in depth analyses.

And finally, thanks to the floor, which has allowed me to indulge in moments of triumph, defeat, reflection, and rest in this great pursuit.

1. INTRODUCTION

1.1 Radar Background Information

The Atmospheric Early Warning System (AEWS) is a United States Air Force program that provides for the atmospheric air defense of North America. It provides radar surveillance of airspace across North America's polar region. In February of 1955, construction of the Distant Early Warning (DEW) Line radar sites commenced. These sites were set up to detect incoming Soviet bombers during the Cold War and provided early warning of a land-based invasion. The DEW Line ran from eastern Canada across the northern coast to western Alaska. The line is comprised of 27 AN/FPS-117 and 36 AN/FPS-124 radars.

The focus of the research will be on the AN/FPS-117 radar. This radar is a three-dimensional, phased array, air search radar produced by Lockheed Martin. The radar is comprised of a primary search radar and a secondary beacon interrogator system. The AN/FPS-117 radar replaced the outdated radars that had been installed in the 1950s. Slight modifications, such as the addition of an adapter plate, were made to the tower to be able to support the larger AN/FPS-117 radar.

The AN/FPS-117 radars report to the North American Aerospace Defense Command (NORAD). This command is a joint organization of Canada and the United States that provides aerospace warning, air sovereignty, and defense for the two

countries. NORAD was formally established in May 1958 to coordinate the defense of North America.

The AEWS mission is to provide air surveillance, detection, identification, and command and control for air sovereignty and defense of the North American atmospheric portion of NORAD's Integrated Tactical Warning and Attack Assessment capabilities. AEWS also supports the national counter-drug campaign.[1]

The purpose of this research is to verify the structural integrity of the AN/FPS-117 Long Range Radar and radar tower. This radar is utilized in extremely remote and desolate locations throughout the United States and Canada. One of the major benefits of this radar is that it is minimally attended. It can be remotely operated and the majority of electronic problems can be diagnosed remotely. Most major mechanical degradation modes are not monitored.

A major concern with this radar is that a mechanical failure is not always detectable. Any mechanical malfunction could affect the ability of the radar to fulfill its mission. Depending on the type of failure, the entire radar could be rendered entirely inoperable. The structural integrity and reliability of the mechanical components of the radar are imperative.

The majority of the AN/FPS-117 radars are located in the arctic. There have been several occasions where major mechanical failures went unnoticed as described by the following case in point. The radar is protected from some environmental effects by a composite radome that is bolted to the radar tower. At a particular site, the radar seemed to be operating normally, but one temperature sensor appeared to be malfunctioning. The temperature it was reading was extremely outside of the typical range. A helicopter was

dispatched to investigate. To the astonishment of the crew, the entire radome had been blown off of the radar tower, miraculously leaving the radar completely intact. The radome was never found.

Failures of this magnitude are rare, but they do occur. It is the responsibility of the engineer to design and maintain a reliable system. As a United States Air Force weapons system, the radar must have a quantifiable reliability, availability, and maintainability. These are essential elements to uphold the mission capability.[2]

1.2 Structural Design Philosophy

As mentioned, the 117 radar was built circa 1980. It is assumed that the radar was not designed with any life criterion. It was assumed by the original designers that the factor of safety was large enough to account for any time-based failure mechanisms such as fatigue, corrosion, wear, etc., or these failure mechanisms were not even considered during the design of the structural components. This is considered the "no-life" design paradigm.[3] No routine inspection for cracks or damage has ever been mandated for this weapon system. There have been instances in the field in which problems have been found and repaired, but these typically were done by diligent maintainers outside of their scope of work.

After time, design engineers began to use the "safe-life" design paradigm. The general idea is that the part is expected to be replaced after a given amount of time. This chosen product life is allegedly less than the fatigue life for the assumed perfectly continuous and homogenous material. Using this paradigm, the designer will build in a safety factor to try and ensure the part is replaced before a critical failure occurs. The

method does not ever specify a failure method other than coming to the end of the prescribed life of the product.

The next design concept that took shape was the fail-safe or fault-tolerant design. This allowed for the product to be designed to have multiple load paths. If one part were to completely fail, the load will be taken by another member and the system will not fail catastrophically.

Finally, the most sophisticated structural design concept is that of a holistic or damage-tolerant design. As defined by the United States Air Force, damage tolerance is the attribute of a structure that permits it to retain its required residual strength for a period of unrepaired usage after the structure has sustained specific levels of fatigue, corrosion, accidental, and/or discrete source damage.[4] In this paradigm, the inherent flaws and discontinuities contained in the material are accepted and evaluation is made of the impact to the structure based on these flaws.

The damage tolerance paradigm uses fracture mechanics to evaluate the remaining life of the component or system containing these flaws, such as fatigue cracks. Nondestructive inspection of the system is a critical part of this method. The output of the damage tolerance and fracture mechanics method is a quantitative prediction of the allowable peak stress for a given crack size, the maximum crack size for a given peak stress, the maximum crack size or peak stress for a given material toughness, the crack size for a given fatigue loading spectrum, initial crack size, and environment, and finally, appropriate intervals for inspection.[5]

No physical inspection of the structural joints or members is specified in the maintenance of this radar. Pending the results of this analysis, appropriate steps should

be taken to determine to what level inspection of critical structure elements should be completed. A holistic or a damage-tolerant approach may also be prescribed in order to quantify damage that may be occurring.

1.3 Research Project Outline

Although these radars are minimally manned, maintenance is performed on the electrical and mechanical components on a routine basis. During these maintenance intervals, necessary repairs and inspections of electronics are conducted. Problems do arise during the times when personnel are not onsite to catch the problem and fix it before it turns into a major repair. These types of problems can go unnoticed until the next maintenance interval. By this time, the effects can be far-reaching.

Even when problems are detected, a large amount of money is spent solely in getting to the radar site. It is essential to use the scheduled time at the radar location to the best of the maintainer's ability. A method needs to be employed to know how to inspect and evaluate mechanical components for the radar to ensure structural integrity. This can be done using a holistic approach. There are seven basic steps in this paradigm.[3] It is imperative to know the following:

1) What to look for
2) Where to look
3) How to look
4) When to look
5) How often to look
6) The probability of detection

7) The detection threshold.

The details and impact for each of the items is discussed more in a subsequent section. Each plays an important role in maintaining the structural integrity of the system.

Utilizing the holistic approach of inspection will save valuable time and money. The result can be a quantifiably more reliable and safe system, capable of fulfilling its designed mission. As stated previously, the objective of the Atmospheric Early Warning System (AEWS) program is to maintain the U.S. Air Force AN/FPS-117 radar fleet and ensure that it can fulfill its mission.

The purpose of this thesis is to determine the structural integrity of the critical load-bearing members of the radar and tower to understand how the fluctuating loads have an impact on the nucleation of crack-like discontinuities and the service life of the components. It will also determine what steps should be taken as a result of the analysis and recommend a holistic inspection criterion that will ensure the longevity of the system to perform its intended mission.

This report focuses on two structural systems as a whole, the radar itself and the radar tower. Fatigue is defined as the process of progressive localized permanent structural change occurring in a material subjected to conditions which produce fluctuating stresses and strains at some point or points and which may culminate in cracks or complete fracture after a sufficient number of fluctuations.[3] The purpose of this report is to investigate how the fluctuating loads have an impact on the nucleation of crack-like discontinuities and the life of the components. It is hypothesized that the rotation of the radar with an out of tolerance level will create increased fluctuating loads in support members that will decrease the life and reliability of the radar.

The hypothesis will be proved or disproved by the following method. A stress analysis will be performed on both the radar and the radar tower to determine the amount of stress and strain placed on the tower. Multiple radars and towers will be instrumented with strain gages in order to measure the strain fluctuations imposed upon the various members by the rotation of the radar antenna. Using a strain-life methodology, a preliminary analysis can be made of the fatigue life of the system. Based on the results of this analysis, a damage-tolerant assessment may be recommended to ensure the integrity of the system.

The radar system will be tested at the Engineering Facility at Hill Air Force Base, Utah to evaluate the impact of radar level on the radar and tower components. The changes in strain due to a quantified change in level will be measured and recorded. The results of the stress analysis will be used in conjunction with the strain gage measurements in order to perform a fatigue and damage tolerance analysis on the structure. Inspections and repairs that have been completed to date will be compared to the results of the damage tolerance assessment. Based on the results of the fatigue and damage tolerance analysis, a holistic inspection criterion will be recommended to ensure the structural integrity of the entire weapon system.

1.4 Research Project Objectives

Listed are the objectives for this research project:

1. Determine the local stresses and strains on radar and tower components.
2. Determine the impact the levelness of the radar has on the life of the system and components.
3. Recommend an attainable unified value for the level specification.

4. Estimate the remaining life of the weapon system by using a strain-life or damage-tolerant approach.
5. Determine the locations of high stress and fatigue prone areas on the radar and tower.
6. Compare results of the stress and fatigue analyses with actual cracks that have been found in the field.
7. Recommend the implementation of a holistic inspection plan for monitoring these locations for cracks.

2. RADAR AND TOWER STRESS ANALYSIS

2.1. Overview

The radar consists of several basic components shown in Figures 1 and 2, namely the array (a), two back supports (b), two pillow blocks (c), platform (d), support plate (e), bearing (f), pedestal (g), adapter plate (h), and the tower structure (i).

The array is the forward face of the radar that transmits and receives radio signals. The back supports are held stationary but allow for positioning of the array. Pillow blocks support the majority of the weight of the array and allow for the array to be tilted in the correct direction. The platform provides the mounting surface for the upper components of the radar. The platform is mounted on top of a support plate and a 5 foot diameter cross roller bearing that are located between the pedestal and the platform. The pedestal remains stationary, mounted to the tower structure, while a motor drives rotation of everything above the main bearing. The weight of the rotating portion of the radar is approximately 27,000 pounds with a total radar weight of approximately 30,000 pounds.

An inherent problem with the design of this particular radar is that the center of gravity for the radar is not located at the vertical axis of rotation. It is approximately 20 inches from the center of rotation toward the front of the array. As the center of gravity travels around its circular path, fluctuating loads and moments are induced on different components. This moment is applied at different locations as the radar turns. The loads

created by the weight of the radar are calculated and shown in the results section. These values will be used in calculating the life of the weapon system.

In order to output accurate target search data, the radar must be mounted horizontally level to within ± 4 arc-minutes (0.0666 degrees). A deviation of an eighth of an inch on the perimeter of the radar can produce height errors greater than 4,500 feet at the end of the radar range. The hypothesis is that differences in level can have a significant impact on the stress imposed on the structure. The Air Force Technical Order specifies that the level is to be checked at least once per year to ensure that it is within the appropriate specification.[6] There are situations that demand that the level be reevaluated on a more frequent basis, for instance, when the radar main bearing has been replaced, or if the radar mounting bolts are re-torqued, etc. If the radar is determined to be out of level, the pedestal is re-leveled. This procedure involves adjusting bolts or placing shims between the bottom of the pedestal and the radar tower, depending on the tower type.

2.2. Model Definition

In order to determine the fluctuating load on the support members, it is first necessary to observe the load path of the radar. A side profile of the radar along with a diagram labeling the dimensions is shown in Figure 3 to illustrate the basic geometry of the array and the back supports. The lengths and angles are determined from research on the radar drawings as listed in the radar Illustrated Parts Breakdown.[7]

The face of the array is positioned 10 degrees clockwise from vertical. The angle beta (β) is complementary to the specified 10 degree backward tilt of the face of the array. The distance on the platform from the pillow block to the back support mount is

given as the length of the base (Lb). The length of the back support (Ls) is also specified in the engineering drawings. To solve for the angle alpha (α) and the length of the array to the point where the back support is connected (La), the Law of Cosines may be utilized. The distance above the point where the back support is connected is labeled (Le). These values are shown in Appendix D.

Now that the geometry of the radar has been determined, a free body diagram of the loads can be created for statically determining the reactions on the pillow blocks and the back supports. The free body diagram is shown in Figure 4.

The pillow block is a pinned joint and can be analyzed as such. On the pin itself, there will be a vertical reaction (R_y) and a horizontal reaction (R_x). The distributed weight (w) of the rotating portion of the radar is shown as a distributed load over the entire face of the radar shown in the negative horizontal direction. The geometry and weight distribution of the radar demonstrates that the center of mass is not found directly on the central vertical axis of rotation.

The purpose of the back support is to fix the rotation of the array about the pin joint. The support is an axial loaded member and acts in the direction of the force (F) shown, based on the angle alpha shown in Figure 3. The back support is pinned between the array and the platform.

Now that the forces have been modeled in a free body diagram, equations of static equilibrium can be used to determine the horizontal and vertical reactions at the pillow block joint as well as the reaction force F on the back support. As shown in Appendix D, the sum of the forces is calculated in the vertical and horizontal directions. The sum of the moments is taken about the pin joint. By summing the forces and moments and

setting them equal to zero to maintain a state of static equilibrium, it is possible to solve for the three unknown reactions. These calculations are shown in Appendix D.

It is important to note that the free body analysis shown previously is only looking at one side of the radar structure. This consists of one pillow block pin and one back support. The same boundary conditions also exist on the opposite side, and they support half of the weight of the radar. Because the boundary conditions are the same on both sides, the resulting forces from the free body diagram in Figure 3 need to be divided in two.

2.3. Model Loading and Constraints

In order to determine the structural integrity and fatigue life of a system, a stress analysis must first be accomplished. A finite element analysis was the method chosen to perform the stress analysis for the radar and radar tower. Due to the complexities of the structure, a three-dimensional model of the radar and tower needed to be created in order to perform an accurate finite element analysis. This was accomplished by using SolidWorks software. This software also has the capability to run the finite element code to estimate the stress and strain. One limitation on this particular license of the software was that it would not perform a dynamic analysis. Multiple static analyses had to be performed in order to simulate the movement and change in loading of the radar due to the rotation.

The models were created in SolidWorks by using the engineering drawings associated with the various structural components. The engineering drawings also specified the types of materials from which the radar and towers are fabricated. Some

material testing has been accomplished to ensure that the components are actually built using the specified materials and that they conform to the associated standards required.[8]

Individual models of each part were created and then assembled together in the program. The model consisted of the platform, support plate, bearing, pedestal, and radar tower, as shown in Figure 5. Once the assembly was complete, the reaction loads that were previously calculated were applied to the top of the platform. This consisted of vertical downward forces (R_y) and horizontal forces (R_x) at the pillow block joints and a reaction force (F) at the angle alpha on the back stay mounting brackets. The reaction force (F) was decomposed into the horizontal and vertical components for input into the model.

Constraints were built into the assembly during the assembly phase. The bottom of the platform had a bonded contact with the top of the support plate. The support plate was bonded to the bearing, and the bearing was bonded to the pedestal. The bonding of the parts in the assembly simulated the manner in which the parts are bolted together. The pedestal, bearing, support plate, and platform were all joined concentrically with the appropriate mounting holes aligned. There are multiple configurations for mounting the pedestal to the tower, but all configurations utilize the 12 bolt holes on the bottom of the pedestal. These bolt holes were aligned with the adapter plate which was fixed to the tower support pads. To determine the stress on the radar components, the bottom of the tower support pads had fixed constraints on the bottom faces of the six support pads. This is the configuration most representative of the mounting condition for the majority of the radars in the field.

Once the material properties, component contact, forces, and constraints were applied to the static study, a mesh could be created. The mesh needed to be modified and refined in certain areas of the model to account for differences in the geometry and local stress concentration factors. A p-adaptive mesh was used to improve the results. The benefit is that rather than using a refined meshed, the method uses progressively higher element order to improve the results.[9] Once the mesh was finalized, the finite element analysis could be run to determine the displacements, stresses, and strains on each of the radar components. These values are shown in the results section. The results from the analysis are then discussed in a subsequent section.

The software license utilized for the analysis did not have a motion or dynamic analysis capability. To determine the variation in stress and strain on the radar, additional static analyses needed to be run. The bearing was essentially "rotated" in the model by 30 degrees and the study was re-run to record the stress changes for a complete 360 degree revolution. There are some inherent dynamic affects that are not considered by modeling the system in this fashion. Based on the slow speed of radar rotation, this is presumed to be a reasonable assumption and simplification.

There are multiple configurations of radar towers, namely AB-259, AB-199, North Warning, Canadian East Coast, and unique cement tower. The AB-259 tower is most common and was the first tower type modeled in SolidWorks for the analysis. The effect of the rotating weight of the radar on the tower was also analyzed in the same software using a separate model. The simulated loads caused by the radar were placed on the model and the analysis was run using a similar approach as the method previously described. The results of these analyses are also discussed hereafter.

2.4. Pedestal Level Calculations

As discussed in section 2, the level of the radar plays an important role in the fidelity of the radar data. It is also presumed that the more out of level the pedestal is, the greater the stress is on certain portions of the radar and tower as well as the greater the magnitude of the fluctuation of the loads imposed on the structure itself. The fluctuating load is a result of the change of the center of gravity of the radar. As the radar is subjected to an incline in the plane of rotation, the forces and reactions change by an amount based on the angle of the plane.

The AB-259 tower utilizes six support pads that are positioned underneath the adapter plate. The levelness requirement was established during the design of the radar. In the process of validating the Air Force Technical Order for the procedures to adjust the radar to within level requirements, the radar had to be leveled multiple times. The data exists for the thickness of the shims necessary for the tower at the Hill Air Force Base Engineering Facility (E-FAC) to be level within varying degrees of accuracy. This testing was done, in part, as one of the objectives of this thesis, which was to provide a unified leveling procedure and specification for the radar level. The testing is described in detail in section 3.2.

Based on the measurements taken with a digital inclinometer, the shim height needed to level the radar is calculated. Using these known height differentials for a known level deviation, the finite element model could be adapted to account for the maximum recorded change in level. This was done by creating models of shims of equivalent thicknesses to obtain the same degree of un-level. These extra shims were added to the model and a secondary finite element analysis was performed. The results

of this additional analysis were compared to the original finite element model to estimate the increase in stress and strain on critical components due to an out of level radar. The results of this analysis are shown in the section 5.1.

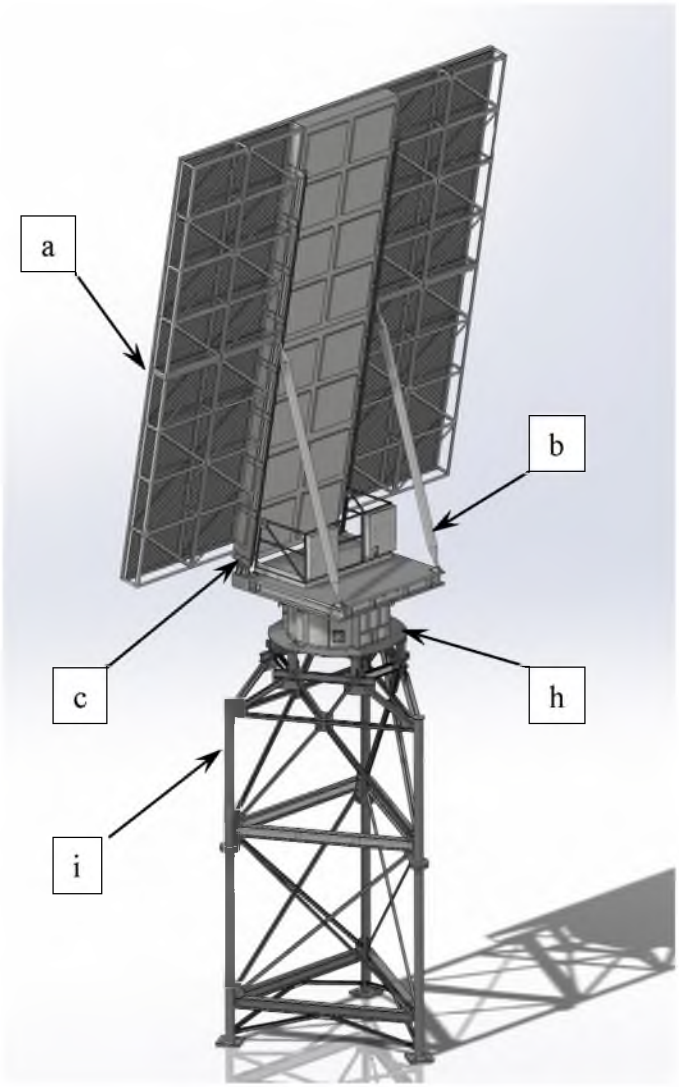

Figure 1 Diagram of radar components. a) radar array b) back support c) pillow block h) adapter plate i) tower structure

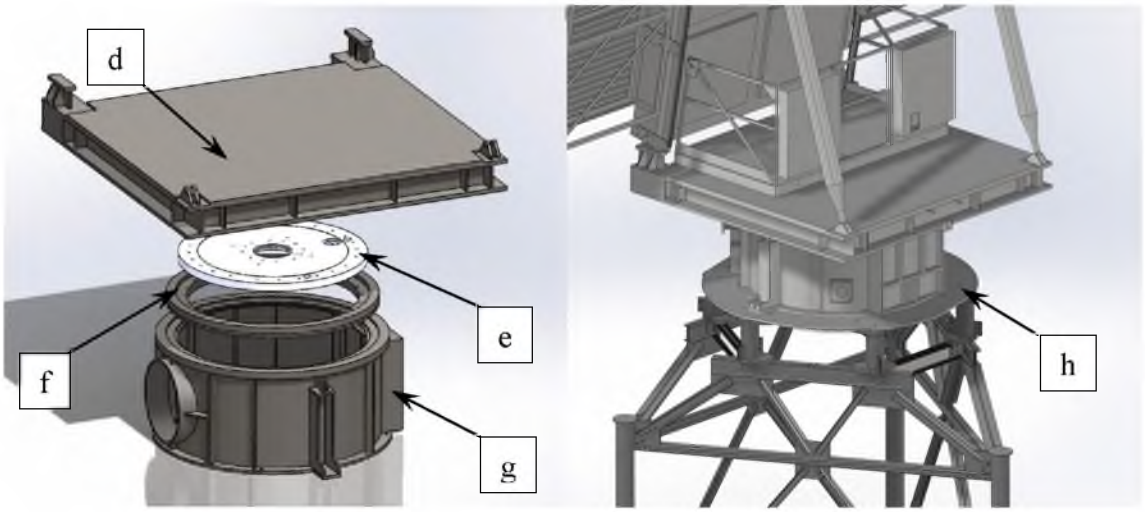

Figure 2 Diagram of radar components. d) platform e) support plate f) bearing g) pedestal h) adapter plate

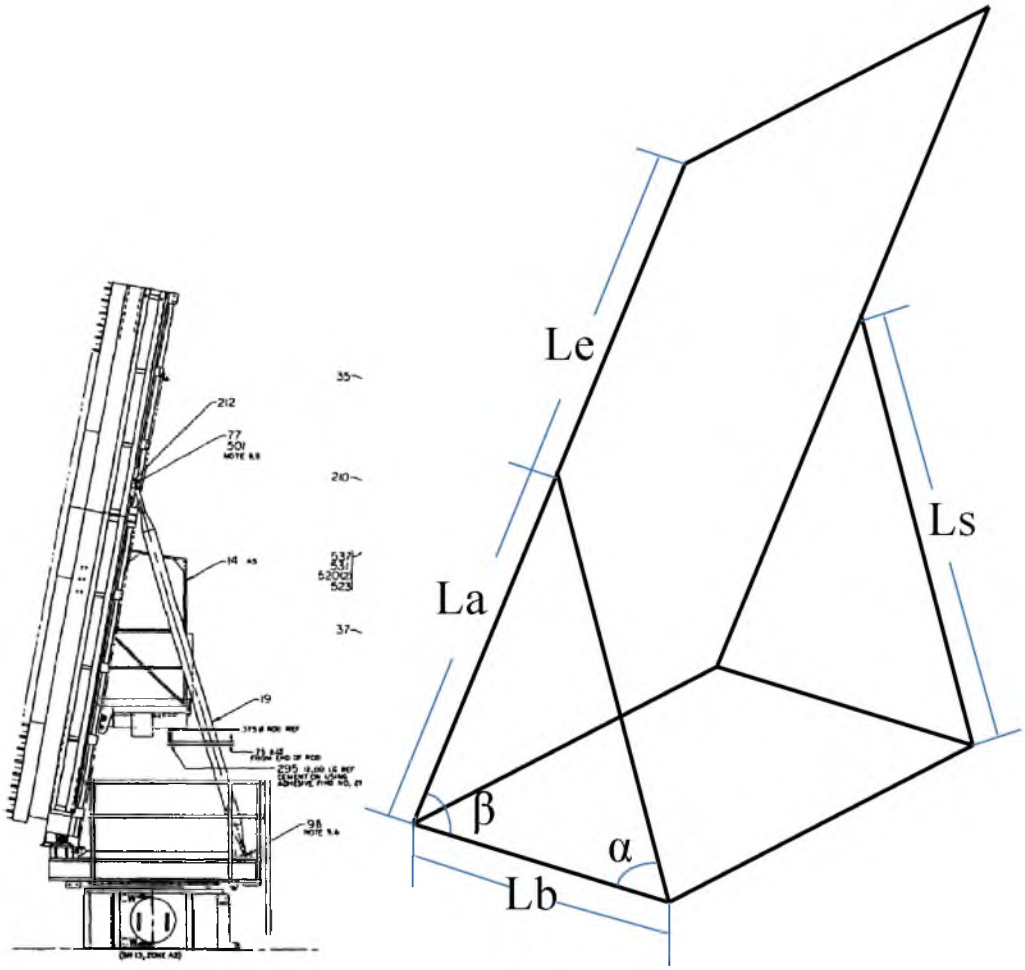

Figure 3 Side profile of the radar showing the angle of the array and back support

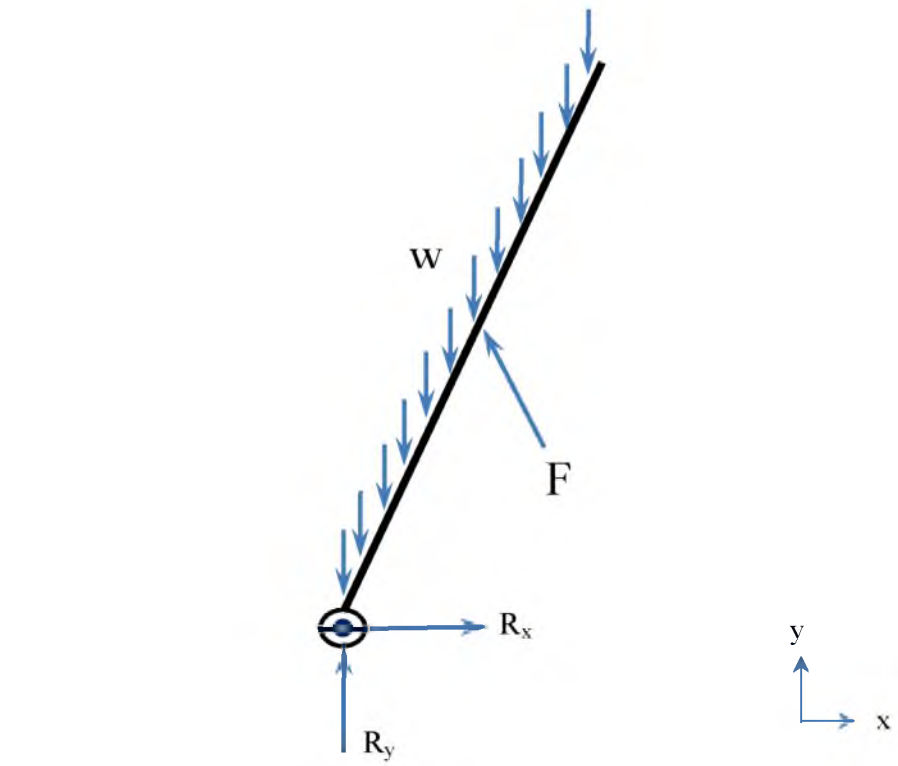

Figure 4 Free body diagram of the pillow block and array

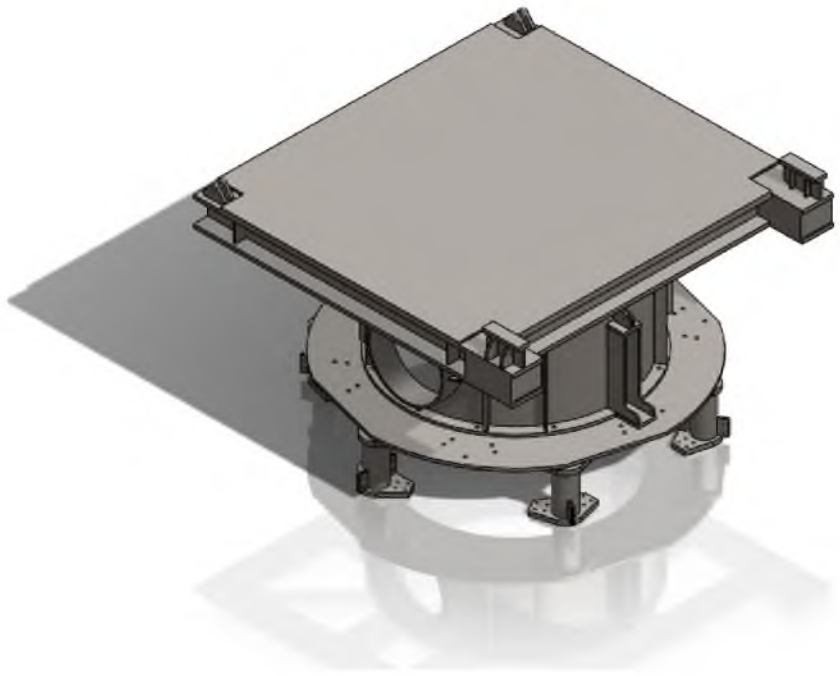

Figure 5 Three-dimensional model of the radar platform, pedestal, adapter plate, and tower.

3. DATA COLLECTION AND PROCESSING

3.1. Strain Gage Installation

To validate the finite element model and to understand actual loads being placed on the radar and the radar tower, it was necessary to instrument the systems with strain gages. The strain gages are the method used to better understand and address the issues related to fatigue cracking and failure of the structural components.[10] These gages measure the strain at discrete locations on the radar and supporting structure. The measurements will be used to ascertain the following information:

1) Calculate the stress changes experienced by the radar and tower.
2) Verify the accuracy of stress ranges predicted by finite element computer models of the towers and pedestals.
3) Gain a better understanding of how the load path is distributed through the structure.
4) Test the hypothesis that the differences in pedestal level can have a significant impact on the stress imposed on the structure.

The strain gages were installed at radar sites at Hill Air Force Base, Puerto Rico, Alaska, and three radar sites in Canada. Because of the different stakeholders involved and the variety of fund sources that were used to pay for the analysis, different methods were employed to install the gages at the different sites. The strain gages were installed by teams that had sufficient training and expertise to perform the task. In general, the

overall recording period was set to be for one year. This allows data to be collected to record changes due to weather, temperature, site conditions, etc. The placement of the strain gages was documented by the installing activity.[10, 11] These locations are shown in Appendix B.

As mentioned previously, the radar systems had been active for decades before the strain gages were installed. The radar rotation was shut down during installation, but there still existed an amount of strain on the structure due to the weight of the radar. The weight is not directly measured by the strain gages because the gages were applied to the structure much later. This total amount of strain needed to be calculated by the finite element analysis. The measured change in strain could also be compared to the analytical to verify that the magnitude of the strains produced were similar.

After the strain gages were installed on a particular site, the radar was placed in an orientation represented by zero degrees. The strain gages were then reset to default values to formulate the baseline. The radar was then turned on and the data acquisition systems began to record strain gage measurements. For the first site, the measurements were taken at different sampling intervals to determine the sampling speed needed to record the fluctuations caused by the radar.

The strain gages installed at the E-FAC were configured to record measurements once per second. The AN/FPS-117 radar rotates at 5 rpm. This allowed for 12 readings per radar rotation. The system monitors the strain on a continuous basis and saves the readings in a data acquisition system that can be accessed wirelessly from within the radar facility.

One of the disadvantages of using strain gages on the radar is that there is not a cost-effective way to install strain gages on multiple rotating components. One component of particular interest is the support plate due to the history of cracks being found. This item, as well as other components that are subjected to rotation, were unable to be instrumented and monitored in service.

A load cell was also used on one of the bolts that mount the radar support pad to the central tower structure. The reason this location was chosen to be evaluated was because there was one instance of several broken fasteners that were found at a radar site in Alaska. The load on the fastener was recorded in addition to the strain on the radar and tower.

3.2. Pedestal Level Change and Strain Data

The first site that was instrumented was at Hill Air Force Base. To test the hypothesis that the radar level has an effect on the supporting structure, the level was quantitatively modified at that radar site. The Air Force Technical Order specifies using a Gunner's Quadrant to verify the level.[6] This tool is no longer procurable and a replacement had to be found. A high precision digital inclinometer was purchased in order to perform the measurements for this study. Before any adjustments were made, a baseline was determined.

The radar pedestal at Hill Air Force Base is mounted directly to an adapter plate. The adapter plate is threaded in three locations for a 1 inch lifting bolt, used to raise the plate and radar above each of the six pads to be able to install shims for leveling the radar. After the level was documented, the original shims were removed. The adapter

plate was then bolted directly to the support pads. The level was then measured and found to be outside the radar level specification.

A gyroscope was used to compare the dynamic level of the radar with that recorded by the static readings. This device is synchronized with the radar data processor and takes measurements of the change in azimuth during rotation and the direction of the radar based on time. Based on measurements from the gyroscope, the location of the offset weight of the radar was known for any given time. The level measurements, strain gage measurements, and gyroscope recordings were taken each time the radar level was adjusted. The times between level adjustments were noted.

The radar was then re-leveled to within specification and the measurements and recordings were repeated. Finally, the radar was leveled to as close as possible to true level. The measurements for all of the various level ranges were then analyzed to compare the changes in strain. The results of the data are presented in section 5.2. The results from this testing was used in the finite element analysis as described earlier to predict the change in stress due to a quantitative level deviation.

4. STRAIN LIFE APPROACH AND DAMAGE TOLERANCE ASSESMENT

4.1. Strain-Life Estimation

As mentioned previously, it is assumed that the radar was not designed with any life criterion. It is somewhat apparent by the design of the structural components that a large factor of safety was used. It is likely that the structure was considered to be safe for the duration of the life of the system due to the large factor of safety for the structural components. However, as seen throughout the history of this system, cracks have developed and problems have arisen, even with a large factor of safety in the design of the components.

At a minimum, a strain-life analysis can be completed to estimate the life of the system. Prior to this research, no fatigue tests had been run to determine the life characteristics for any radar or tower components. Due to the fluctuating loads caused by the rotation of the antenna, the number of cycles to failure can be estimated using a strain-life approach.

There are standard practices that exist to appropriately collect fatigue data. These are specified in order to compare fatigue data that have been collected by other sources. Before using fatigue data from other sources, it is important to understand if the results can be correlated to the components in question. There are several important aspects to consider when evaluating fatigue data, which were taken from a selection of Fatigue and

Fracture, Volume 19 in the ASM Handbook. Some of the important questions that need to be answered before selecting usable data are listed.[12]

- What are the coupon size and geometry?
- Was there a stress concentration?
- What was the temperature?
- Was an environment other than lab air employed?
- What was the specimen orientation in the original material?
- Does the line represent minimum, mean, or median response?
- How many samples were tested?
- What was the scatter?
- What were the frequency and waveform?
- What was the failure criterion?
- If there were run outs, how were they handled and represented?
- Is it data for a thin sheet response?
- Is the R value for the test the same as the application in the field?

Based on these questions and after an extensive search of the literature, it was difficult to find fatigue testing data that would correlate to the radar components in question. With the absence of the data, an estimation of the fatigue life could be made analytically. However, the correlation between the samples used to compile the fatigue data used to create the strain-life curve and the radar component in question may not be any better than published data. Using these values may suffice for an initial estimate. The recommendation would be to statistically design a fatigue test to simulate the stresses

and strains found in the radar.[3,13] A discussion of this is presented in a subsequent section.

An idea of the number of fluctuations, or stress cycles, that the radar has already been subjected to was determined by estimating the number of revolutions of the radar to the present date. The radar rotates at 5 revolutions per minute. It operates continuously 24 hours per day, 7 days a week. The average availability of this radar has been calculated by the US Air Force to be at 99.6%. If the radar was activated in 1980, this corresponds to approximately 89 million (8.9×10^7) revolutions to date.

Due to the offset center of gravity of the radar, each time the radar rotates, the structural components are subjected to an increase in load and a decrease in load through one revolution. For each rotation, one strain cycle is imposed on the components. This is helpful in looking at the number of cycles or reversals to failure on a strain-life diagram and how it equates to time.

There are two basic relationships when considering the fatigue life of a metal component. The "Low Cycle Fatigue" range is dominated by the strength of the specimen. The second section of the relationship, or "High Cycle Fatigue" range, is based on the ductility of the component. This is due to the fact that at a high stress, the strength of the component will be the main factor that determines the life, whereas, at a low stress, the specimen can be subjected to a greater number of reversals before failure will occur.

The relationship between strain range and fatigue life is found based on the addition of these two components. The strength dominated component or plastic strain amplitude versus life relation is shown in Equation 1 that follows.

$$\frac{\Delta\varepsilon_e}{2} = \frac{\sigma_f'}{E}(2\,N_f)^b \qquad [1]$$

The exponent (b) in the equation is the Fatigue Strength Exponent. The coefficient (σ'_f) is the Fatigue Strength Coefficient, and ($2\,N_f$) is the number of stress reversals.

The ductility dominated component or elastic strain amplitude versus life relation of the plot is shown in Equation 2.

$$\frac{\Delta\varepsilon_p}{2} = \varepsilon_f'(2\,N_f)^c \qquad [2]$$

The exponent (c) is the fatigue ductility exponent and the coefficient (ε'_f) is the Fatigue Ductility Coefficient.

By summing these two components, an equation for strain range and fatigue life can be produced. It is shown by the following in Equation 3.

$$\frac{\Delta\varepsilon}{2} = \frac{\Delta\varepsilon_e}{2} + \frac{\Delta\varepsilon_p}{2} = \frac{\sigma_f'}{E}(2\,N_f)^b + \varepsilon_f'(2\,N_f)^c \qquad [3]$$

Values for the fatigue coefficients and exponents in Equation 3 are empirically determined. For a given material, these values can be found in handbooks or textbooks. For this study, the direct values were not empirically determined due to funding constraints. However, static tensile tests have been accomplished in accordance with ASTM E8 and the results are shown in Appendix A.[8]

In absence of (σ'_f), (ε'_f), (b), and (c), Collins has suggested setting the strain-life parameters to the following static tensile test results.[14]

$$\sigma_f' \cong \sigma_f \quad \varepsilon_f' \cong \varepsilon_f \quad c \cong -0.6 \quad b \cong -\frac{\log\left(\frac{2\sigma_f}{S_u}\right)}{\log(2\,N_e)} = -0.16\log(2\,\sigma_f\,S_u), \qquad [4]$$

where (σ'_f) is the true stress at fracture, and (ε'_f) is the true fracture ductility. The true stress and strain at fracture are found by the actual cross-sectional area of the specimen and final length, but can be determined by the following equation:

$$\sigma_f = \sigma_E(1 + \epsilon_E) \quad and \quad \varepsilon_f = \ln(1 + \epsilon_E), \qquad [5]$$

where (σ_E) and (ε_E) are the engineering stress and engineering strain at fracture as determined from the static tensile test.

These estimations are calculated and shown in Appendix D. A comparison was made for the values determined from the tensile test and those from a standard text. Different values were retrieved from the ASM Metals Reference Book.[15] The values that were used are listed in Table 1.

The range for the fatigue strength exponent (b) typically varies from -0.05 to -0.15 and for most metals has an average value of -0.085.[16] As shown in Table 1, the value calculated from the static tensile test results is well outside of this range. For this reason, the Modified Universal Slope method for determining the fatigue properties were used in place of the standard Static Tensile Test calculations as shown previously in Equation 4.[17]

The Modified Universal Slopes Method uses a slightly different method for the determination of the strain life curve, as shown by Equation 6. This is also evaluated as an alternative way of determining fatigue properties for materials based on a static tensile test.[18]

$$\frac{\Delta\varepsilon}{2} = 0.623\left(\frac{S_u}{E}\right)^{0.832}(2N_f)^{-0.09} + 0.0196(\epsilon_f)^{0.155}\left(\frac{S_u}{E}\right)^{-0.53}(2N_f)^{-0.56} \qquad [6]$$

Once the curve was established for the strain amplitude versus the number of cycles to failure, the strain range needed to be determined. This value can be ascertained by the application of Hooke's Law as shown in Equation 7. For a more accurate result, the actual strain range for the specific components was found by using the finite element analysis in conjunction with the strain gage measurements. The strain amplitude was then determined by Equation 8.

$$\varepsilon = \frac{\sigma}{E} \quad [7]$$

$$strain\ amplitude = \frac{\Delta\varepsilon}{2} = \frac{\varepsilon max - \varepsilon min}{2} \quad [8]$$

Due to the rotation of the radar, the components experience a quantifiable change in strain for each radar cycle. Based on the strain amplitude found in Equation 8, an estimation of the fatigue life can be made using the strain-life curve shown in Equation 3 and Equation 6. These curves are shown in section 5.3.

4.2. Damage Tolerance Assessment

As discussed previously, there are several methods of structural design that are available to a designer to account for time-based failure modes. In safe-life design, the material is assumed to be continuous, homogeneous, and free from damage. However, this can be a dangerous assumption. Materials are not homogeneous, nor continuous.[19] The damage tolerance design methodology uses a fracture mechanics failure theory based approach. This method accounts for the fact that the materials may contain inherent discontinuities. The benefit of this approach is that a determination can be made of the integrity of the structure as to whether or not it can continue to sustain the required loads.

The failure process is summarized by the following steps:

1) Fatigue loading

2) Fatigue damage accumulation

3) Development of a fatigue crack

4) Micro structurally short crack growth

5) Physically short crack growth

6) Long crack growth (Linear Elastic Fracture Mechanics)

7) Continued crack growth (Elastic Plastic Fracture Mechanics)

8) Plastic collapse

9) Fracture

During steps 1 through 3, a durability analysis can be conducted such as a strain-life or stress-life, which has been discussed previously.[20] During the short crack growth phases, steps 4 and 5, the fatigue analysis can transition from the durability method to linear elastic fracture mechanics. The crack will experience stable crack growth during the long crack growth phase in steps 6 and 7, after which the crack will become unstable and failure will occur.

There are two types of strength related failures, namely yield dominant and fracture dominant. In yield dominant, the loading exceeds the structures ability to carry load without resulting in failure or permanent deformation. In fracture dominant, the stress intensity in the presence of a crack and an applied load exceed the fracture toughness of the material.[20] In the case of the radar, the failures that have been found to date have been fracture dominant.

The purpose of any fracture mechanics assessment is to provide a quantitative prediction of the following:

1) Allowable peak stress for a given crack size

2) Maximum crack size for a given peak stress

3) Maximum crack size or peak stress for a given material toughness

4) Crack size for a given fatigue loading spectrum, initial crack size, and environment

5) Appropriate intervals for inspection.

For this research, the desired outcome is a prediction of the maximum crack size or peak stress for a given material toughness as well as specific intervals for inspection. This will aid in the holistic approach for prescribing the inspection criteria to ensure the structural integrity of the system.

The basis of the fracture mechanics assessment is an energy balance.[19] In the early days of fracture mechanics, Griffith proposed that crack extension will only occur when the available energy exceeds the energy required to form new surfaces. Irwin expanded on the energy balance by determining a relationship for the stress intensity factor. The form of the stress intensity relationship is shown in Equation 9, where (K_I) is the Mode I stress intensity, (σ) is the far field stress, (a) is the crack size, and (β) is the geometric correction factor. The units of stress intensity are [stress √ length].

$$K_I = \sigma\sqrt{\pi\, a}\,\beta \qquad [9]$$

In Linear Elastic Fracture Mechanics, the failure criteria is reached when the stress intensity becomes greater than the fracture toughness of the material. Or in other words, as the stress intensity approaches the fracture toughness, unstable fracture occurs. The fracture toughness is also referred to as the critical stress intensity factor (K_{IC}). The critical stress intensity factor is a property of the material. This property is determined by

standardized test methods such as ASTM E399, Standard Test Method for Linear-Elastic Plane-Strain Fracture Toughness K_{IC} of Metallic Materials.

On the towers and radars in the field, fatigue cracks have been found and identified as such. Due to the presence of the cracks, the analysis to be conducted is that of a fracture mechanics analysis to quantify the remaining life of the part. In the strain-life analyses, the presence of a crack constitutes a failure. However, in a fracture mechanics paradigm, there may be residual life for the part. This residual life calculation can be determined based on the stress intensity of the part and fracture toughness of the material as well as the consideration of other influencing factors. Some of the influencing factors are the change in stress intensity, maximum stress intensity, stress ratio, frequency, environment, load waveform shape, temperature, load history, etc.[20]

Stress intensity solutions can be derived a number of different ways. Some of these methods include finite elements, boundary integral, conformal mapping, superposition, and experimental.[21] Due to the complex nature of the radar system, the calculations of the stress intensity for the parts in question need to be performed numerically using the finite element method. This is done using StressCheck software.

A 3D model of the support plate was used for the damage tolerance analysis. This part was chosen because of the history of cracks found in this part. The support plate at the LAB-6 radar site in Canada was replaced due to 4 cracks that were found in the structure. The locations of the cracks are shown in the results section 5.5. The failure analysis of the support plate is also shown in the results section 5.6.

To perform the analysis, the solid model file was imported into StressCheck. The software was then used to simulate the crack in the part by inserting a plane to disconnect

the material at the crack location. The location of the plane was fixed, but the width of the plane was parameterized to allow for the simulated growth of the crack in the material. The stress analysis performed is very similar to the finite element analysis of the entire structure as described in a previous section. The same basic sequence of steps was performed. The only difference was the modification to the mesh around the crack and on the crack face. The mesh was refined at these locations in order to produce the stress intensities at the crack tip.

Using an excel macro, the crack length was parametrically increased to specified values and the model was solved. The stress intensities were recorded at 45 segments along the crack face. The largest stress intensities at the crack tip were then averaged together and tabulated to show a singular value for each of the parameterized crack lengths. The far field stress was found by comparing the stress on a support plate spoke that was not cracked. The beta correction factor was determined by using Equation 9. This is tabulated in section 5.4.

The fatigue crack growth rate is defined as the change in length of the crack (delta a), over the change in cycles (delta N). The fluctuating stress in the relationship also causes the stress intensity to change. This change in stress intensity is defined as (ΔK). Paris, et al., have established a correlation between the fatigue crack growth rate (da/dN) and the stress intensity factor range (ΔK).[19] Standardized test methods have been written in order to develop da/dN versus ΔK curves for different types of materials. Using these curves, a prediction of the crack growth rate, and ultimately the fatigue life, of a component can be calculated based on the stress range for the given part.

A section of the tower was removed from the E-FAC to perform this fatigue testing to determine the fatigue crack growth rate curve for the structural material. The structural member removed was cut into five samples for the fatigue test and eight samples for the tensile tests. The fatigue tests were run in accordance with ASTM E647 *Standard Test Method for Measurement of Fatigue Crack Growth Rates*. A sample of the results from this test is shown in Figure 6.

Based on the fatigue crack growth rate curve for the material and a calculation of the stress range of critical radar parts, the crack growth rate can be determined. To aid in this effort, AFGROW software is utilized. The software allows for a 2D crack to be modeled using geometry from the structural component.

Two separate damage tolerance analyses were run. The first was modeled based on the support plate spoke being completely fixed to the out rim of the bearing. For this analysis, a user-defined through crack was used which had an initial crack length of 0.125 inches. Figures 7 through 10 show the input parameters used to model the crack growth in the part.

Once the failure analysis from the support plate was received from the lab, it was apparent that the geometry from the original damage tolerance analysis had been incorrectly modeled. The spokes were only attached to the outer rim of the support by a weld around the perimeter of the spoke. The geometry was remodeled to include a small gap between the end of the spoke and the outer rim with a crack going through the welded portion. The second damage tolerance assessment was then completed based on this geometry.

For the second analysis, the initial crack length was 0.05 inches. The following figures show the input parameters used to model the crack growth in the part. The model of the crack was modeled to only pass through the welded material along the perimeter of the spoke as shown in Figure 9. The AFGROW input parameters used to model the crack growth in the part are shown in Figure 10.

The stress ratio (R) was also modified in the different analyses to account for the different possible loading magnitudes as well. The equation for the stress ratio is shown in Equation 10 as follows.

$$R = \frac{K_{min}}{K_{max}} = \frac{\sigma_{min}}{\sigma_{max}} \quad [10]$$

In StressCheck, the radar load is included in the model as an applied stress rather than a force. The stress induced by the weight of the radar was applied to the top of the support plate. The outside rim of the support plate was fixed where it rests upon the bearing. The model was solved with these loads and boundary conditions. This produced a compressive stress in the vicinity of the crack locations, which ultimately resulted in a negative stress intensity condition. The loading orientation had to be reversed in order to produce tensile stresses in the region of interest. This reversal of loading orientation is acceptable because of the cyclic loading of the radar. Due to the linear characteristic of this analysis, the magnitude of stress is not critically important when solving for stress intensities and betas at a crack face.

The AFGROW input parameters had to also be reversed in order to account for the loading reversal in StressCheck. This was accomplished by multiplying the stresses by negative one. The new minimum and maximum values were used to recalculate the revised stress ratio.

As shown in Figures 8 and 10, the spectrum is constant amplitude loading. This is representative of the loading condition imposed by the offset center of gravity of the radar. The stress multiplication factor (SMF) was modified to represent possible loading magnitudes. For both the full height through crack and the cracked weld, the input SMF values started at 0.430 ksi, which was the maximum stress found in the part from the finite element analysis. The SMF values were increased to obtain different life predictions for this part. These results are shown and discussed in subsequent sections.

The three values for the stress ratio were -1 for fully reversed loading, -11.2 which was representative of the absolute maximum and minimum principal stress fluctuations in the part, and -90.1 which was representative of the average maximum and minimum principal stress fluctuations in the part as determined by the finite element analysis.

As shown in Figures 8 and 10, the user-defined beta values from StressCheck are included in the analysis. This accounts for the change in stress intensity at the crack tip as the crack propagates through the part. Using the input results from StressCheck, AFGROW can calculate the number of cycles it will take for the crack to propagate through the part. The analysis in AFGROW will stop based on a given failure criteria or when the crack reaches a free edge in the part. In the support plate, the multiple spokes will carry the load of a single failed spoke, so the net section yield failure criteria was disabled and failure occurred when the crack reached the opposite side of the part. The results from this analysis are shown in the results section 5.4.

4.3. Nondestructive Inspection

Nondestructive inspection is a critical factor in a holistic design paradigm. Part of the inherent truths of the damage tolerance philosophy is that crack-like discontinuities are present in the structural members of the system. In order to maintain structural integrity, it is essential to be able to find these discontinuities. Nondestructive inspection provides the method to evaluate the product.

No routine inspection for cracks or damage has ever been mandated for the radar system. There have been instances in the field in which problems have been found and repaired, but these typically were done by diligent maintainers outside of their scope of work. As part of this research, a baseline inspection was completed at several radar sites. The inspection was conducted by a Level II certified inspector from Hill Air Force Base. A sample of the results found from these inspections is shown in the results section 5.5.

A method needs to be employed to know how to inspect and evaluate mechanical components for the radar to ensure structural integrity. This can be done using a holistic approach. There are seven basic steps in this paradigm. It is imperative to know what to look for, where to look, how to look, when to look, how often to look, the probability of detection, and the detection threshold.[3]

Defining what to look for is the first step in this holistic process. Based on the damage tolerance assessment, the critical crack size for a given component can be determined. However, there are other important failure modes that should be considered when deciding what to look for. The AN/FPS-117 radar site in Puerto Rico is located directly on the coast. This site experiences a high degree of corrosion issues. This failure mode may be included in knowing what kinds of things to look for.

For the analysis of the structural integrity of the radar and radar tower, a stress analysis was completed to locate the areas of high stress. These areas are typically where problems may arise. Any part in the structure that contains a stress concentration may be prone to damage. The results of the stress analysis should pinpoint the locations on the structure that are likely to exhibit indications.

There needs to be a definition of how to look for structural damage. In the past, this has been accomplished by an electronics technician who is on site performing maintenance on the radar. These technicians have often noticed cracks in the structure. The determination needs to be made regarding the qualifications of the person performing the nondestructive inspection. This determination will be partly based upon the size of the flaws and the method of detection.

The inspection interval can be determined in part by the crack growth rate for critical components. As discussed previously, a large amount of money is spent solely in traveling to these remote radar sites. Typically the site is visited at least on a quarterly basis to perform maintenance. It is essential to use the scheduled time at the radar location to the best of the maintainer's ability. The inspection interval of the radar and tower may also be driven by cost. In an effort to reduce the costs of this inspection, the interval may be lengthened if it is determined to be safe to do so.

There are a wide range of nondestructive inspection techniques that can be utilized to locate cracks. Some common inspection techniques are listed as follows: visual inspection, magnetic-particle, liquid penetrant, ultrasonic, radiographic, and eddy-current testing.[22] Each of these techniques will have a specific probability of detection and a detection threshold. Depending on the criticality of the structure being analyzed, a

specific method may be chosen to ensure that the size of the flaw can and will be found with a quantified probability. The location of the cracks as well as the type of material will be important in choosing a method to use. The results of the damage tolerance analysis will assist in determining the inspection technique.

Utilizing this holistic method of inspection will save valuable time and money. The result can be a quantifiably more reliable and safe radar system, which is capable of fulfilling its designed mission.

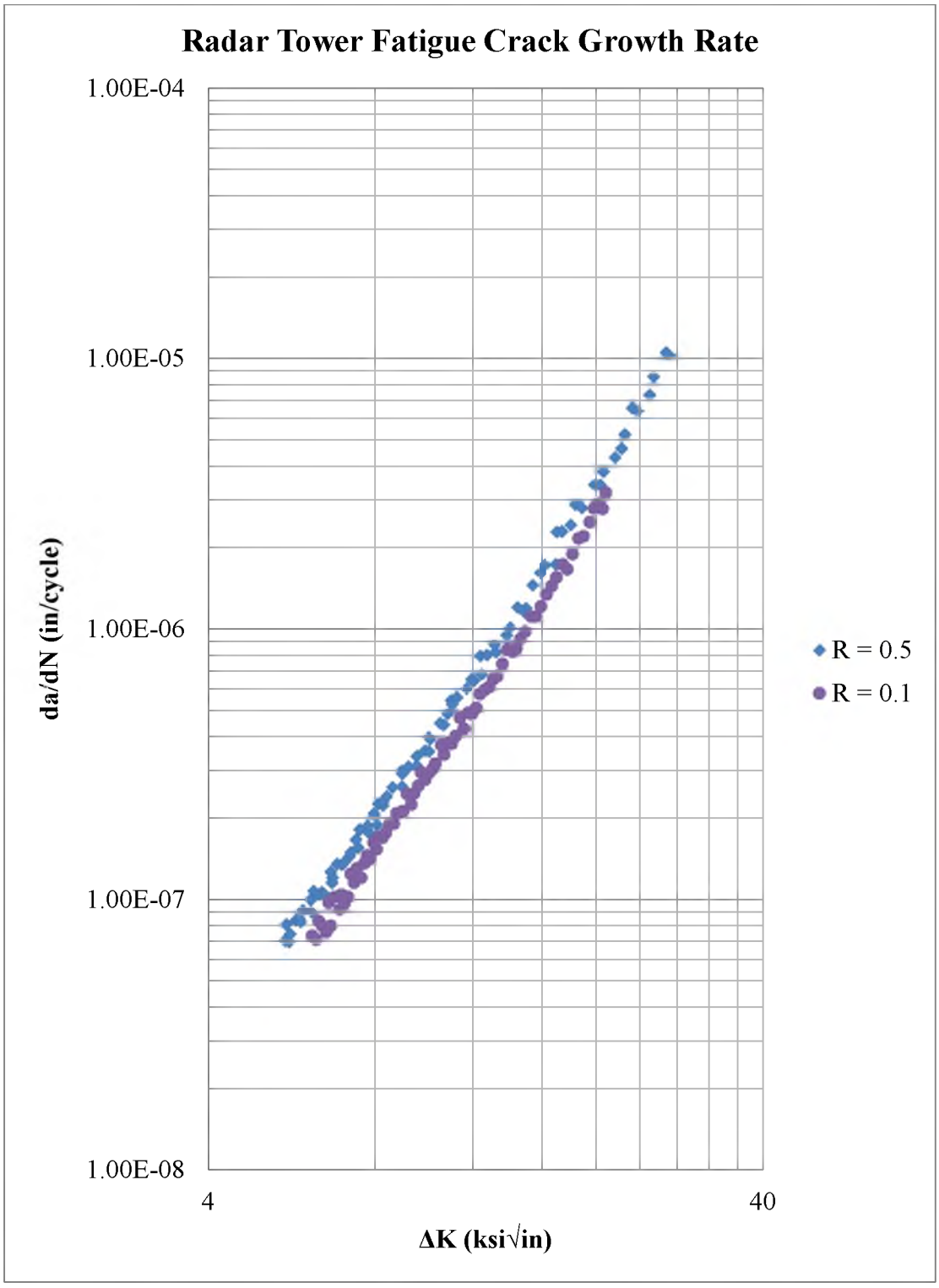

Figure 6 Fatigue crack growth rate testing results for radar tower steel samples

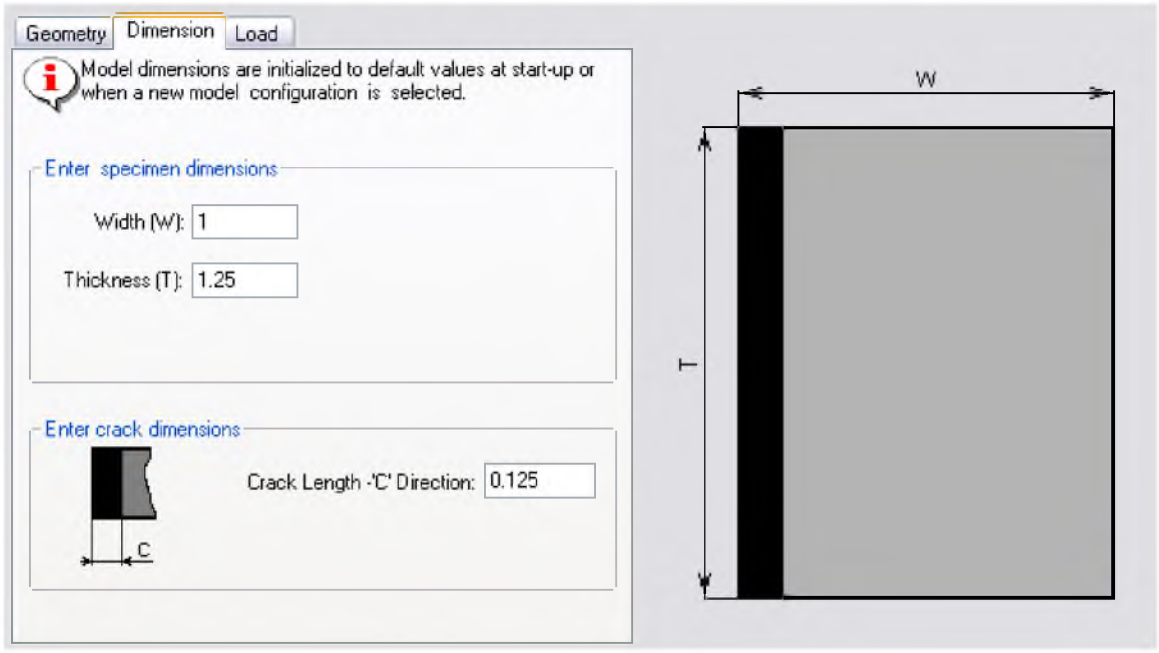

Figure 7 AFGROW geometric dimensions for first damage tolerance model

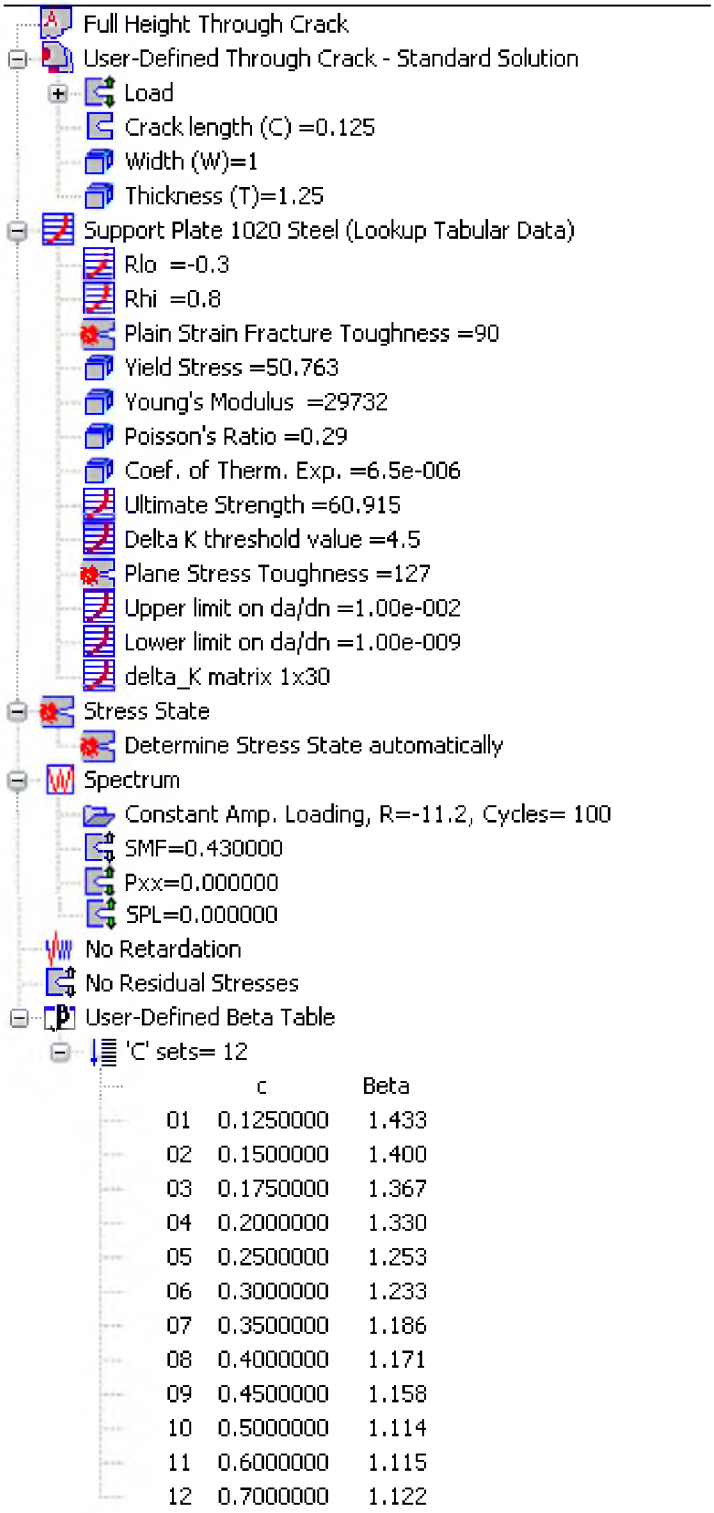

Figure 8 AFGROW input file for first damage tolerance model

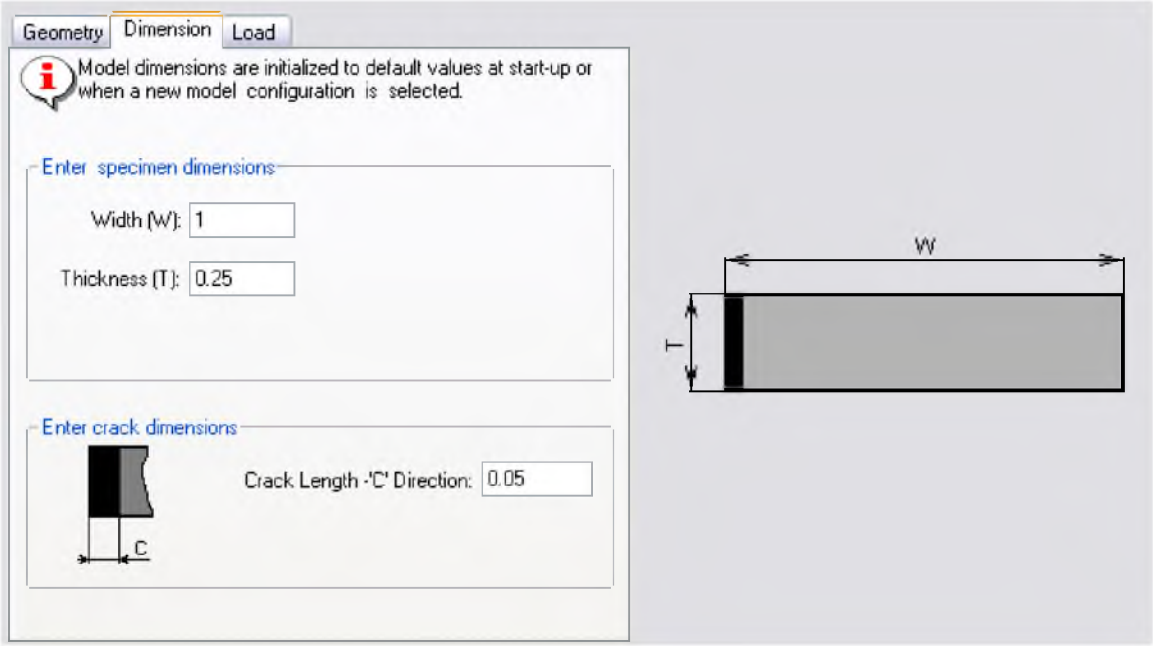

Figure 9 AFGROW geometric dimensions for revised damage tolerance model

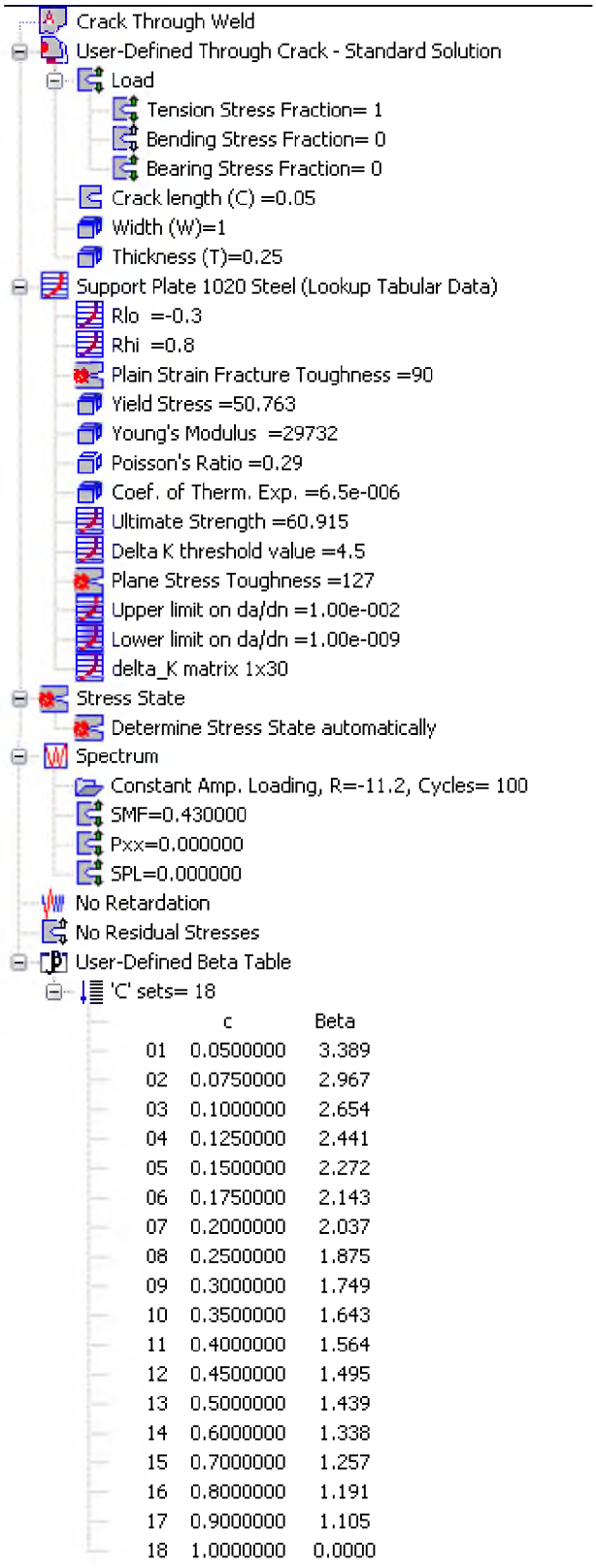

Figure 10 AFGROW input file for revised damage tolerance model

Table 1 Fatigue properties for radar materials

	AISI 1020 Hot Rolled Steel [13]	Static Tensile Test Results [8]	Modified Universal Slope Method [17]
σ'_f	130,000 psi	54,971 psi	54,971 psi
E	29,000 ksi	28,928 ksi	28,928 ksi
b	-0.12	-1.58	-0.12
ε'_f	0.41	0.35	0.35
c	-0.51	-0.60	-0.60

5. RESULTS

5.1. Stress Analysis

The reaction loads that were calculated from the weight of the radar antenna are shown in Table 2. The results from the SolidWorks finite element analysis are shown in the following figures. Figures 11 through 15 show the Von Mises stress, first principal stress, strain, deflection, and factor of safety results for the radar set at the zero degree orientation, respectively.

The tabulated results from the SolidWorks finite element analysis are shown in Table 3. The measurements were taken at the same locations as the strain gages that had been instrumented on the tower for comparison. SolidWorks includes various plot tools to select individual elements and output the location, stress, strain, and displacement values for the selected elements. The element locations that were selected corresponded to the locations on the radar and tower where the strain gages were located. The finite element analysis strains were then compared to the fluctuating strains measured by the strain gages.

Figures 16 through 19 show the change in strain at the 15 strain gage locations on the pedestal as the weight of the radar is repositioned every 30 degrees. Strain gage 7 was positioned on the oil pan, which was not included in the finite element model.

The high stress areas are found using the finite element analysis. These were typically located where a stress concentration is present. Some high stress areas are

shown in Figures 20 through 22. The load path for the radar will also provide insight into the areas that will feel the most stress. SolidWorks has a design optimization feature that will highlight the load path through the structure. A sample of this feature is shown in Figure 23.

5.2. Strain Gage Results

A small selection of the results from the data collected from the strain gages is plotted in Figure 24. A sample of the strain gage impact based on the changes in radar and platform level at the radar engineering facility is shown in Figure 24. The full complement of the 48 strain gages are shown in Appendix C.

The LAB-6 strain measurements were collected over a period of time when the level of the radar was being adjusted. The measurements show one cycle recorded every two hours over a four day period. A sample of this is displayed in Figure 25. The full results for the sixteen pedestal strain gages are shown in Appendix C.

The iterations of changes in radar level are tabulated for the E-FAC at Hill Air Force Base. This is shown in Table 4. For each of the level readings, the shim thicknesses, or suggested shim thicknesses on the tower posts are shown.

5.3. Strain-Life Results

The curves for the strain amplitude versus the fatigue life are shown in Figure 26. The dotted line is based on the ASM material properties. The thin orange line is based on the Modified Universal Slope material properties. The thick blue line is based on the Static Tensile Test properties. As discussed previously, the fatigue strength exponent (b)

was well outside of the range of typical values. This is evidenced by the plot shown in Figure 26, which tends to follow the strength dominated component of the fatigue life. The Modified Universal Slope material properties are used due to the fact that this will predict the shortest life, thus being the more conservative approach.

The strain amplitudes for the strain gage readings at the E-FAC were calculated. These calculations are shown in the Appendix D. They range on the order of 17 to 46 microstrain. The strain amplitude calculations using the SolidWorks finite element analysis were also calculated. The FEA strain amplitudes were calculated at locations that corresponded with the pedestal strain gage installations at the LAB-6 radar site in Canada for comparison purposes. These calculations range on the order of 0.5 to 16 microstrain. These strain gage readings are plotted against the fatigue failure curve in Figure 27.

The vertical line in Figure 27 represents the number of cycles that the radar has experienced at the current time (8.9×10^7 cycles). The value corresponding value for the strain amplitude at 8.9×10^7 cycles is 485 microstrain for the ASM material properties and 752 microstrain for the Modified Universal Slope material properties.

The strain gage placement at the LAB-6 radar site did not always correspond with the highest stress locations on the radar and tower. Using the results for the maximum strain amplitudes as determined by the finite element analysis, a larger strain amplitude was predicted. This was on the order of approximately 138 microstrain. This is shown in Figure 28.

The intersection of the maximum strain amplitude line and the fatigue life curve is shown in Figure 29. This value was calculated to be approximately 2×10^{12} cycles. This estimation is discussed in a subsequent section.

As discussed in section 3.1, the total weight is not directly measured by the strain gages because the gages were applied to the structure much later. This total amount of strain is determined by adding the finite element analysis strain results to the measured strain range. The results from this analysis are plotted against the strain-life fatigue curve shown in Figure 30.

The highest value for strain amplitude was estimated to be 144 microstrain. As shown previously, the critical strain amplitude at 8.9×10^7 cycles is 485 microstrain. This estimated value is only 30% of the critical strain amplitude.

5.4. Damage Tolerance Results

The results from the two damage tolerance assessments are as follows. The results from the StressCheck finite element analysis are presented. Figure 31 shows the first principal stress in the radar support plate. Figure 32 shows a close up image of the stress in the part surrounding the full height crack. Figure 33 shows a view from the interior of the support plate spoke as if it was hollow. The planar crack face is visible traveling through the full height of the part from right to left. This is from the first analysis.

Figures 34 and 35 show the first principal stress from the crack in the weld. This is from the second damage tolerance analysis. As shown in Figure 35, the square in the

center of the spoke that is visible is the gap between the end of the spoke and the outer rim.

The output of the StressCheck analysis is the stress intensity at the crack tip for increasingly larger crack lengths. The stress intensity at the crack tip is averaged and shown in Tables 5 and 6. Using Equation 9, the beta correction factor can be calculated.

Table 7 shows the principal stresses in the support plate as determined by the finite element analysis. Due to the high degree of variability in the analysis as compared to actual site conditions, the absolute maximum and minimum and the average maximum and minimum stresses were used to calculate stress ratio. These were also compared to fully reversed loading with a stress ratio of -1.

AFGROW has a feature to be able to input the cyclic stress-strain parameters to calculate the life to "crack initiation". The Modified Universal Slope Method material properties were used in AFGROW to determine when a crack would presumably nucleate in the part. The output is from AFGROW was the following: "The number of cycles to initiation is greater than 2×10^9. Prediction stopped." This correlates with the results from the strain-life analysis as shown in a previous section.

Tables 8 and 9 as well as Figures 36 and 37 show AFGROW results for both the full through thickness crack and the crack traveling through the weld with a gap between the end of the spoke and the outer rim of the support plate. Both analyses were conducted at three different stress ratio values, and multiple stress levels as shown. The life is calculated to be infinite at the stress levels predicted by the finite element analysis. This topic is discussed in a subsequent section.

The analysis was run at increasingly higher stress levels until the program predicted failure. For the full height through crack, the stress required to cause the crack to propagate through the part was 5.012 ksi. For the model with the crack through the weld, the stress required to cause the crack to propagate was 3.351 ksi.

5.5. Nondestructive Inspection Results

During this research, several sites have been inspected for cracks using nondestructive inspection techniques. The NDI program office at Hill Air Force Base was utilized to perform the inspection. The first site that was inspected was Point Barrow, Alaska. Three of the four corners of the central enclosure on the tower directly underneath the radar were found to be cracked. One of the cracks is shown in Figure 38.[23]

In July of 2012, a similar inspection was completed at three additional radar sites in Alaska. During this inspection, crack-like indications were also found. Some of these problems areas are shown in Figure 39 and 40. The size of the cracks that were found at these three sites ranged from less than half of one inch to upwards of several inches in length.

The pedestal oil pan has also exhibited cracking at certain corners of the part. Figures 41 and 42 show a crack in the oil pan that had been repaired, but have nucleated additional cracks at the repaired location.[24]

In September of 2012, nondestructive inspection of the support plate at the LAB-6 radar site identified cracks. They were found using a magnetic particle examination

performed by an NDE technician. The locations of the cracks and an image of one of the cracks are shown in Figure 43.[24]

5.6. Failure Analysis Results

The failed radar support plate that was removed at LAB-6 was sent to the Materials Laboratory at Hill Air Force Base for a failure analysis. The remainder of this section contains excerpts from the failure analysis report.[25] The four cracked spokes shown in Figure 43 were removed from the original part. Figures 44 and 45 show the sectioned part.

Three point loading was applied to open cracks 1, 2, and 4, to expose the fracture surfaces. The exposed fracture surfaces exhibited a considerable amount of debris which had been trapped between the spoke ends and the rim during manufacture. The spoke ends exhibited possible cutting marks from a torch cutting process and the rim exhibited what appeared to be machining lines. The fracture surfaces appeared stained/corroded and exhibited multiple crack origins nucleating at the weld root and propagating outwards. The weld roots exhibited undercutting, inadequate penetration, pores, and inclusions all of which produced stress risers.[25] This is shown in Figures 46 and 47. The figures for cracks 2 and 4 were very similar to crack 1 and were omitted for brevity.

The fourth spoke, numbered crack 3, was also sectioned but with cross sections running down the center of the spoke and across the crack to expose the weld cross section as shown in Figures 48 and 49. Another cut was made through the separated spoke end perpendicular to the top cut going through the side welds near the midpoint of the spoke, shown in Figures 50 and 51.

A gap was visible at the end of the spokes between the spoke and the rim. The two cut surfaces were examined for cracks in the weld. These surfaces were later polished and are shown in subsequent figures.

Fractography was conducted using a scanning electron microscope to study the fracture topography. Figure 52 shows the fracture topography across the side of one spoke end surface, typical for all spokes. Figure 53 shows a magnification of two locations from Figure 52. Multiple prior crack regions were detected on the surface of each of the cracked spokes. The cracks appeared to originate in the weld root and fan out towards the outer surface propagating through the weld material and forming multiple plateaus. The cracks exhibited faint beach markings typical of fatigue; however, corrosion products and staining obscured the detail of the fracture surfaces. Some of the prior cracks exhibited a crack front which ended at a band of overstress which extended outward to the weld surface.[25]

Polished cross sections from crack 3 were examined where the spoke was welded to the rim. Figures 54 through 57 show images of the polished surfaces taken with a Keyence microscope. Refer also to Figure 51. The specimens were prepared in accordance with ASTM E3 and etched using a diluted Nital etchant. Cracks are visible in each weld nucleating at the root and growing outward through the weld material.[25]

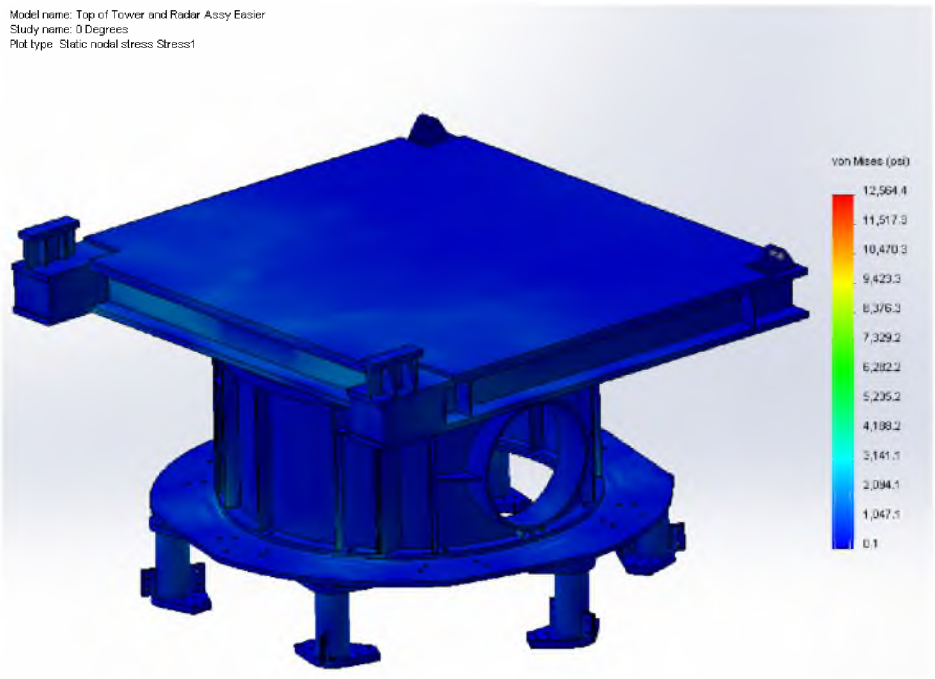

Figure 11 Von Mises stress results for the radar platform, pedestal, and tower

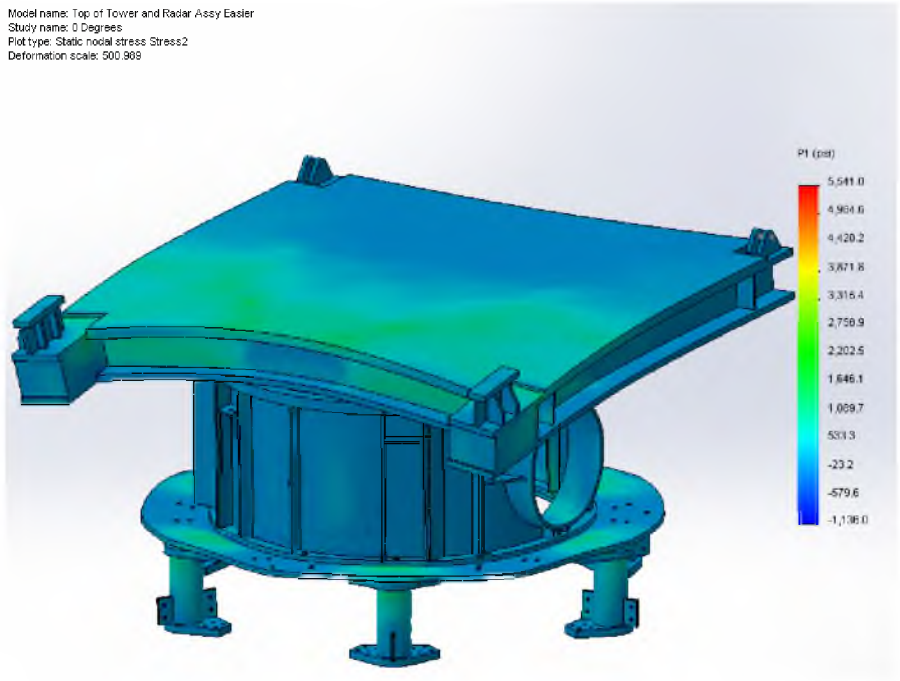

Figure 12 First principal stress results for the radar platform, pedestal, and tower

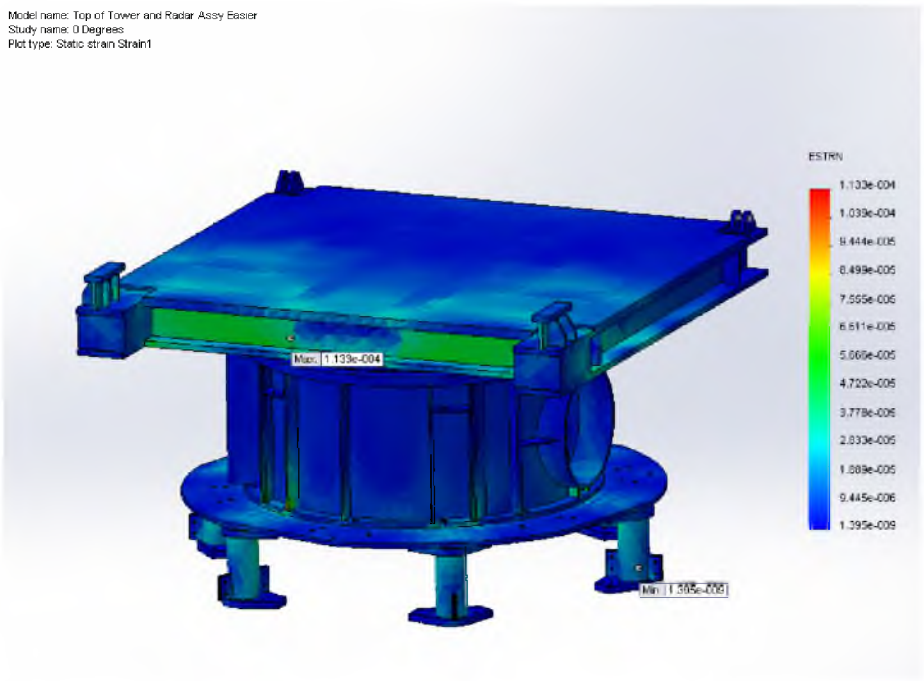

Figure 13 Strain results for the radar platform, pedestal, and tower

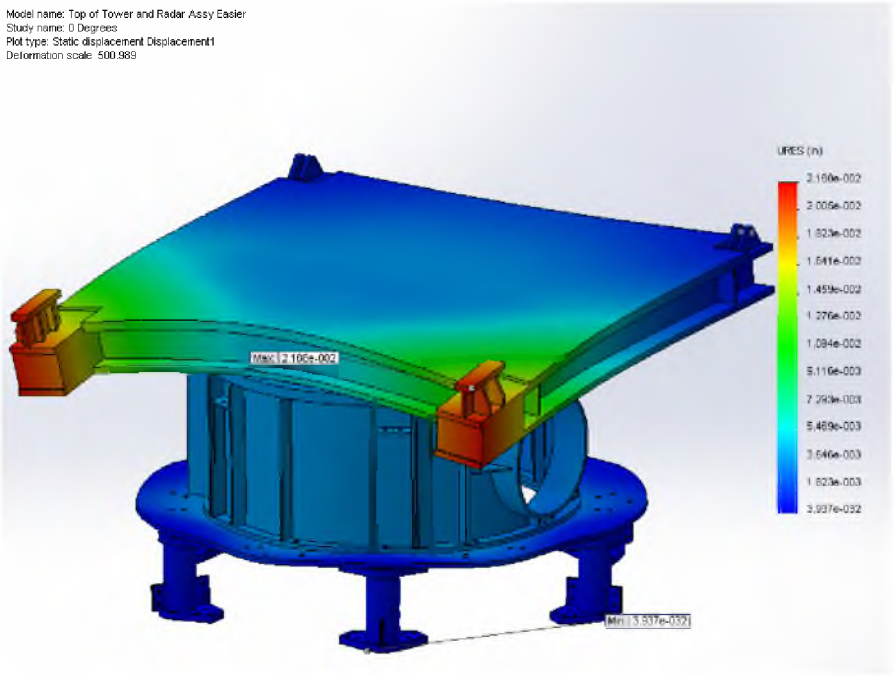

Figure 14 Deflection results for the radar platform, pedestal, and tower

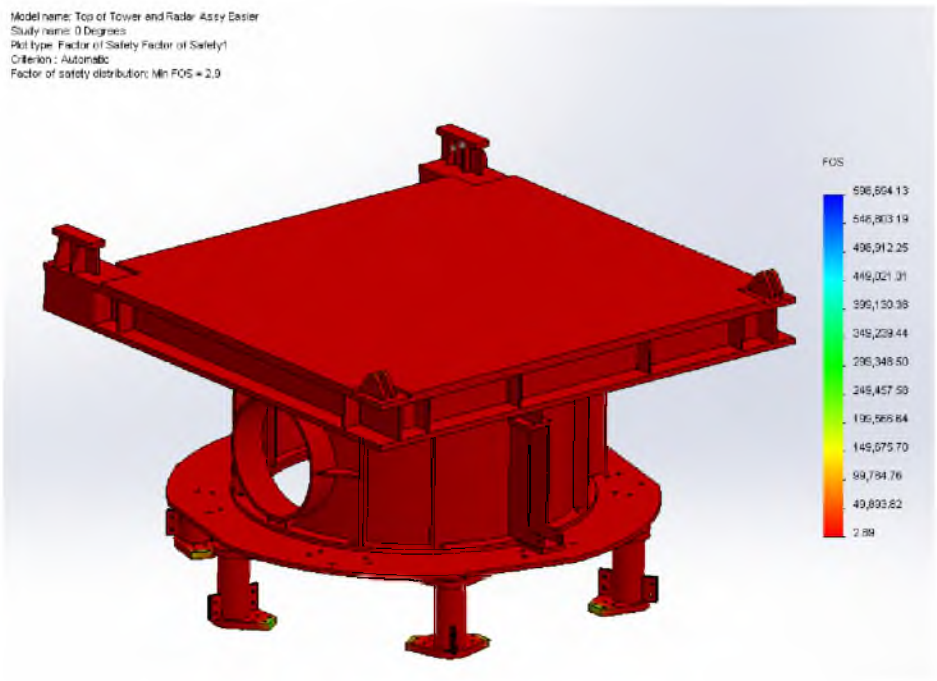

Figure 15 Factor of safey results for the radar platform, pedestal, and tower

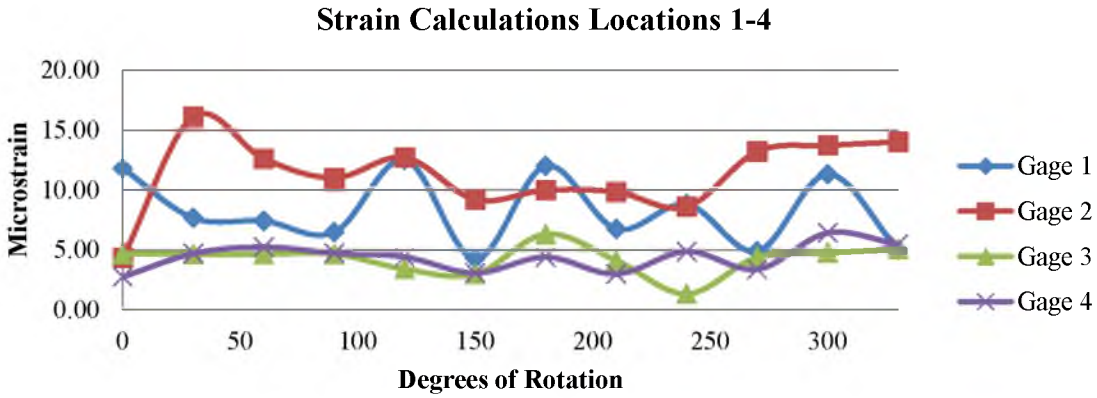

Figure 16 Finite element strain fluctuations based on radar rotation

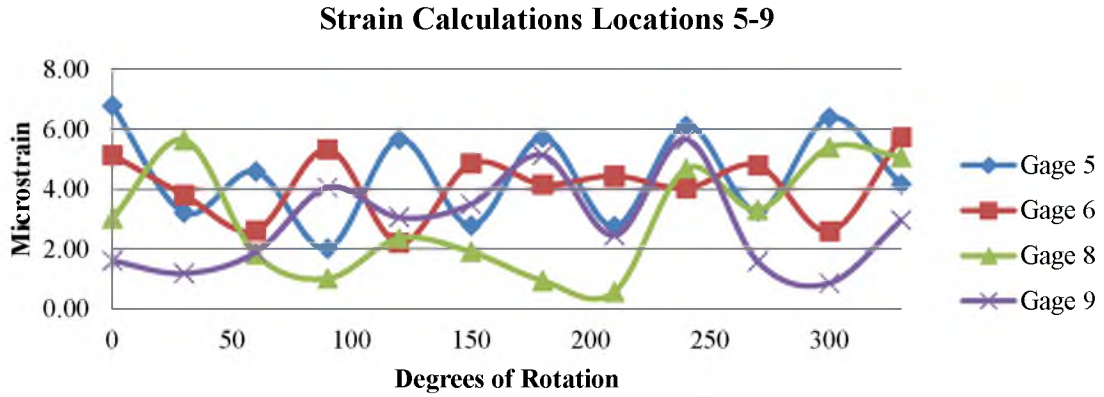

Figure 17 Finite element strain fluctuations based on radar rotation

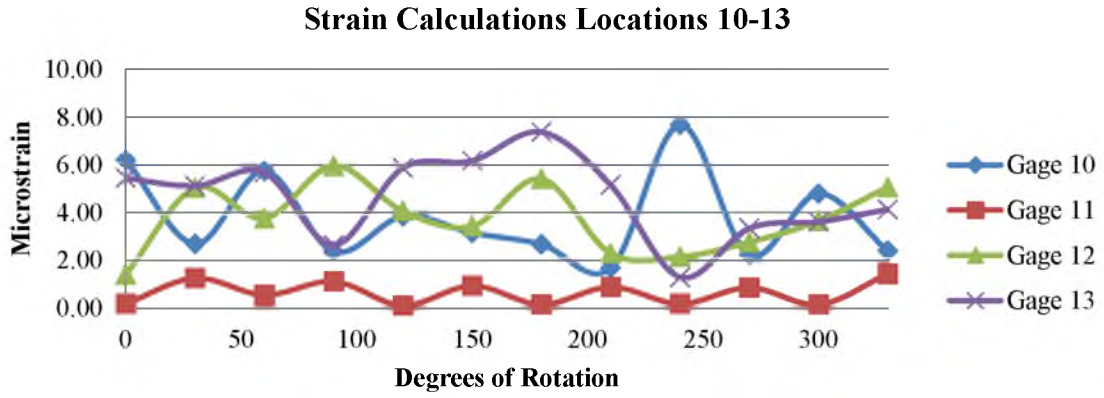

Figure 18 Finite element strain fluctuations based on radar rotation

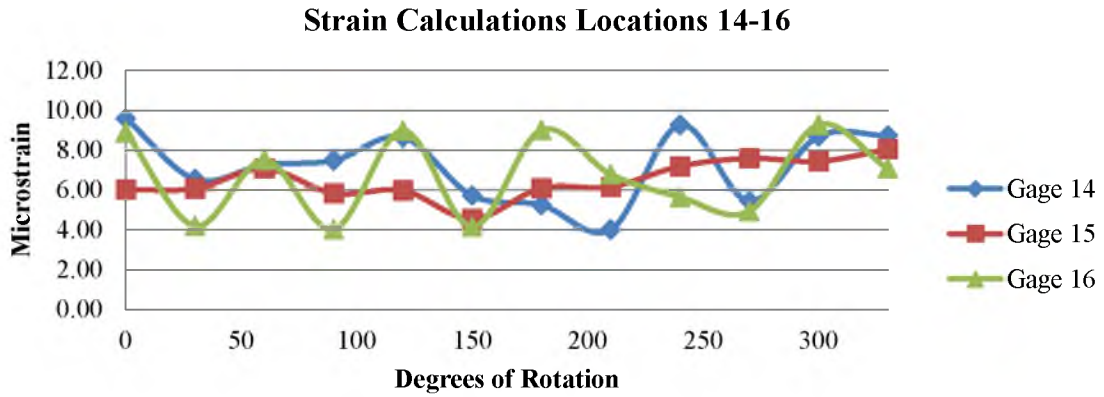

Figure 19 Finite element strain fluctuations based on radar rotation

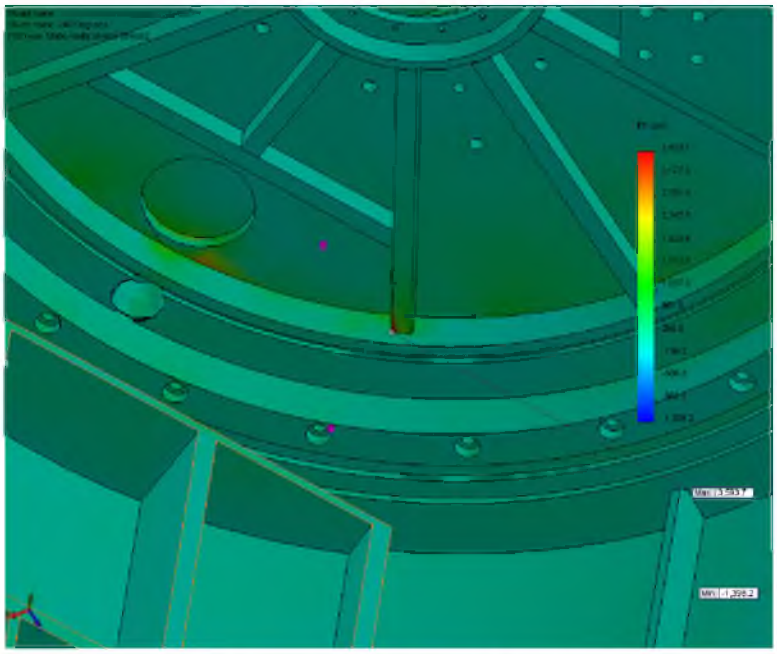

Figure 20 Predicted areas of high stress on the radar adapter plate

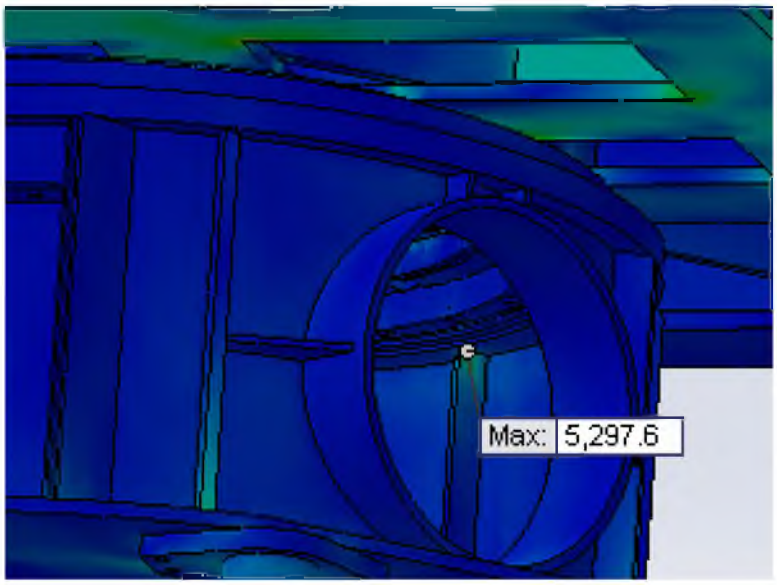

Figure 21 Predicted areas of high stress on the radar platform and pedestal

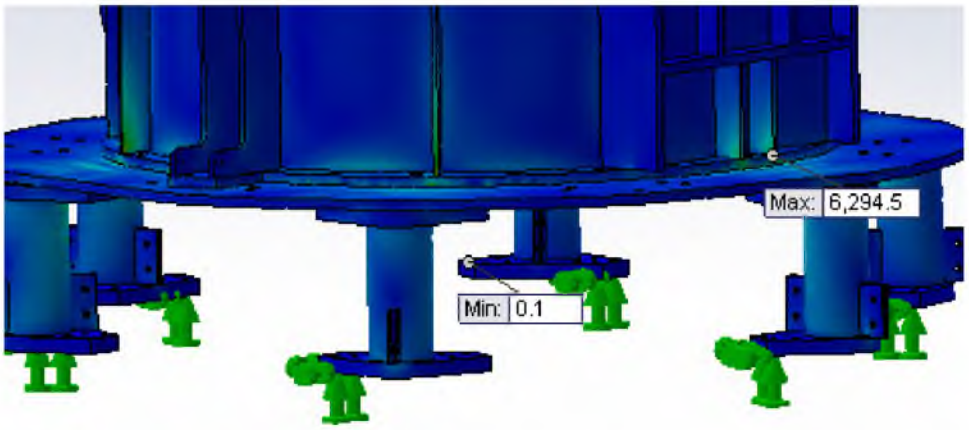

Figure 22 Predicted areas of high stress on the radar pedestal

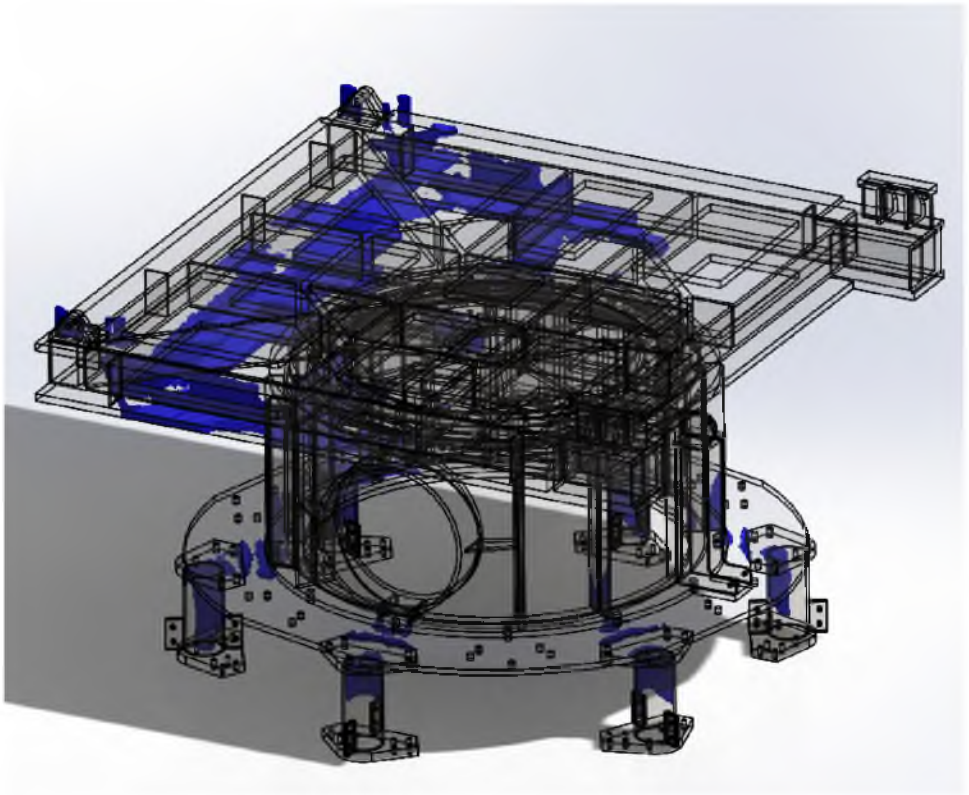

Figure 23 Design optimization feature showing load path and locations of higher stress

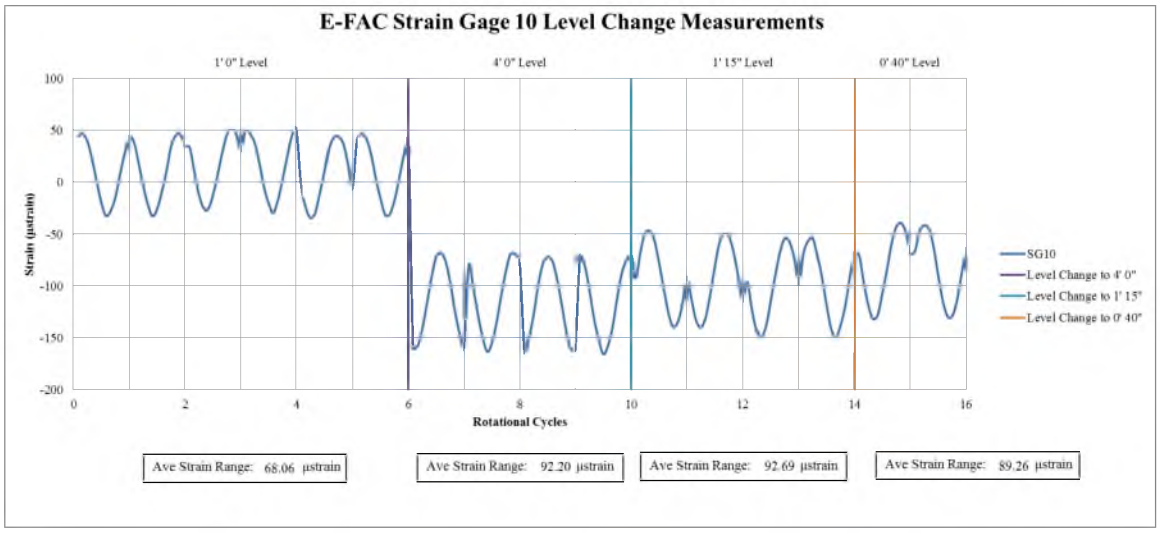

Figure 24 Plot of microstrain versus cycle for the E-FAC Strain Gage 10

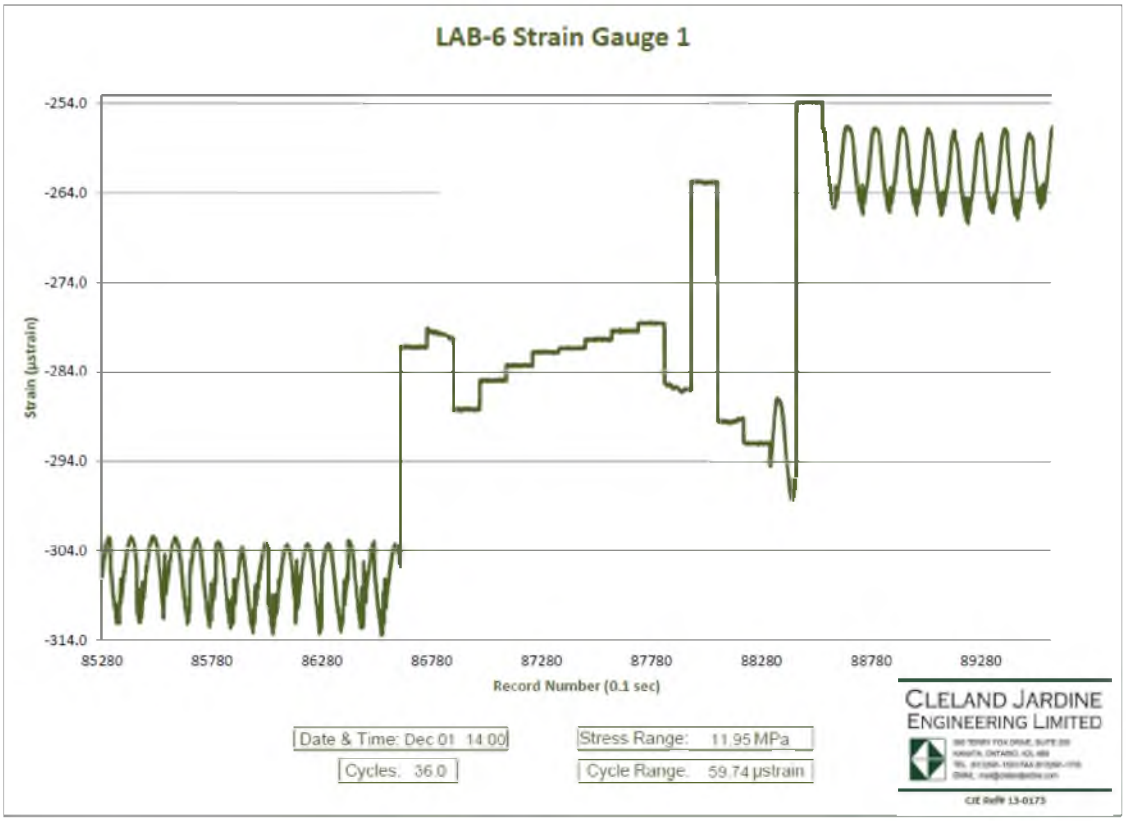

Figure 25 Plot of microstrain versus time for the LAB-6 Strain Gage 1

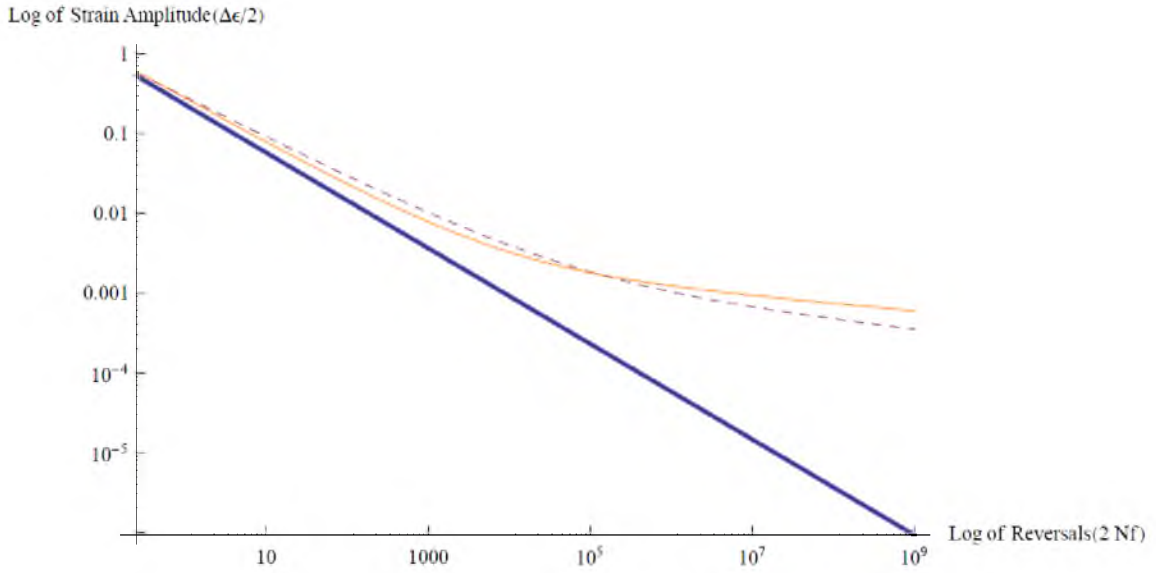

Figure 26 Log-log plot of the strain amplitude versus reversals to failure for the ASM, static tensile test, and Modified Universal Slope Method derived material fatigue properties

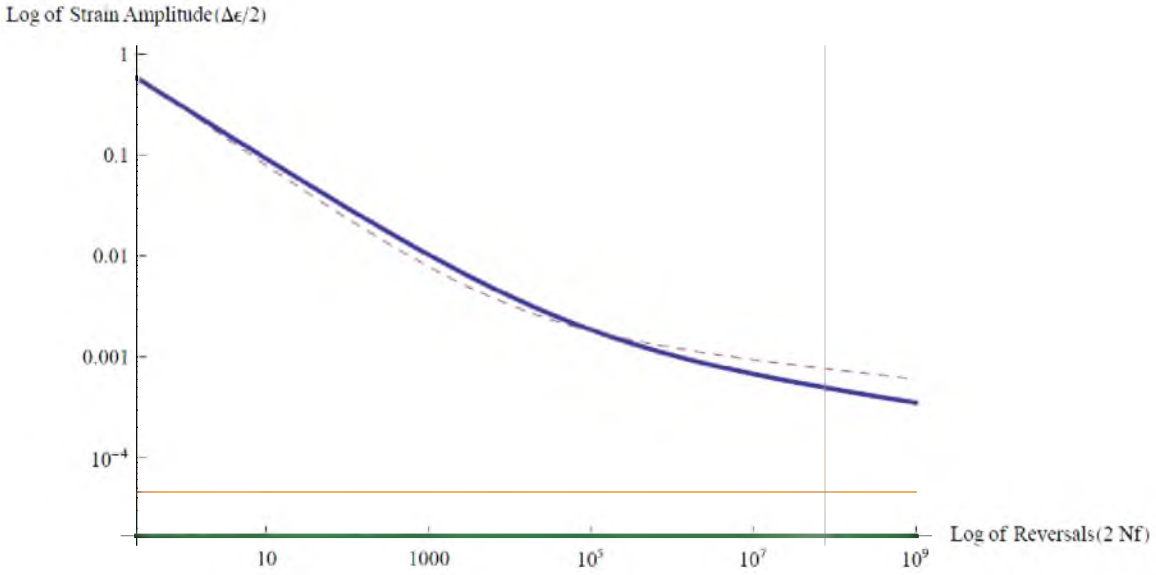

Figure 27 Log-log plot of the strain amplitude versus reversals to failure for the radar engineering facility and FEA strain gage readings

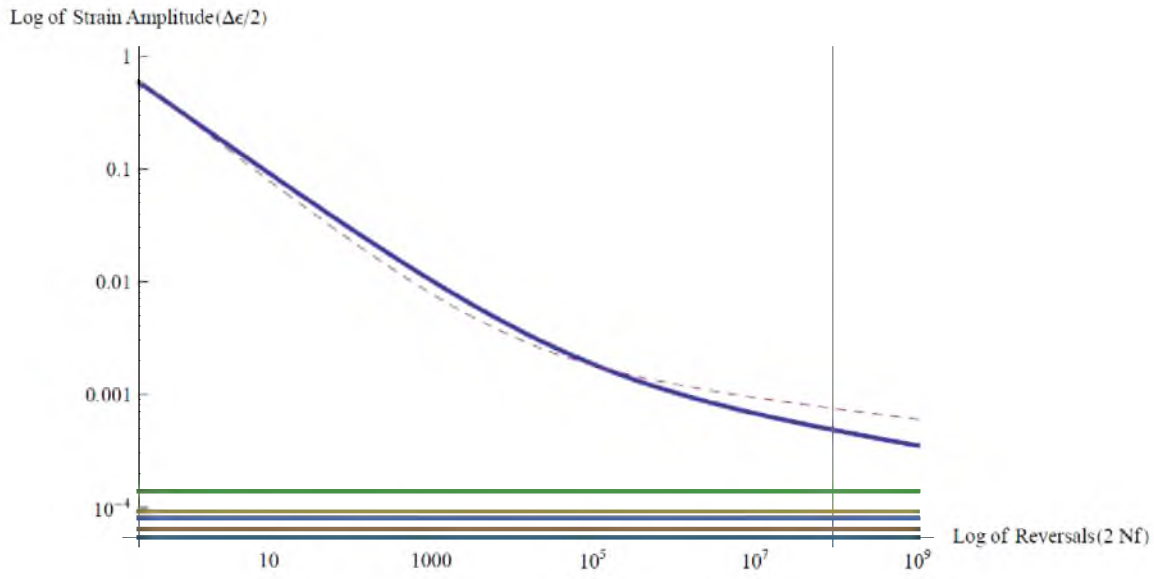

Figure 28 Log-log plot of the strain amplitude versus reversals to failure for the FEA maximum strain gage readings

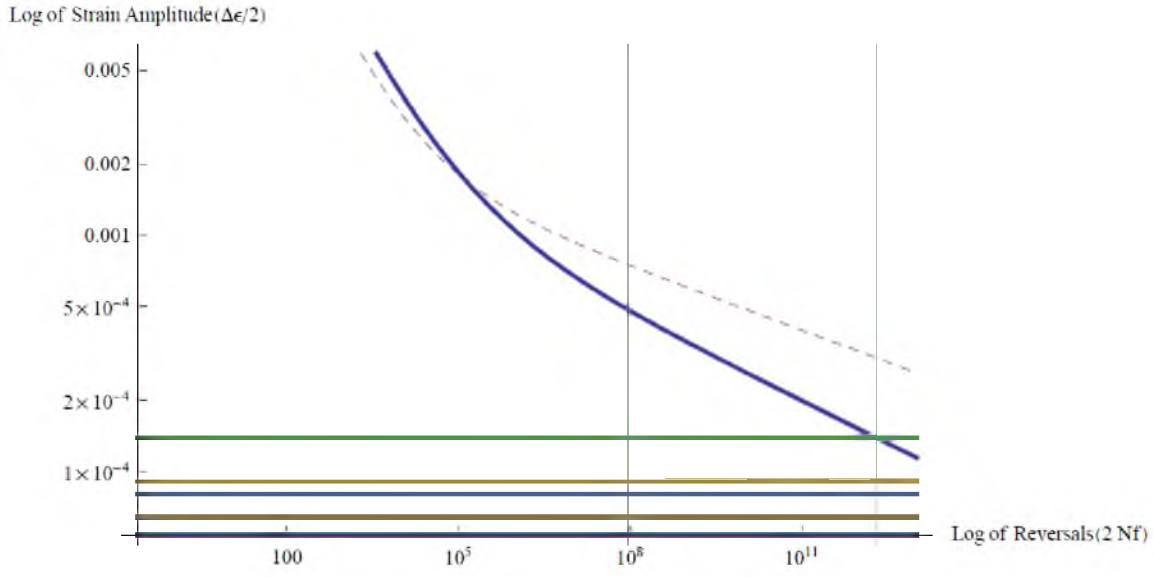

Figure 29 Intersection of strain amplitude range with fatigue life curve

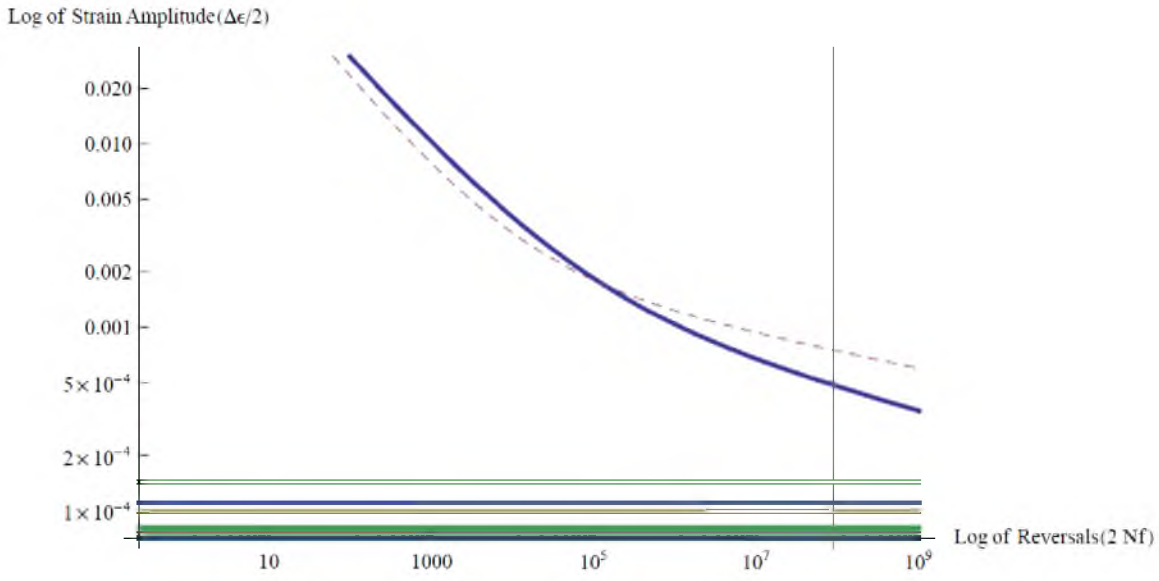

Figure 30 Total strain amplitude to include measured values and finite element results plotted against the fatigue life curve

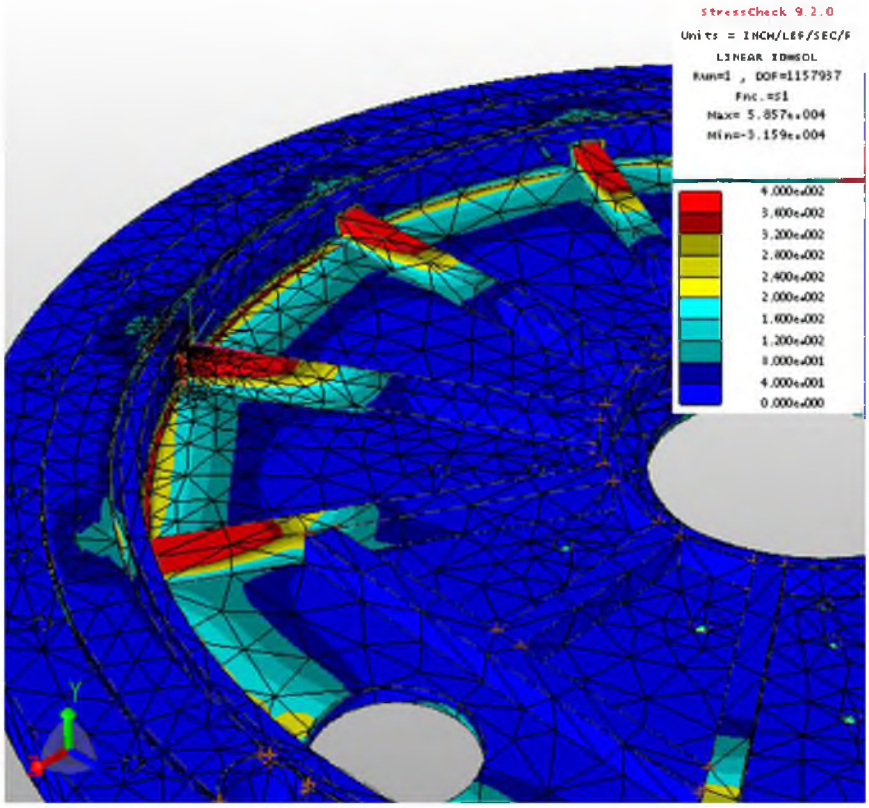

Figure 31 First principal stresses on the radar support plate

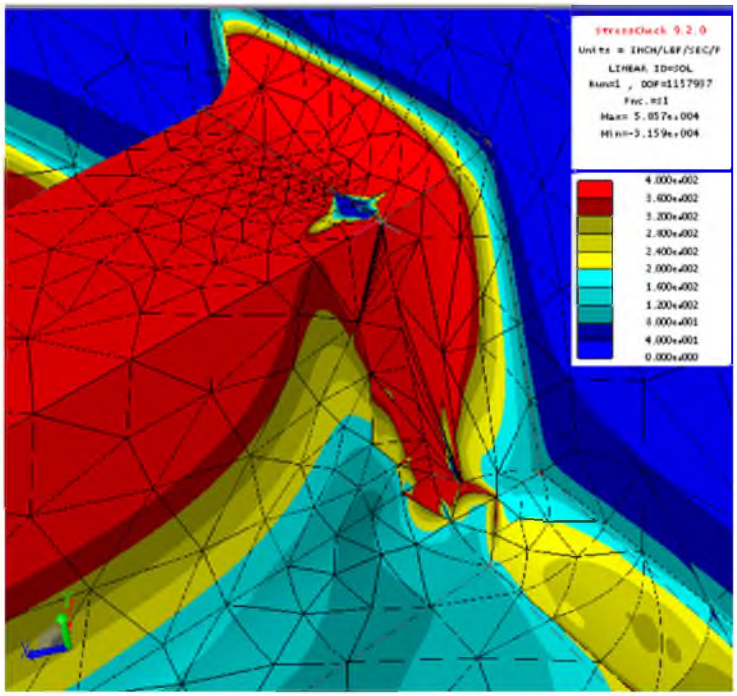

Figure 32 First principal stresses on the radar support plate near the full through crack

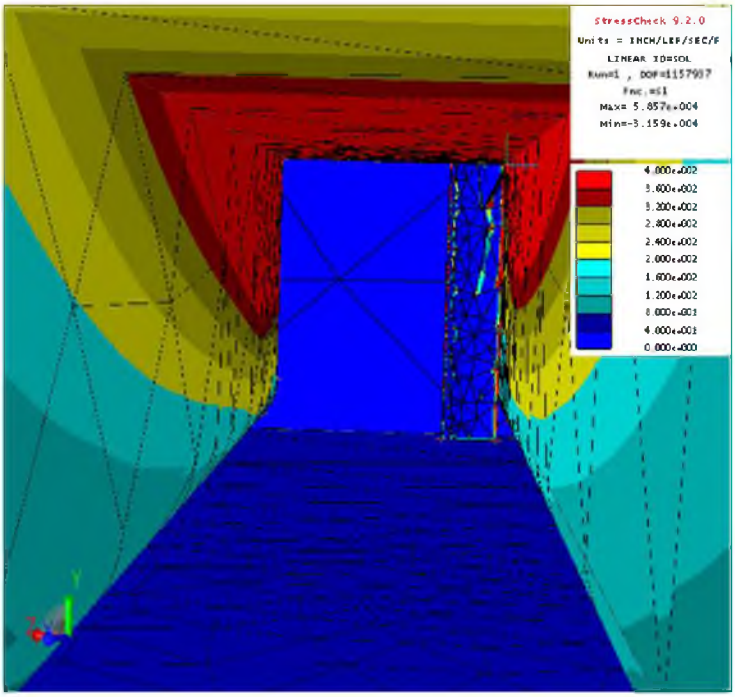

Figure 33 View of the full through fatigue crack from interior spoke of the support plate

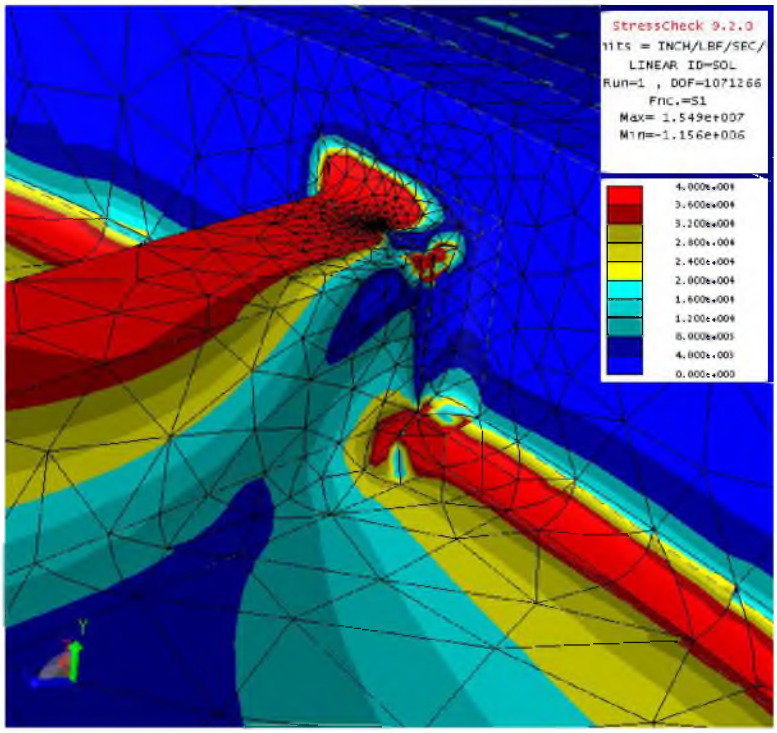

Figure 34 First principal stresses on the radar support plate near the crack through the weld

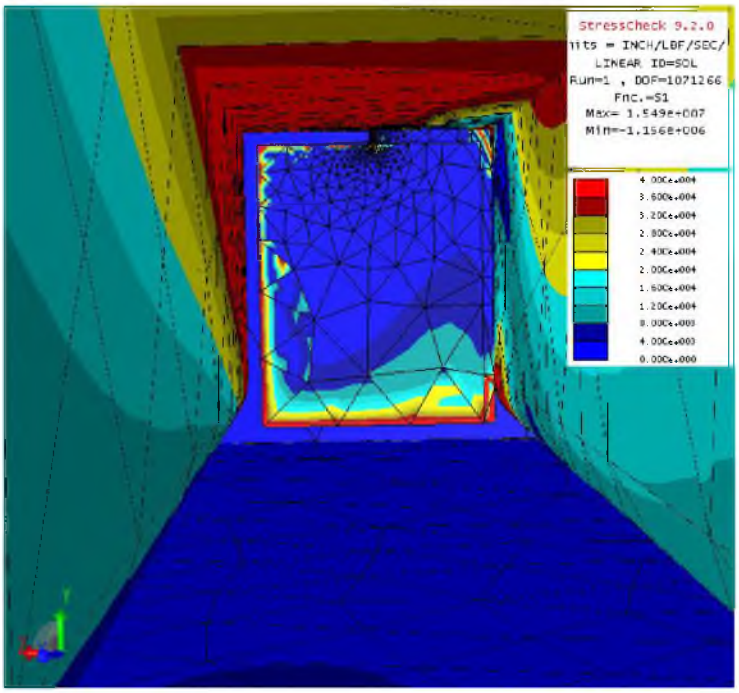

Figure 35 View of the weld fatigue crack from interior spoke of the support plate

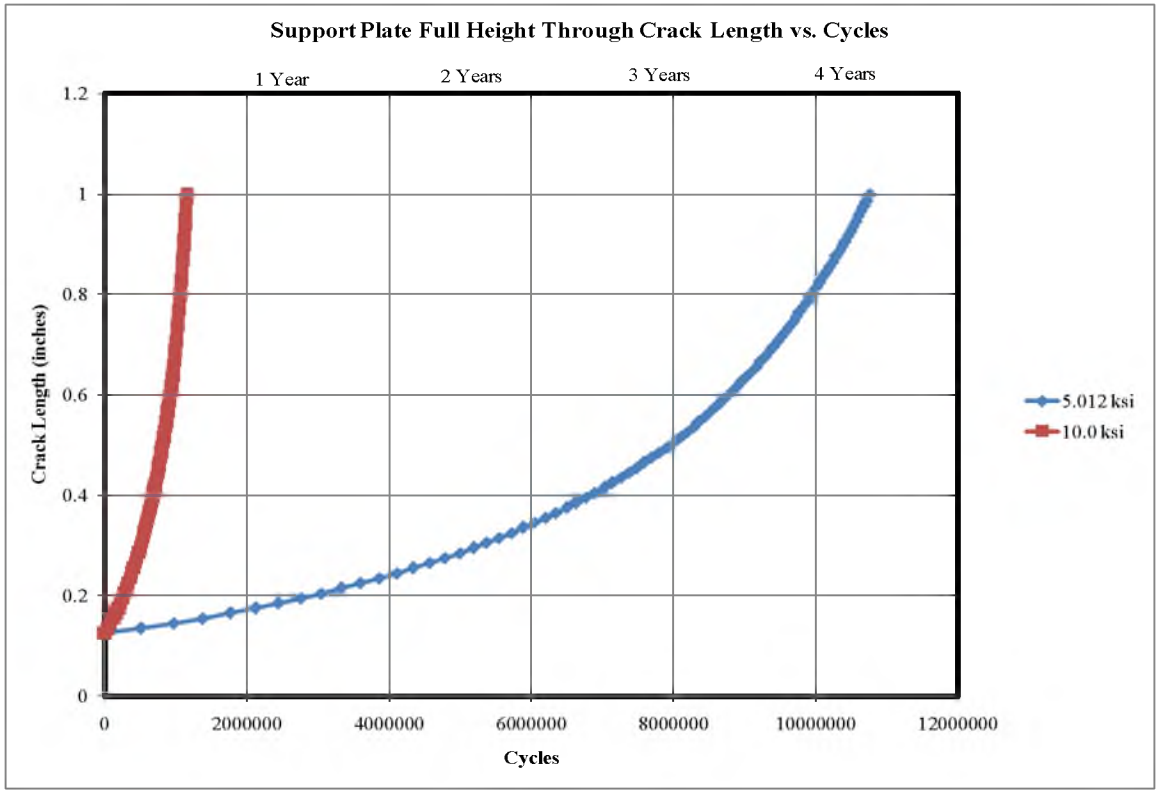

Figure 36 AFGROW crack length vs. cycle results for the full height through crack in the support plate

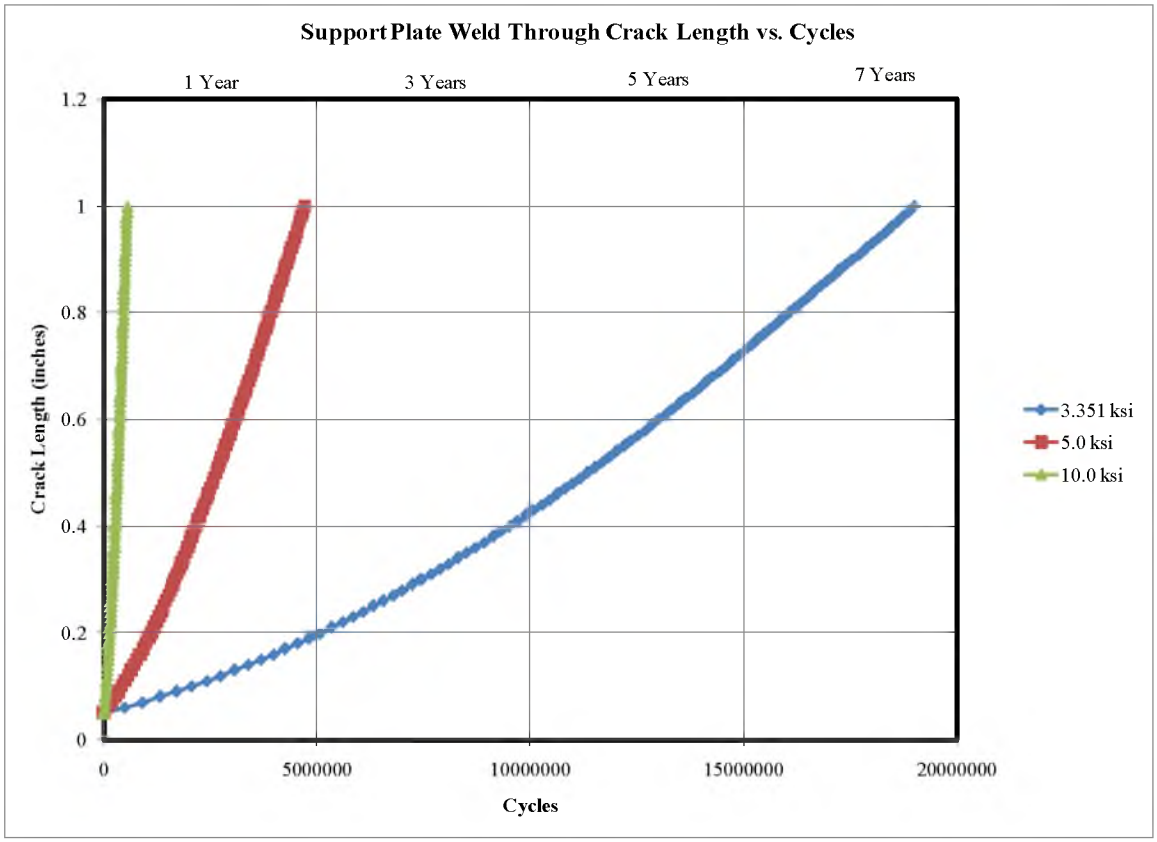

Figure 37 AFGROW crack length vs. cycle results for the crack through the weld in support plate

Figure 38 Fatigue crack found visually at Point Barrow, Alaska in July 2011

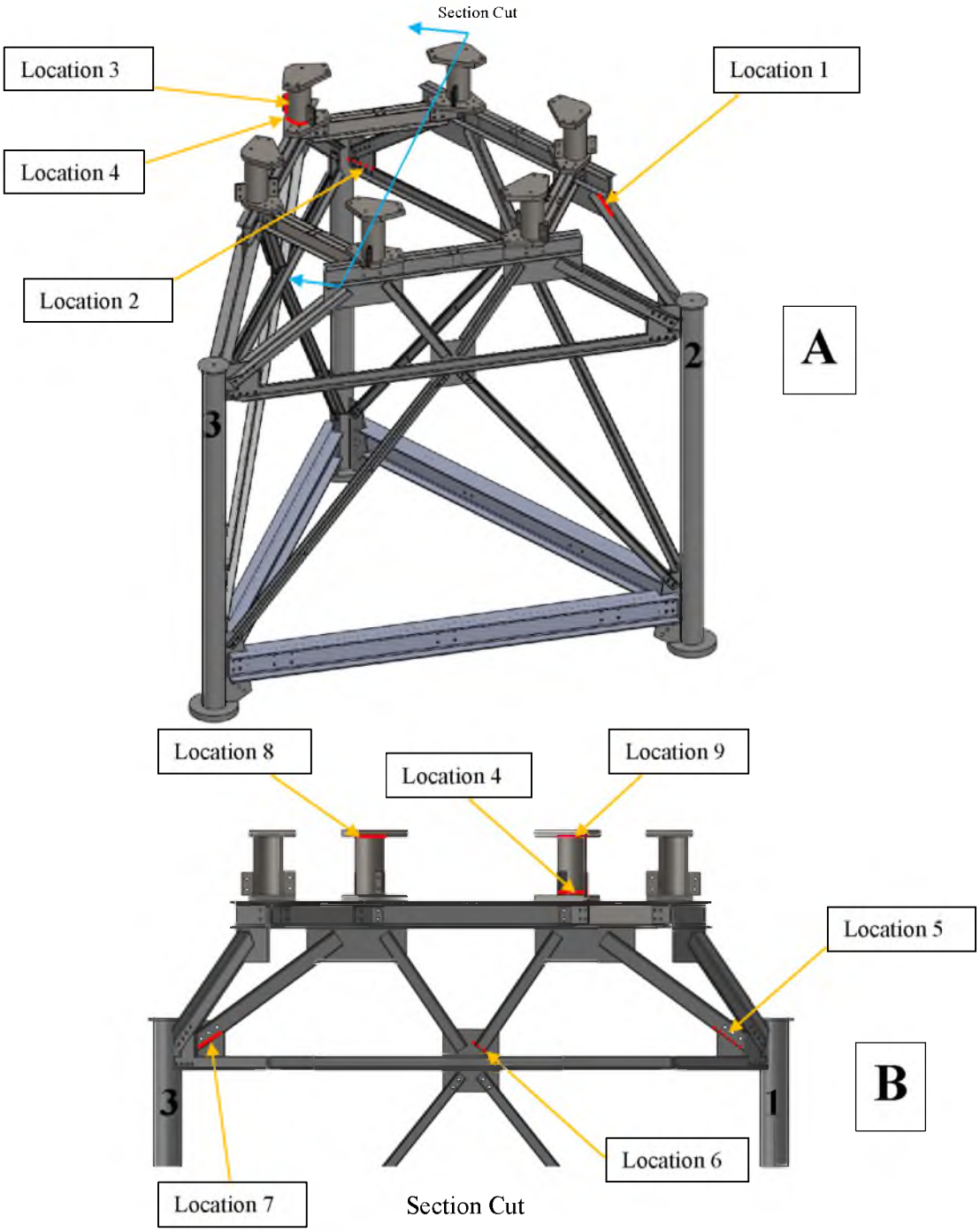

Figure 39 Tower crack locations found visually at Sparravohn, Alaska in July 2012.[23] A) isometric view showing crack locations 1 through 4 B) side profile showing crack locations 4 through 9

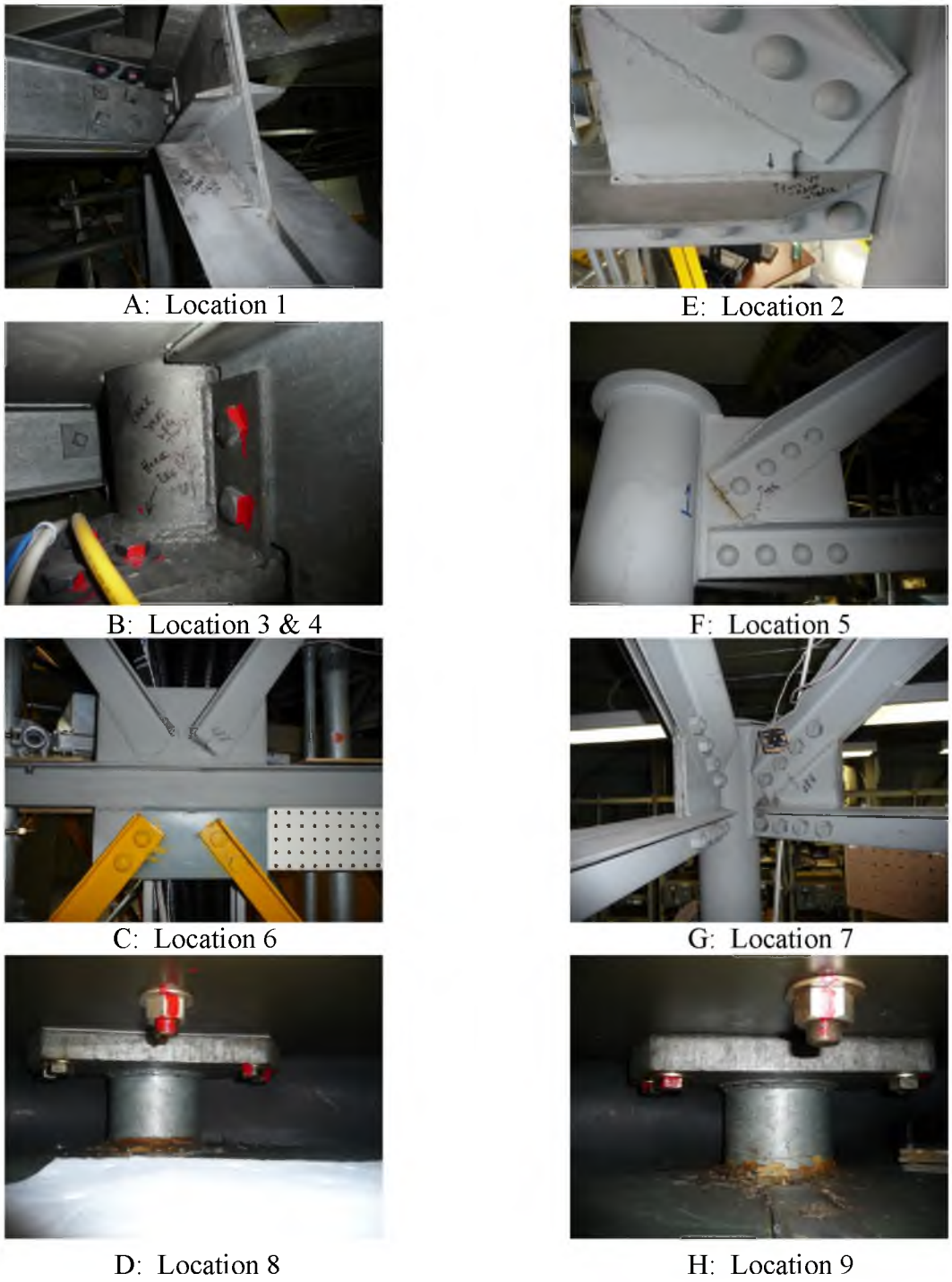

Figure 40 Images of tower crack locations found visually at Sparravohn, Alaska in July 2012.[23] A) crack location 1 B) crack locations 3 & 4 C) crack location 6 D) crack location 8 E) crack location 2 F) crack location 5 G) crack location 7 H) crack location 9

Figure 41 Repaired pedestal oil pan crack shown from above

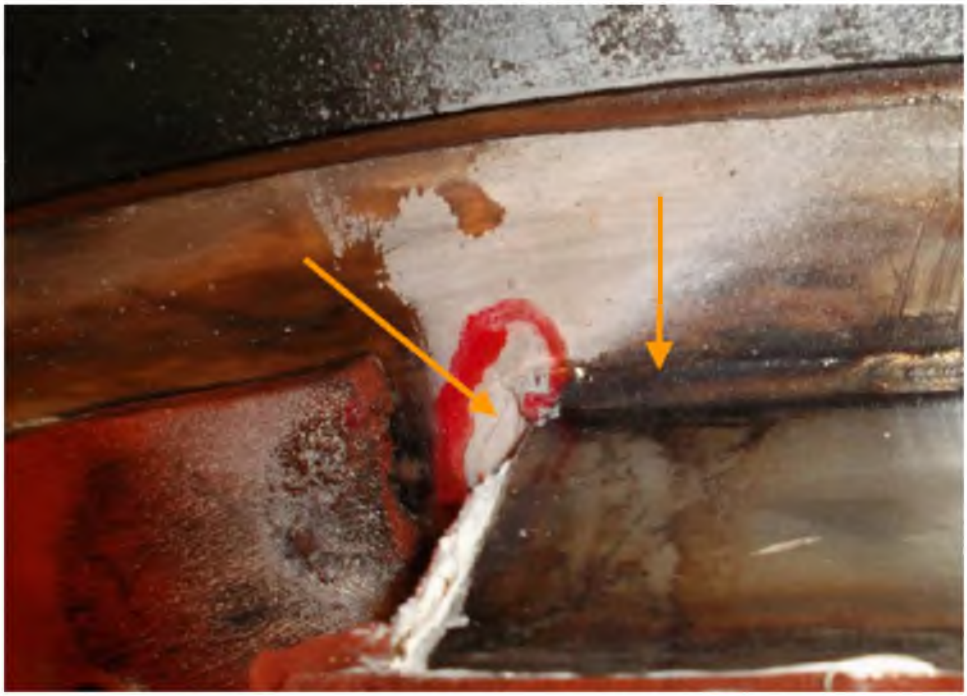

Figure 42 Crack in pedestal oil pan formed after the repair

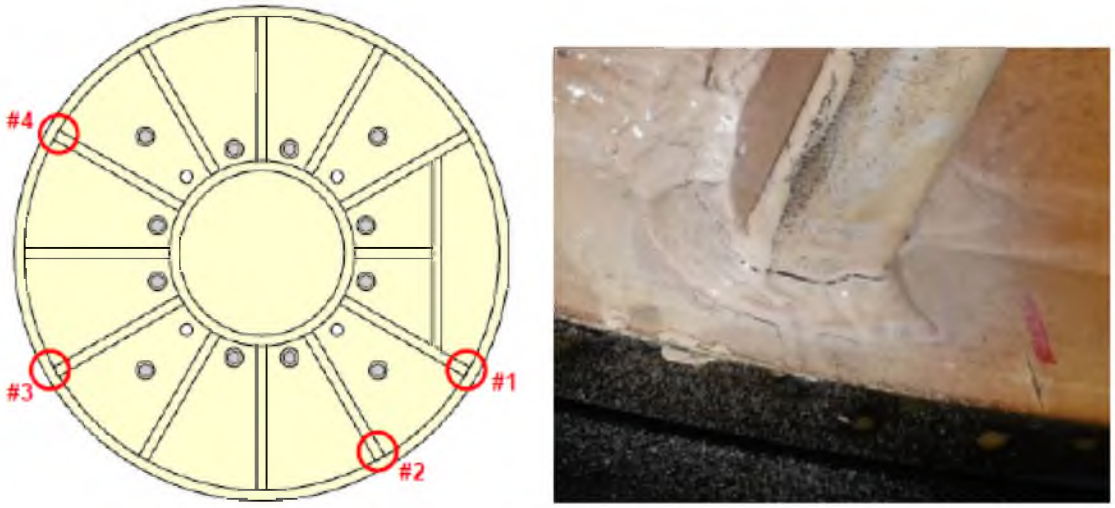

Figure 43 Location and image of cracks found at the LAB-6 radar site on the adapter plate

Figure 44 Bearing support sections containing cracks 1 & 2 at ends of the spokes

Figure 45 Bearing support sections containing cracks 3 & 4 at ends of the spokes

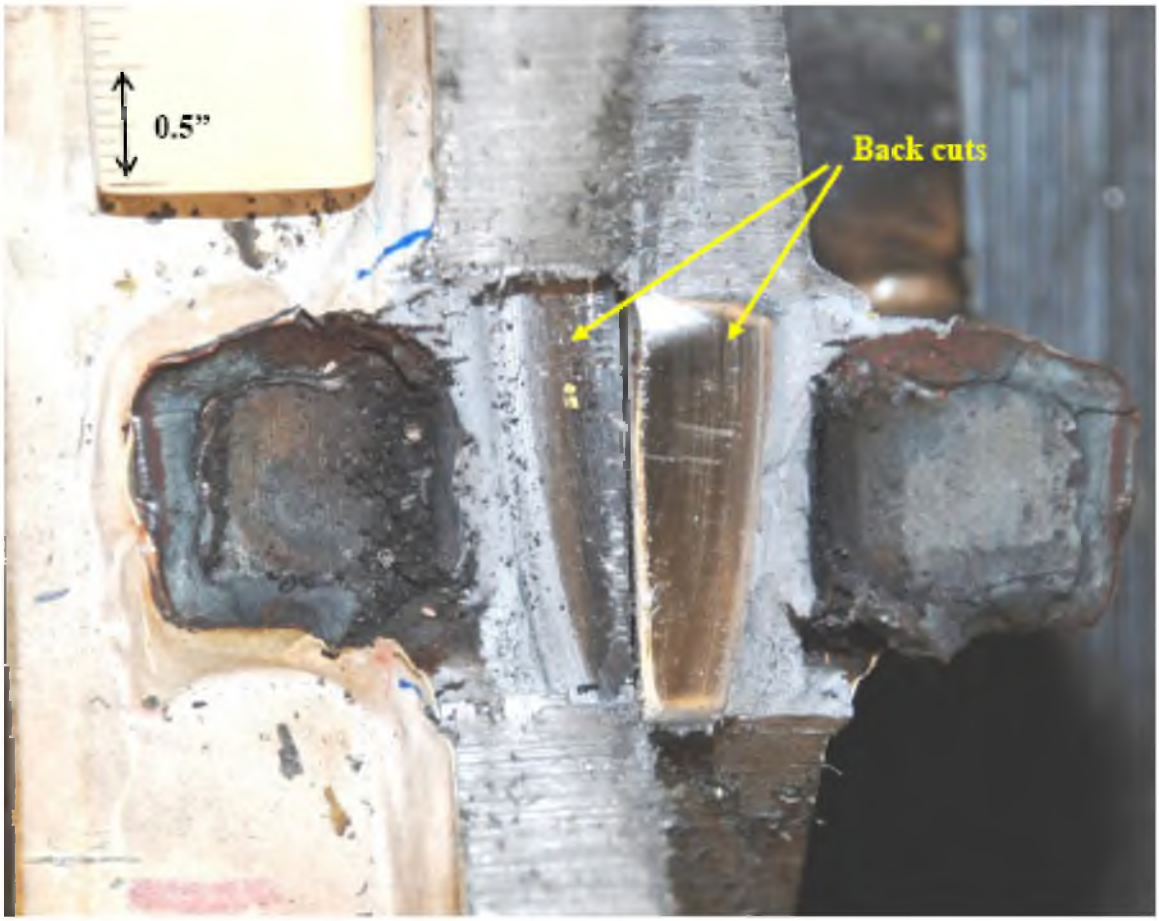

Figure 46 Section with crack 1 fracture surface exposed

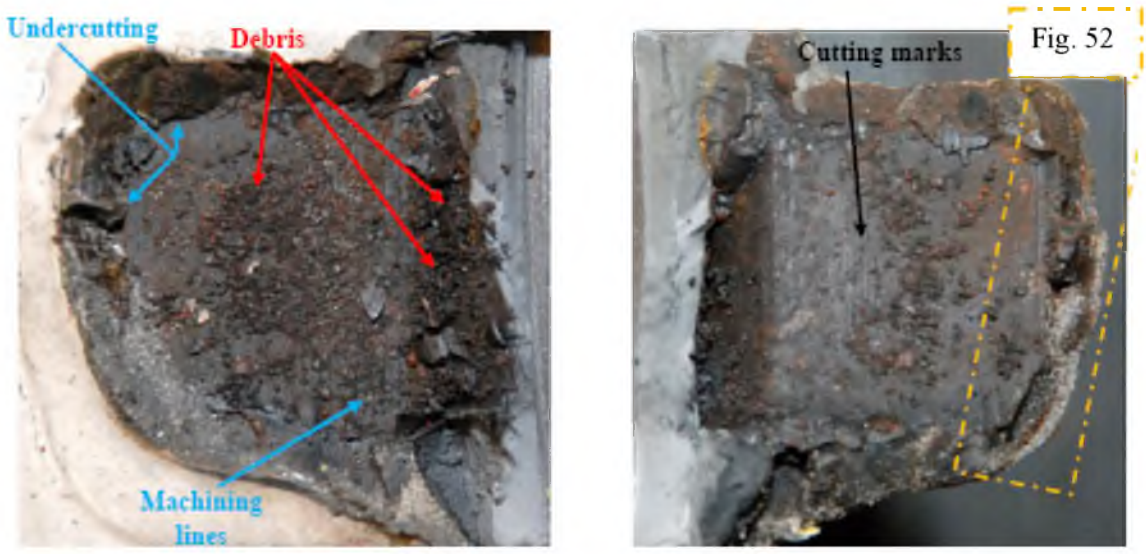

Figure 47 Close-up of crack 2 fracture surface

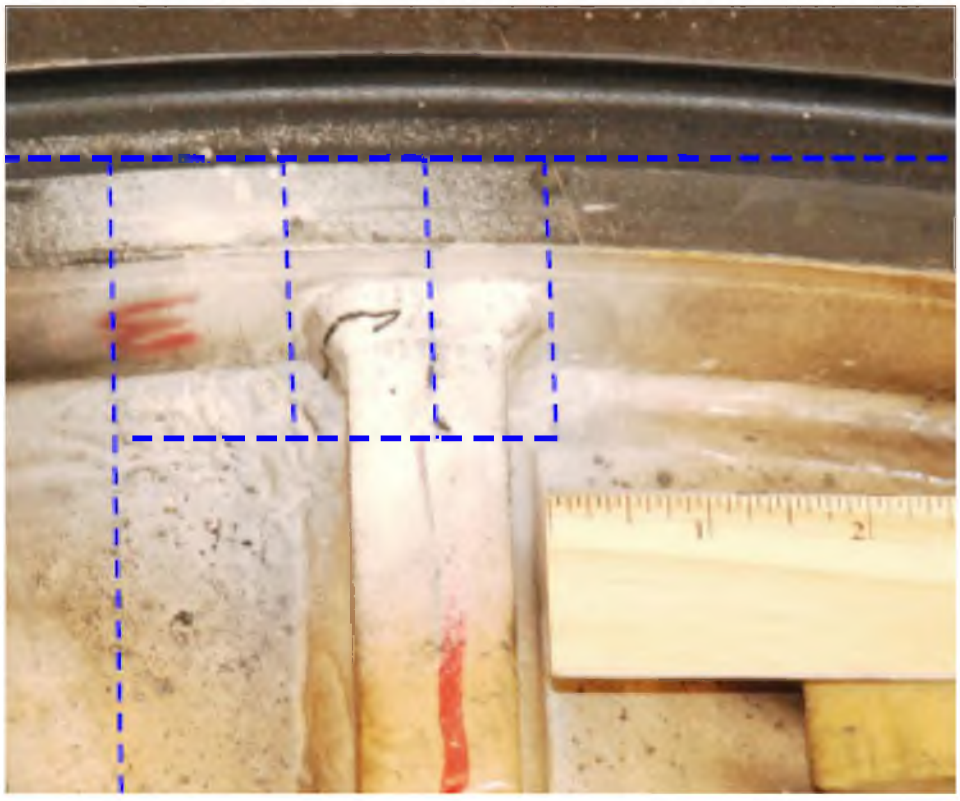

Figure 48 Section numbered crack 3 showing sectioning lines

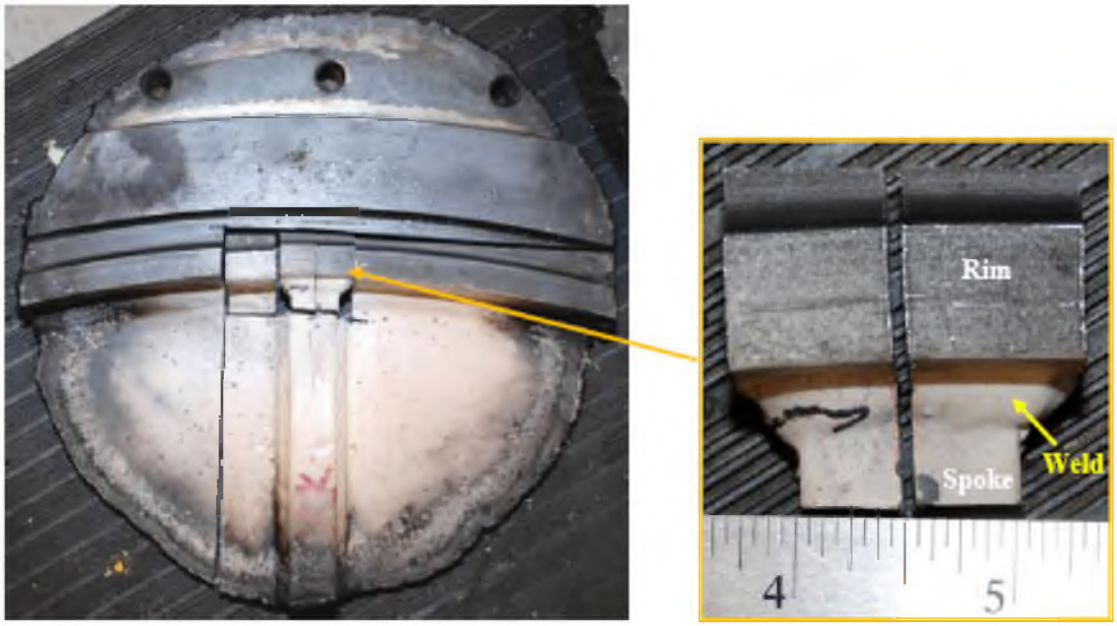

Figure 49 Cross section through end of spoke, crack 3

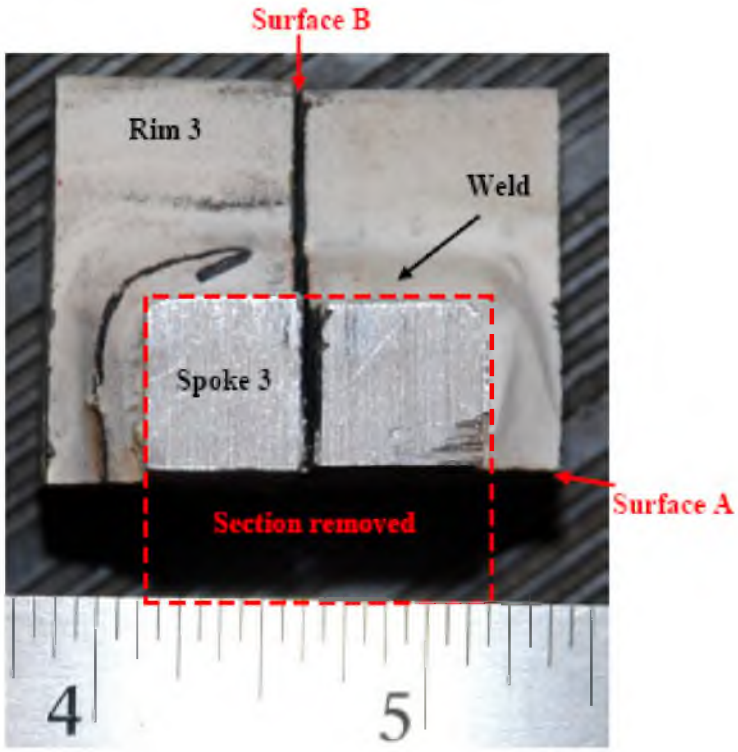

Figure 50 Second cross section perpendicular to first at spoke end, crack 3

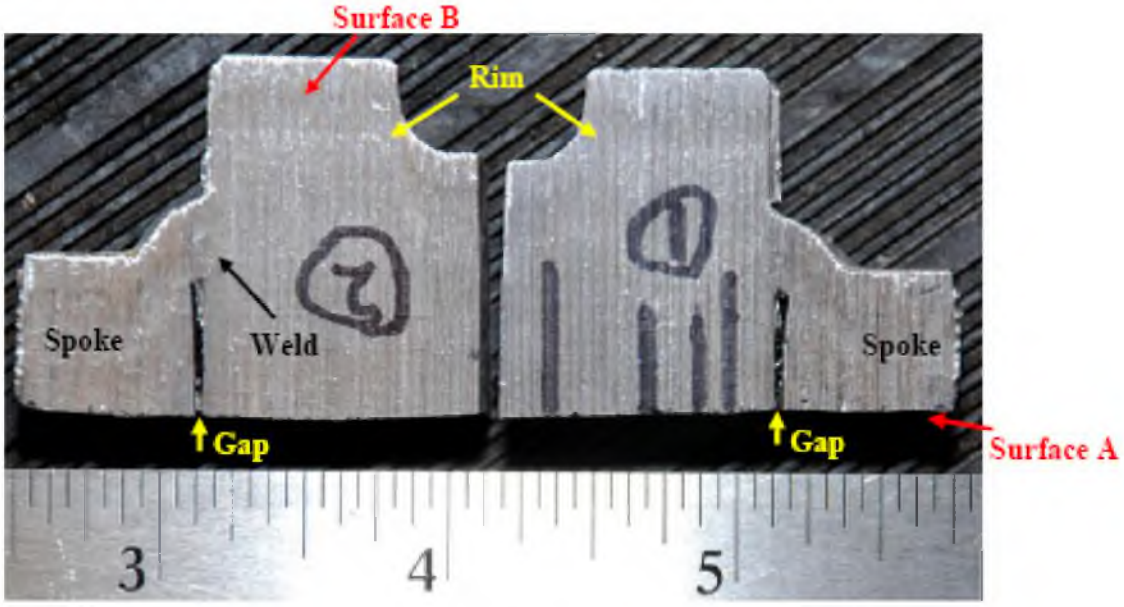

Figure 51 Two halves of crack 3 at spoke end

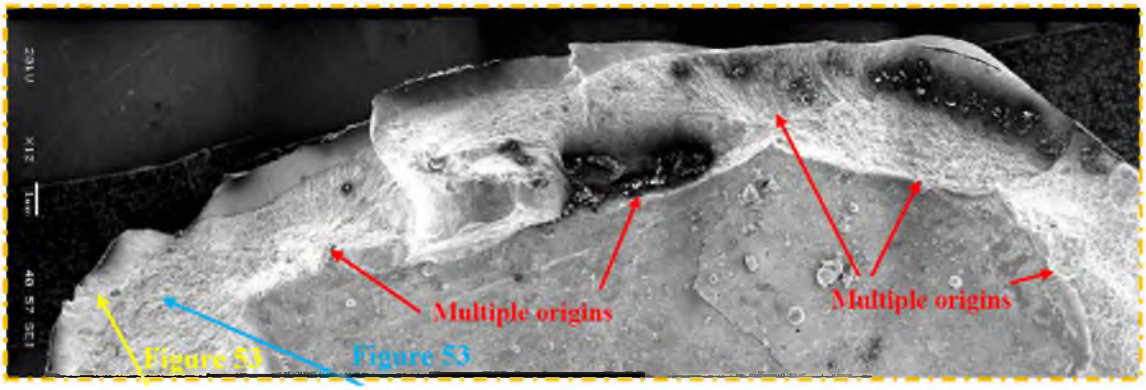

Figure 52 Composite SEM micrograph showing crack 2 fracture surface along top surface (originals at 12X)

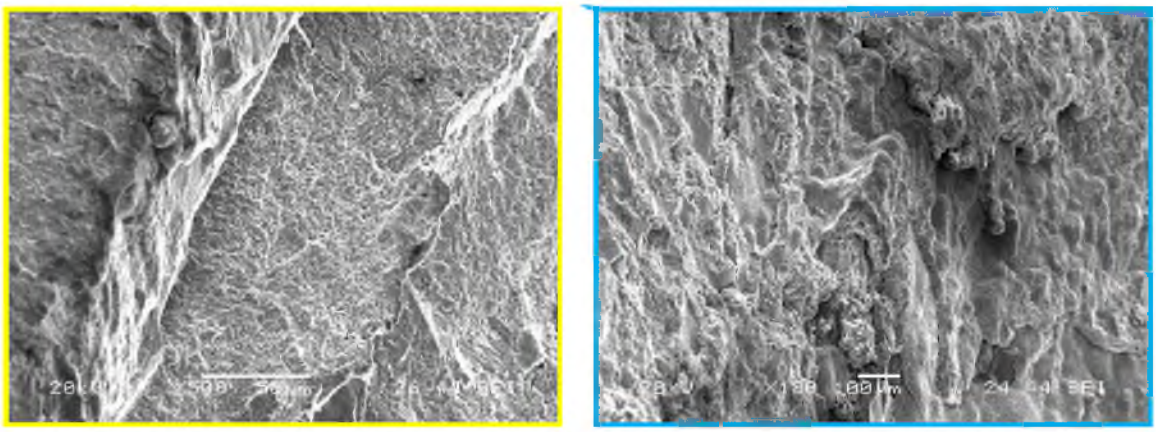

Figure 53 SEM micrographs showing close-ups of obscured fracture topography as highlighted in Figure 52 (originals at 500X and 100X)

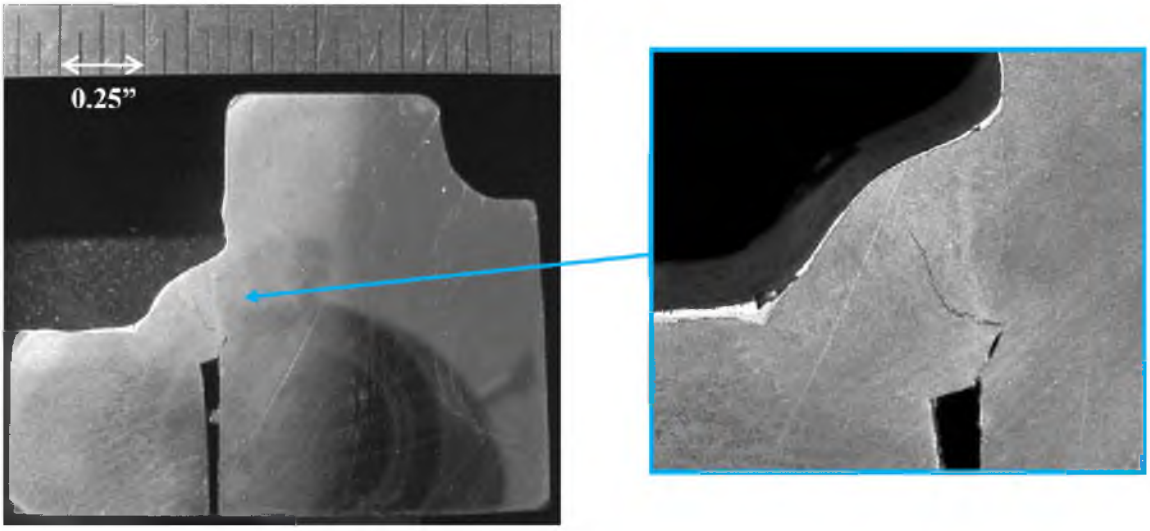

Figure 54 Surface B, left section of crack 3 spoke to rim weld (original at 5X)

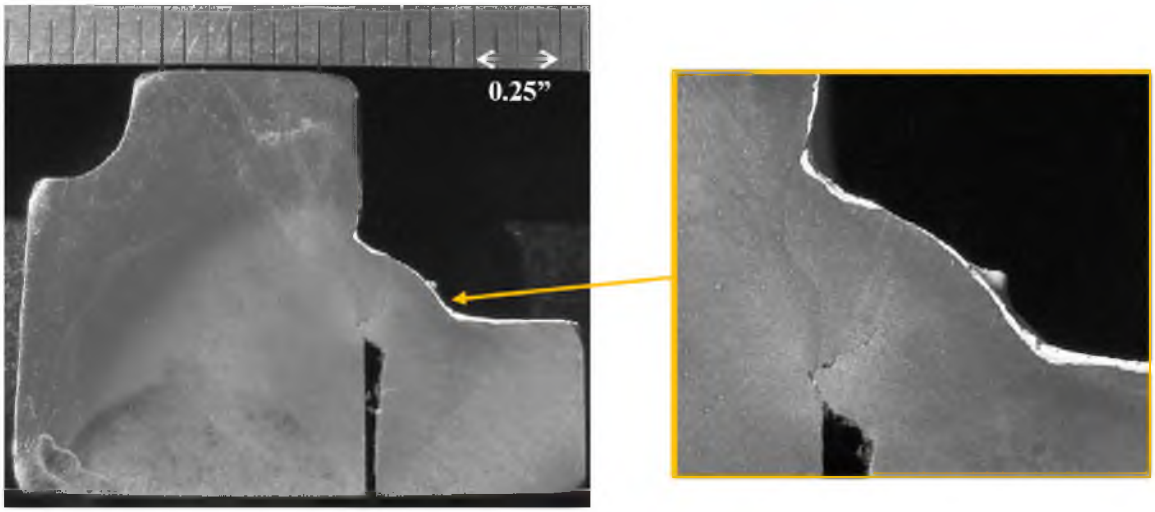

Figure 55 Surface B, right section of crack 3 spoke to rim weld (original at 5X)

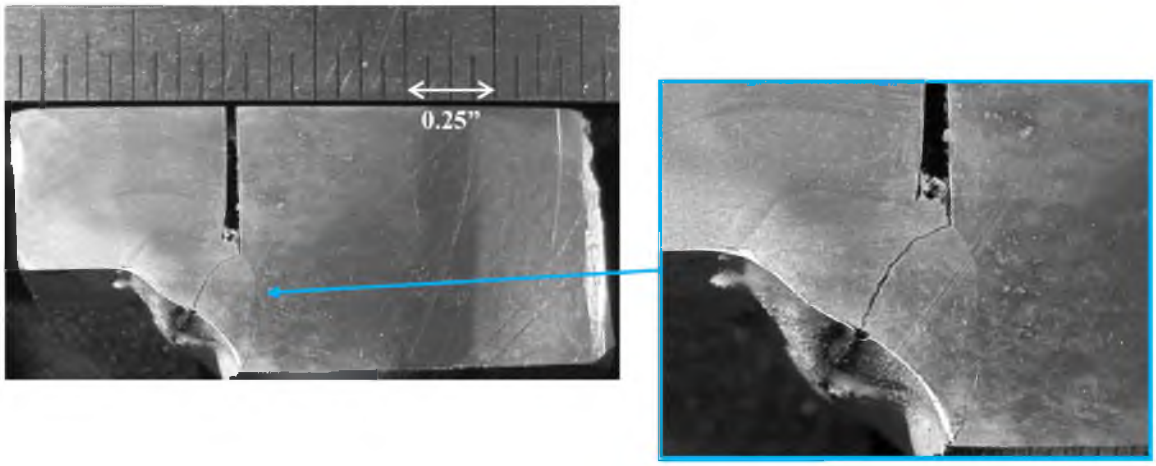

Figure 56 Surface A, left section of crack 3 spoke to rim weld (original at 5X)

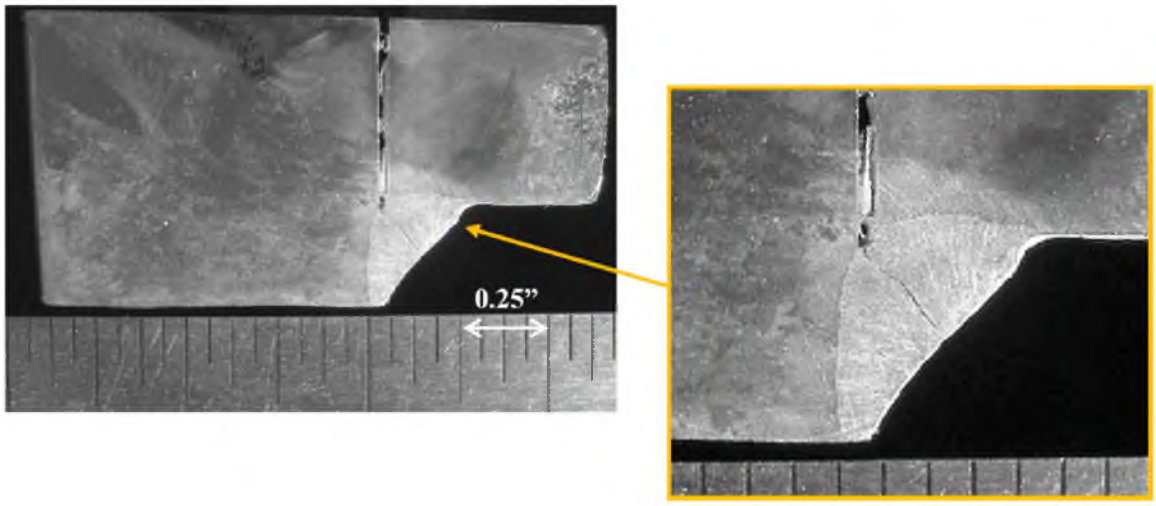

Figure 57 Surface A, right section of crack 3 spoke to rim weld (original at 5X)

Table 2 Reaction loads found from equations of static equilibrium

	Load (pounds)
R_y	20,058
R_x	2,203
F_y	6,942
F_x	2,203

Table 3 Finite element analysis results for the radar and tower

Finite Element Results Recorded at Strain Gage Locations							
Point	Location (mm)	Normal X (N/m^2)	Normal Y (N/m^2)	Normal Z (N/m^2)	Shear XY (N/m^2)	Shear XZ (N/m^2)	Shear YZ (N/m^2)
1	987.99, -1081.14, -504.78	-881843	-102916	-313562	5584	-523400	15584
2	557.9858, -631.6147, -1103.7588	-73660	-401474	616601	72892	102789	188147
3	530.7247, -424.0530, -1089.3285	-49862	-53867	-374793	21366	15390	12201
4	507.6288, -569.2549, -1303.9757	-15176	478216	80184	64430	1848	-4630
5	539.1157, -1174.750, -1496.4084	-580804	-144796	-1354468	-400318	-930292	-353307
6	382.6885, -1200.150, -1494.1887	-109036	239738	-84875	-141904	-124512	-145661
7	659.6399, -1049.250, -1684.8800	-529130	-2149729	-1664406	-355677	998596	603125
8	880.6851, -931.4259, -1936.3973	-446435	38273	-300975	-465461	309888	314751
9	1131.8138,-893.8260, -2163.6736	62972	-7612	51337	-4647	-24713	16035
10	1613.0646,-1174.750, -2143.8438	-529459	-123900	-2279783	-88518	-547639	-822125
11	1841.9611,-1046.737, -1991.1902	-601415	332297	-234817	194775	-541729	287633
12	1980.9747,-562.4275, -1887.5457	175139	-896098	137914	194497	212305	182013
13	2013.8232,-424.0530, -1898.0260	197394	-11426	262958	-19114	359400	10545
14	2144.7815,-569.2616, -1755.1179	-41435	310468	-102289	479406	-76466	-330694
15	2142.3188,-1069.800, -823.9232	-684018	-2479499	-1951547	-46559	1168813	169741
16	2492.1418,-1444.724, -711.8903	159446	-1278779	30832	1804540	136069	2157383
17	1470.5306,-1466.254, -80.9086	361301	-2721173	284253	493662	-133885	3118101

Table 3 Continued

Finite Element Results Recorded at Strain Gage Locations							
Point	Location (mm)	Normal X (N/m^2)	Normal Y (N/m^2)	Normal Z (N/m^2)	Shear XY (N/m^2)	Shear XZ (N/m^2)	Shear YZ (N/m^2)
18	422.3916, -1466.254, -605.7656	-120916	-3827453	302472	-2431312	-199977	2815725
19	344.4638, -1466.254, -1765.4030	175492	-3827749	-82001	-3045721	-6035	-958891
20	1327.7207,-1466.254, -2423.9626	-62516	-3328476	-42306	-898872	-68004	-3918549
21	2473.7817,-1466.254, -1774.8693	87565	-2987917	-22261	2128515	-57888	-1497064

Table 4 Shim thickness values for various radar level measurements

Level Reading	Post 1	Post 2	Post 3	Post 4	Post 5	Post 6
1' 0"	0.102"	0.073"	0.022"	0.057"	0.095"	0.045"
4' 0" *(Suggested Thicknesses)*	*0.119"*	*0.085"*	*0.022"*	*0.067"*	*0.107"*	*0.052"*
1' 15"	0.057"	0.034"	0.004"	0.000"	0.022"	0.045"
0' 40"	0.062"	0.040"	0.012"	0.016"	0.034"	0.045"

Table 5 Stress intensity and beta correction factor results for the full height crack in support plate spoke

Run	Crack Length (a)	Stress Intensity (K)	Beta Correction Factor (β)
1	0.125	449.14	1.43
2	0.150	480.68	1.40
3	0.175	506.70	1.37
4	0.200	527.18	1.33
5	0.250	555.11	1.25
6	0.300	598.49	1.23
7	0.350	622.06	1.19
8	0.400	656.15	1.17
9	0.450	688.65	1.16
10	0.500	697.93	1.11
11	0.600	765.16	1.11
12	0.700	831.65	1.12

Table 6 Stress intensity and beta correction factor results for the crack through the weld in the support plate spoke

Run	Crack Length (a)	Stress Intensity (K)	Beta Correction Factor (β)
1	0.050	671.50	3.39
2	0.075	720.22	2.97
3	0.100	743.82	2.65
4	0.125	764.73	2.44
5	0.150	779.67	2.27
6	0.175	794.44	2.14
7	0.200	807.35	2.04
8	0.250	830.98	1.88
9	0.300	848.76	1.75
10	0.350	861.39	1.64
11	0.400	876.44	1.56
12	0.450	889.03	1.50

Table 7 Principal stresses in the support plate calculated by FEA

Support Plate Principal Stresses (psi)		
Rotation	**Tension**	**Compression**
1	-1505.2	20.3
2	-2146.5	272.9
3	-1779.5	271.9
4	-2132.2	430.2
5	-236.6	248.5
6	-562.9	81.8
7	-3406.0	-135.9
8	-2238.6	-302.5
9	-745.1	-93.3
10	-1587.9	-323.8
11	-4806.0	-338.6
12	-2122.4	132.0
Min/Max	-4806.0	430.2
Stress Ratio (R)		-11.2
Average	1939.1	22.0
Stress Ratio (R)		-90.1

Table 8 AFGROW life calculations for the full height through crack in support plate

Stress Ratio (R)	Stress Multiplication Factor (SMF)	Cycles (N)	Life (years)
-1	10	1159200	0.44
	5.012	10767000	4.10
	0.430	Infinite*	Infinite*
-11.2	10	1159200	0.44
	5.012	10767000	4.10
	0.430	Infinite*	Infinite*
-90.1	10	1159200	0.44
	5.012	10767000	4.10
	0.430	Infinite*	Infinite*

*The output from AFGROW stated the following: "After the pass of the spectrum, growth was less than 1e-013. Total cycles [100]. Program halted."

Table 9 AFGROW life calculations for the crack through the weld in support plate

Stress Ratio (R)	Stress Multiplication Factor (SMF)	Cycles (N)	Life (years)
-1	10	547500	0.21
	5	4717700	1.80
	3.351	19014300	7.24
	0.430	Infinite*	Infinite*
-11.2	10	547500	0.21
	5	4717700	1.80
	3.351	19014300	7.24
	0.430	Infinite*	Infinite*
-90.1	10	547500	0.21
	5	4717700	1.80
	3.351	19014300	7.24
	0.430	Infinite*	Infinite*

*The output from AFGROW stated the following: "After the pass of the spectrum, growth was less than 1e-013. Total cycles [100]. Program halted."

6. DISCUSSION

6.1. Observations

6.1.1. Stress Analysis

The results from the overall radar and tower stress analysis were in the expected range based on the loads that were subjected by the radar. The maximum Von Mises stress predicted was much less than the yield strength of the materials used for the structure. This is also shown in the Factor of Safety plot. The minimum factor of safety was calculated to be 2.89. This is within the appropriate range for structures of this type. As discussed previously, based on the size of the structural members, a high factor of safety is expected.

The first principle stresses for the radar and tower posts fluctuate from a positive value where the structure is in tension, to a negative value where the structure is in compression. In fatigue, the primary areas of concern are where tensile stresses are present. In areas strictly in compression, the probability of fatigue cracks occurring is greatly reduced. The stress analysis highlights areas where the stress is fluctuating between tensile and compressive forces.

The strain results from the finite element analysis are relatively similar in magnitude to the readings taken by the strain gages installed on the structure. This shows a good correlation between the model and the actual strains being measured.

The deflection induced on the structural members by the weight of the radar was relatively low. This is also expected based on the physical size of the structure. The small deflections would likely be even less due to the increased rigidity in the system by members that were not included in the model.

The high stress locations on the radar were typically found in areas of stress concentrations. The highest stress areas were found to be on the corners of the adapter plate as shown in Figure 20, the top and bottom connections of the vertical supports on the pedestal as shown in Figures 21 and 22, and near the counter sunk bearing mounting holes in the pedestal. The strain gages that were installed on the pedestal were not in the areas of highest stress as predicted by the finite element analysis. Based on the results from the stain gages alone, an enhanced life may be inaccurately calculated. For this reason, the maximum stresses and strains were included in the strain-life approximation.

SolidWorks has a feature that shows the load path through the structure. This feature is typically used as a design feature to be able to optimize the size of the part. Based on the load path through the radar, the higher stressed areas are visually depicted as shown in Figure 23. These areas are useful in determining the locations to inspect for fatigue damage.

6.1.2. Strain-Life

The strain gage measurements that were taken during the changes in level were noticeable. In general, when the radar was more out of level, the strain would increase. When the radar was more level, the strain would decrease. Although the change in strain range was noticeable and measureable, the magnitude of the fluctuations did not increase

dramatically. The small amount of strain change did not reduce the fatigue life by a significant amount.

Even though the level did not greatly reduce the life of the part, there is still an advantage to keeping the radar as level as possible. For example, if a crack has developed in the part, the increased strain will lead to an increased stress level at the crack tip. The level deviation could have more of a detrimental effect than an increase in strain in a part that is not cracked.

It was observed that the strain amplitudes as calculated from the strain measurements intersected the strain-life curve at approximately 2×10^{12} cycles. Using only this information alone, one would conclude that a failure would never happen, or at least not for another 7,500 years. This is absolutely not the case as demonstrated from the cracking evident in the structure, found by the nondestructive inspections. There could be several reasons why such failure could be occurring. The vacillation in strain is not the only mechanism that could cause a fatigue failure. Other mechanisms will be discussed that are not included in the life model.

There are various types of failure mechanisms that may be occurring that would increase the susceptibility to fatigue. There are multiple locations on the radar where two metals would be in direct contact. Any movement between these components could result in fretting fatigue damage. Some examples of damage that may occur from fretting are: pits, oxide and debris, scratches, metal transfer, extensive surface plasticity, subsurface cracking, fretting craters, etc.[26] An analysis of fretting fatigue should be conducted resulting in a quantifiable inspection. The life reduction from fretting fatigue

may lower the strain-life curve to a point that the strain amplitude that is currently experienced may cause failure.

Environmental conditions may impact the fatigue life of these components as well. The radars are typically located along the coast. In this environment, they are subject to a large degree of corrosion from the high salt concentration in the air. Corrosion will accelerate the crack growth rate by several orders of magnitude.[27] Corrosion fatigue is another failure mechanism that should be considered and modeled in the fatigue life estimations.

There are a number of sources of uncertainty in the analysis of fatigue results in the use of the stress-life approach.[27] They are summarized as follows:

1) Uncertainties in the estimation of material properties, which include microstructural variability from one specimen or batch to another as well as experimental errors in the measurement of properties in the same batch of materials.
2) Uncertainties in the modeling of applied stresses, for a given service condition and environment. These could stem from such things as vibrations or also a lack of knowledge about the exact distribution of stress cycles that occur over the design. An example in this test may be wind loading on the tower in conjunction with the rotation of the tower.
3) Uncertainties in the *a priori* estimation of the environment and in loading intensity.

A recommendation for further examination of these uncertainties would be to utilize concepts from the ASTM STP 744 titled "Statistical Analysis of Fatigue Data".[13]

This publication discusses the standard practices for statistically analyzing stress-life and strain-life fatigue data. This would provide a quantifiable confidence level of the data being used.

6.1.3. Damage Tolerance

The damage tolerance analysis for the radar support plate had significantly different results for the variances in stress levels. The stress state required for crack growth is not plausible using the average and maximum stresses from the finite element analysis. If a larger stress was used, the crack would propagate through the part. This demonstrates conflicting results. As shown by the cracks found in an actual radar, the stress state was high enough for the crack to grow. This suggests that there is a difference between the simulated model and the actual conditions on the structure.

There are a multitude of variables that would have an impact on the stress state in fatigue prone areas. Subsequently, this will have a dramatic effect on the damage tolerance life prediction. Some examples of these variables would include residual stresses, material differences, multiple damage sites, inaccurate spectrum, load distribution differences, etc. Each of these will be discussed.

The stress state near the cracks found in the weld could be significantly different than what was used in the model. There may be residual tensile stresses near the weld due to the process of manufacturing the part. This would increase the stress state near the weld and cause the crack growth rate to accelerate. This is largely unknown and could not be modeled.

The increased hardness of the welded material will have an impact on the crack growth rate. The material properties and crack growth rate curve used in the analysis were that of the parent plate material. The harder material will exhibit a higher crack growth rate due to the higher stress concentrations in areas adjacent to the normalized bulk metal. The model takes on the assumption of homogenous, continuous material properties.

The failure analysis showed that the poor quality of the weld resulted in inclusions, pores, and inadequate penetration. As stated previously, each of these defects will produce stress risers that could potential act as crack nucleation sites. As cracks nucleate at each of these individual sites, they could combine into a single crack which will accelerate the crack growth in the entire part. The model was built with a continuous material without flaws.

The loading spectrum could also be refined. The spectrum that was used was based on a finite element analysis representation of the stress state near the cracked feature. A higher fidelity model can be created by locating strain gages on the structure in the vicinity where actual cracking is occurring. By doing this, the model can be refined to use a more realistic stress state and spectrum. The model could then be revised until it more closely approximates the actual stress state found by the strain gages.

The solid model used for the damage tolerance assessment was for the support plate only. The full assembly was not used in the finite element analysis. The load from the weight of the radar was placed on the top of the support plate. The full assembly model accounted for the offset center of gravity of the radar. The load distribution in the support plate was approximated in the damage tolerance analysis. The weight

distribution could provide differences in the locations of tensile and compressive stresses in the support plate. These changes in load distribution could potentially have an effect on the life prediction.

Although the results from the damage tolerance assessment were diverse, the predictions seemed viable based on inspections that have been done in the field. At a minimum, an annual or biannual visual inspection can be recommended based on the crack growth rates that were determined in the analysis. In order to recommend more accurate inspection criteria for the holistic approach, the model would need to be refined.

6.1.4. Support Plate Failure Analysis

Cracks were detected at the spoke ends of the four suspect bearing support sections. The cracks were opened to reveal the fracture surfaces surrounding three sides of the spoke ends. The welds exhibited poor qualities including undercutting, inadequate penetration, pores, and inclusions, all of which produced stress risers. Fractography of the fracture surfaces revealed prior cracks. All of the fracture surfaces exhibited multiple prior cracks which grew outward forming different plateaus. Evidence suggested that the cracks nucleated at the weld root and propagated by fatigue outward towards the surface. Some cracks reached the surface while others exhibited a band of overstress between the crack front and the surface.[25]

Microscopy revealed the microstructure of the welds to be significantly finer grained than the bulk metal. It was also noted that the weld hardness was considerably harder than the base metal. Harder weld metal results in higher stress concentrations in areas adjacent to the normalized bulk metal which also leads to crack nucleation,

commonly in the heat affected zones. It was apparent that no post weld normalizing heat treatment was performed to normalize the grain structure and hardness in the weld zones.[25]

Failure of the support plate is attributed to lack of weld penetration and poor weld quality. The lack of a post weld normalization heat treatment may also have been a contributing factor. Multiple prior cracks were detected emanating from undercut areas, inclusions, and pores.[25] Based on the results of the failure analysis, a future repair of the support plate can be better understood.

6.2. Predictions

Utilizing a better method to level the radar will result in lowering the stress on the radar. A digital leveling application was developed in conjunction with this research that will allow the maintainer to effectively level the radar within the specification. This application reduces the subjectivity of the adjustments and saves valuable time when performing this maintenance procedure. The obsolete gunner's quadrant will be replaced fleet wide by the new digital level for use in leveling the radar.

The digital leveling application will make leveling the radar a simpler task. This will ensure that the radar maintainers will successfully level the radar not only within the tolerance, but well below the maximum level. The predicted result will be a lower stress on the radar and structural components.

Based on the research for the height accuracy requirement of the radar, the recommend attainable unified value for the level specification will be changed from ± 4 arc-minutes (0.0666 degrees) to ± 2 arc-minutes (0.0333 degrees). By using the digital

level and the leveling application, this has proved to be an attainable requirement. This will have a positive impact on the radar fatigue life by lowering the stresses on the components, even though the stress reduction is minimal.

The originally designed shims underneath the radar did not distribute the weight evenly onto the tower support pads. These shims were square and one stack of the appropriate thickness was placed on each side of the tower support pad. This would have resulted in areas of higher stress concentrations. A custom designed shim set was developed in conjunction with this thesis to provide even distribution of the weight onto the tower support pads. This shim set was also fabricated in smaller increments to obtain a more level radar. By allowing the radar to be as level as possible, the stress and strain felt by the tower is also lowered, thus prolonging the life of the weapon system. This modification has already begun to be implemented in the field.

To increase the life of the radar, some steps may be taken. One recommendation may be to investigate High Frequency Mechanical Impact (HFMI). The durability and life of dynamically loaded, welded steel structures are determined often by the welds, particular by the weld transitions. By selective treatment of weld transitions with the HFMI treatment method, the durability of many designs can be increased significantly. This method is universally applicable, requires only technical equipment, and offers high reproducibility and a high grade of quality control.[28]

6.3. Nondestructive Inspection Methods

The nondestructive inspections that have been completed to date have been successful in locating crack-like indications. The methods that are typically utilized are

magnetic particle, dye penetrant, and visual inspection. Once the cracks were located, the organization responsible for the maintenance of the facilities funded the effort to repair the structure. The AEWS program office was typically utilized to provide recommended instructions for the repair of the structure.

The majority of the cracks that have been found are located at or near weldments in the structure. It was also the opinion of the inspector that a majority of the welds were not considered "high quality" welds that would be expected to be found in a similar support structure. In the failure analysis of the support plate, the welds were found to be porous and low quality.[25]

As discussed previously, in a fracture dominant strength related failure, the defects are typically macroscopic.[5] Some examples of these defects are weld flaws, porosity in the material, fatigue or stress corrosion cracks, corrosion pits, etc. As shown by the failure analysis of the support plate, the poor quality of the welds was considered to be a significant factor in the failure of the part. The voids and discontinuities in the weld potentially act as stress risers and crack nucleation sites.

There were some problems that arose while performing a visual inspection of the tower. Undocumented modifications had been made to the tower structure. Part of the periodic maintenance is to paint the tower structure. The thickness of the paint in some areas made inspection very difficult. Often, the paint had to be removed to obtain a higher level of confidence that no cracks were present.

Due to the number of cracks found in the support plate at the LAB-6 radar site, this part was taken out of service and replaced with a refurbished spare part. The spare part had undergone thorough inspection to ensure that no cracks were evident in the

structure. The failed part was sent to a lab at Hill Air Force Base to undergo a detailed failure analysis. The stress analysis pin pointed the same locations on the support plate to be high stress areas. This gives merit to using the finite element analysis results to help determine the locations on the radar to be inspected.

In nearly all instances, the cracks found in the field have been found in welded connections. This is shown in the results section in Figures 39 through 43. As discussed previously, weld flaws can act as stress risers and crack nucleation locations. This is evidenced in the poor quality of welds that were seen in the field. The strain-life equations do not account for the inherent flaws in the welds. The damage tolerance assessment has the ability to take these problems into consideration to determine a more realistic life prediction.

As discussed, a complete inspection of the structure had never been mandated. Based on the results of the inspection and the magnitude of the defects found, it is essential to shift to a paradigm that maintains awareness and control of these safety critical components. It is necessary to establish a program to continually inspect the radar and radar tower for cracks. The results from the fatigue life and damage tolerance assessments are instrumental in determining the method to employ to ensure that issues are identified. An overall damage tolerance analysis of the system will be a large undertaking, given the different tower types and subtle differences in the radar support structure. However, this is highly recommended in order to mitigate the risk of a catastrophic system failure.

7. SUMMARY

7.1. Conclusions

This thesis research was conducted in order to verify the structural integrity of the AN/FPS-117 Long Range Radar and radar tower. The following conclusions are reported in the order they were stated in the objectives.

1. The local stresses and strains on radar and tower components were determined using a combination of finite element analysis and strain gage measurements.
2. The impact the levelness of the radar has on the life of the system and components was determined to be minor.
3. An attainable unified value for the level specification was recommended to be changed to ± 2 arc-minutes (0.0333 degrees) for improved system performance and a greater structural life.
4. The remaining life of the weapon system was estimated by using a strain-life approach and a damage-tolerant approach.
5. The finite element analysis determined the locations of high stress and fatigue prone areas on the radar and tower.
6. Results were compared of the stress and fatigue analyses with actual cracks that have been found in the field.
7. Suggestions for the implementation of a holistic inspection plan for monitoring the structural integrity of the system were made.

7.2. Significance

The radar system structure as a whole was found to be in acceptable condition. The areas of concern are at or near welded connections. The quality of the welds has a significant impact on the life of the structure. With the ability to locate problem areas on the radar, a unique inspection plan can be created in order to ensure the longevity of this system. If left alone, the cracks in the structure may advance to a catastrophic result.

This research highlights the inherent flaw that a sufficient factor of safety will guard against failure for the entire life of the weapon system. This simply is not true. All systems are susceptible to cumulative damage and the risk of failure needs to be understood. This research can be used to provide direction on a path to mitigate the risk of system failure.

7.3. Future Research and Recommendations

The following are future research suggestions and recommendations:

1. Implement a standardized, efficient, and uniform leveling procedure in the Air Force Technical Order.
2. Utilize the redesigned shims to evenly distribute the weight of the radar evenly over each of the six tower pads.
3. Perform a dynamic analysis of the radar, using a more robust version of finite element analysis software.
4. Provide detailed instructions on determining the criticality of an identified flaw and specify when repairs need to be made.

5. Prescribe repair techniques and solutions to cracking in localized areas to reduce the susceptibility of fatigue damage in the future.
6. Model all other tower types in addition to the AB-259 tower to determine high stress and fatigue prone areas.
7. Implement a holistic nondestructive inspection plan based on the results of this research to ensure the structural integrity of the system.
8. Implement a specific plan to utilize opportunistic inspections.
9. Research the impact of specific environmental concerns and how they can reduce fatigue life.
10. Statistically design a fatigue test to simulate the stresses and strains found in the radar.
11. Locate additional strain gages at areas of interest based on the results of the stress analysis.
12. Refine the finite element model and perform a damage tolerance analysis for a more accurate estimation of the fatigue life of the critical structural members.

APPENDIX A

TENSILE TEST RESULTS

Table 10 Tensile testing results from the Science and Engineering Laboratory, Hill AFB, UT Saturday, November 17, 2012

Sample Number	Maximum Load (lbf)	Load at Break (lbf)	Tensile Extension at Maximum Load	Tensile Stress at Break (ksi)
1	9760.0	7707.2	0.28250	53.18950
2	9978.4	7882.2	0.07532	54.66126
3	9825.5	7779.1	0.21393	53.53071
4	9797.6	7726.8	0.21635	54.24254
5	9943.6	8002.3	0.18777	57.92959
6	9905.4	7806.8	0.20731	55.12312
7	10159.0	8217.3	0.19074	56.37956
8	9923.8	7874.1	0.21391	54.71143
Mean	9911.7	7874.5	0.19848	54.97096
Range	399.1	510.2	0.20718	4.74009
Standard Deviation	125.52739	167.91937	0.05767	1.54470

Table 11 Tensile testing results from the Science and Engineering Laboratory, Hill AFB, UT Saturday, November 17, 2012

Sample Number	Tensile Stress at Yield (ksi)	Load at Yield (lbf)	Area (in^2)	Local Peak Maximum (ksi)
1	67.35664	9759.97648	0.14490	49.71818
2	69.19828	9978.39154	0.14420	48.89385
3	67.61277	9825.48806	0.14532	50.02206
4	49.77199	7090.01997	0.14245	49.77199
5	54.18044	7484.37788	0.13814	54.18044
6	50.87837	7205.64895	0.14163	50.87837
7	53.71426	7828.85356	0.14575	53.71426
8	50.12941	7214.62404	0.14392	50.03417
Mean	57.85527	8298.42256	0.14329	50.90167
Range	19.42629	2888.37157	0.00761	5.28659
Standard Deviation	8.60653	1309.44583	0.00251	1.96017

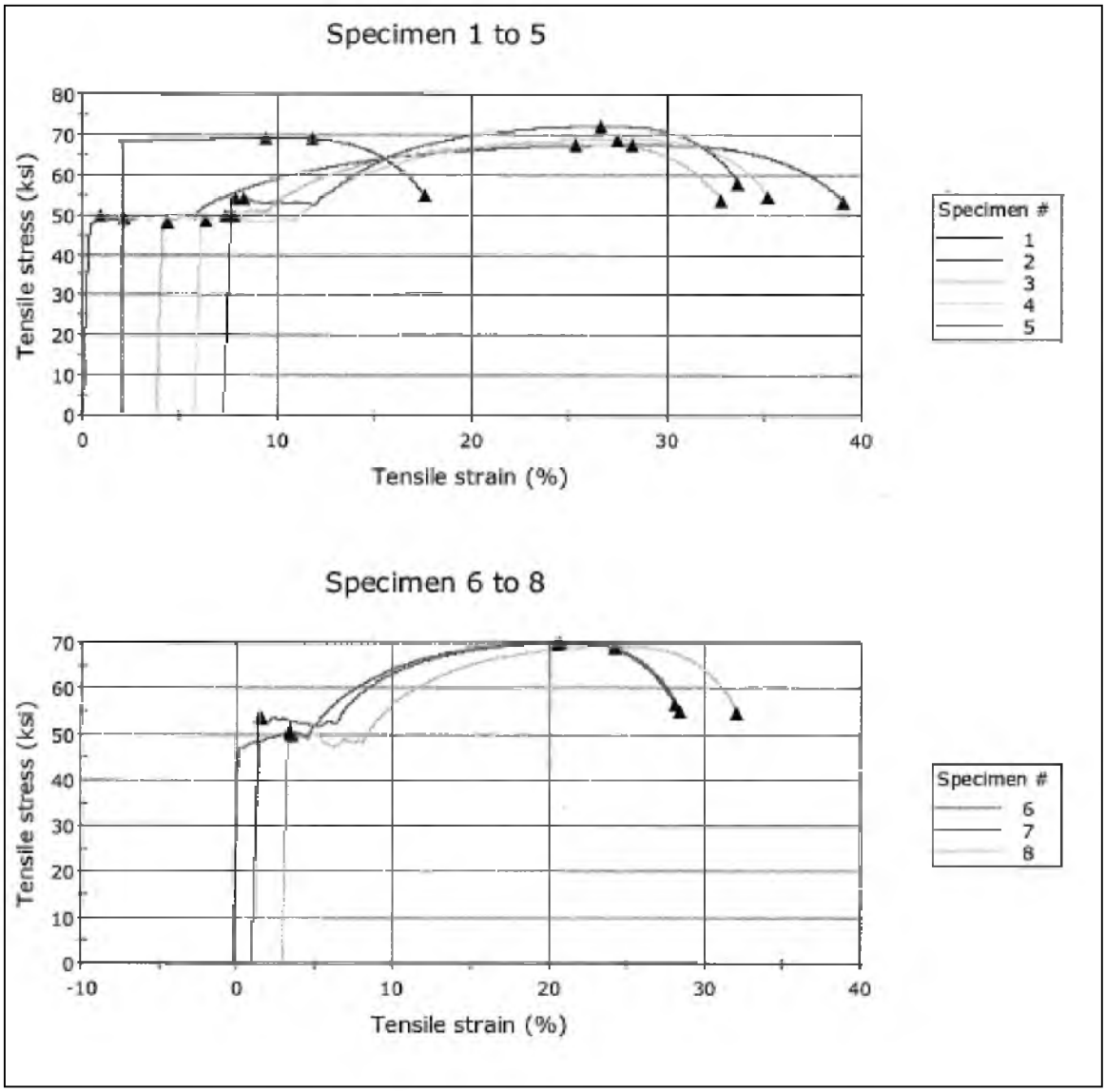

Figure 58 Tensile testing results from the Science and Engineering Laboratory, Hill AFB, UT Saturday, November 17, 2012

APPENDIX B

STRAIN GAGE MOUNTING LOCATIONS

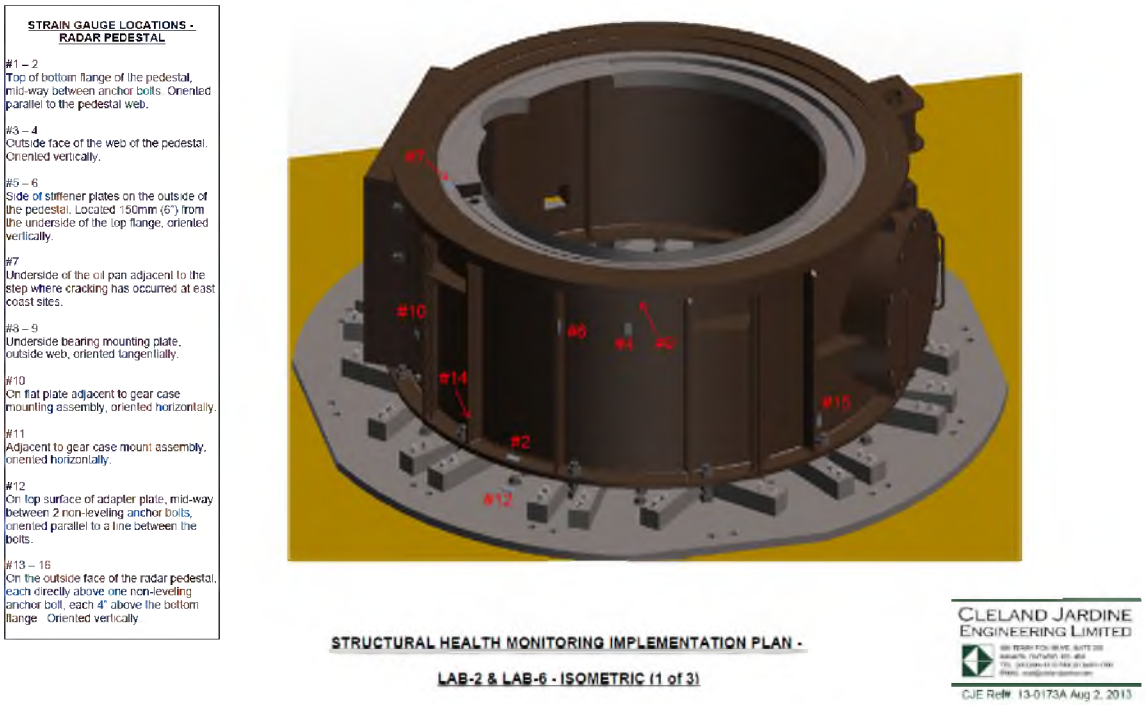

Figure 59 Strain gage mounting locations on the radar pedestal

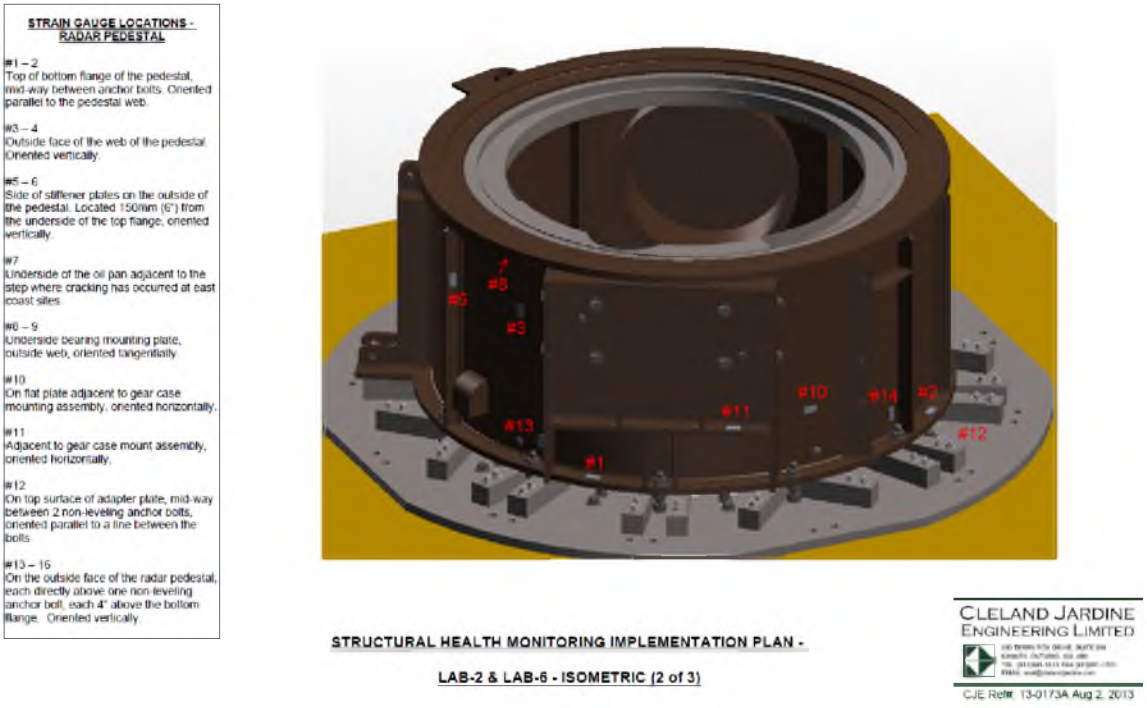

Figure 60 Strain gage mounting locations on the radar pedestal

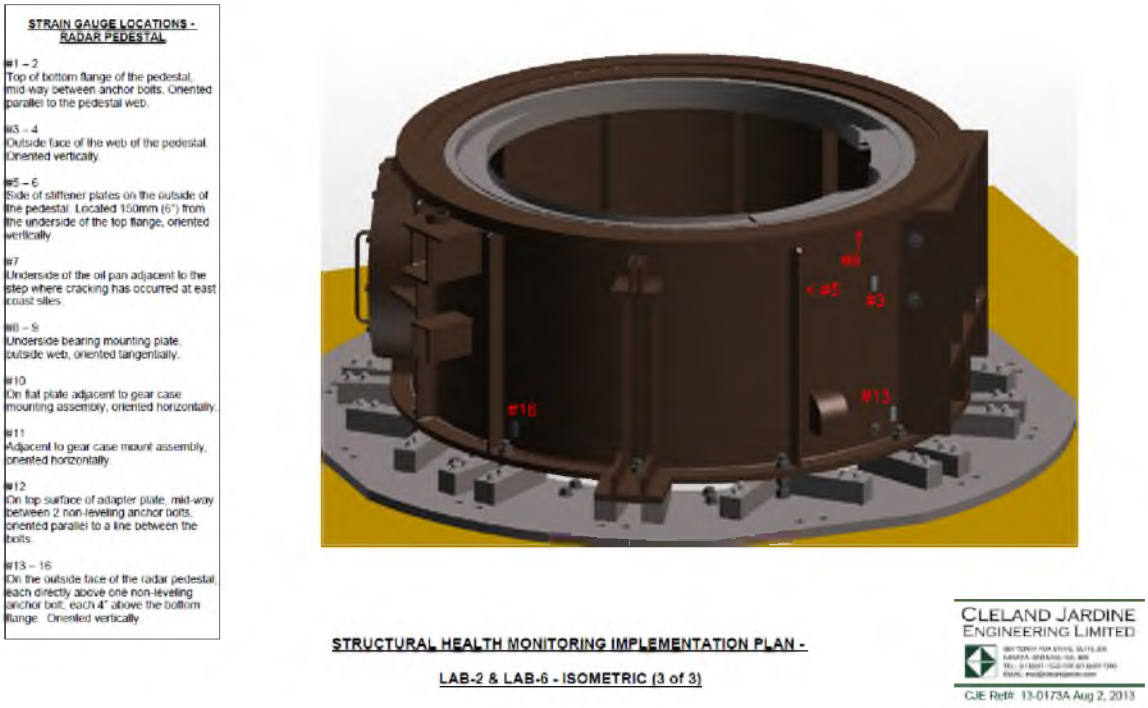

Figure 61 Strain gage mounting locations on the radar pedestal

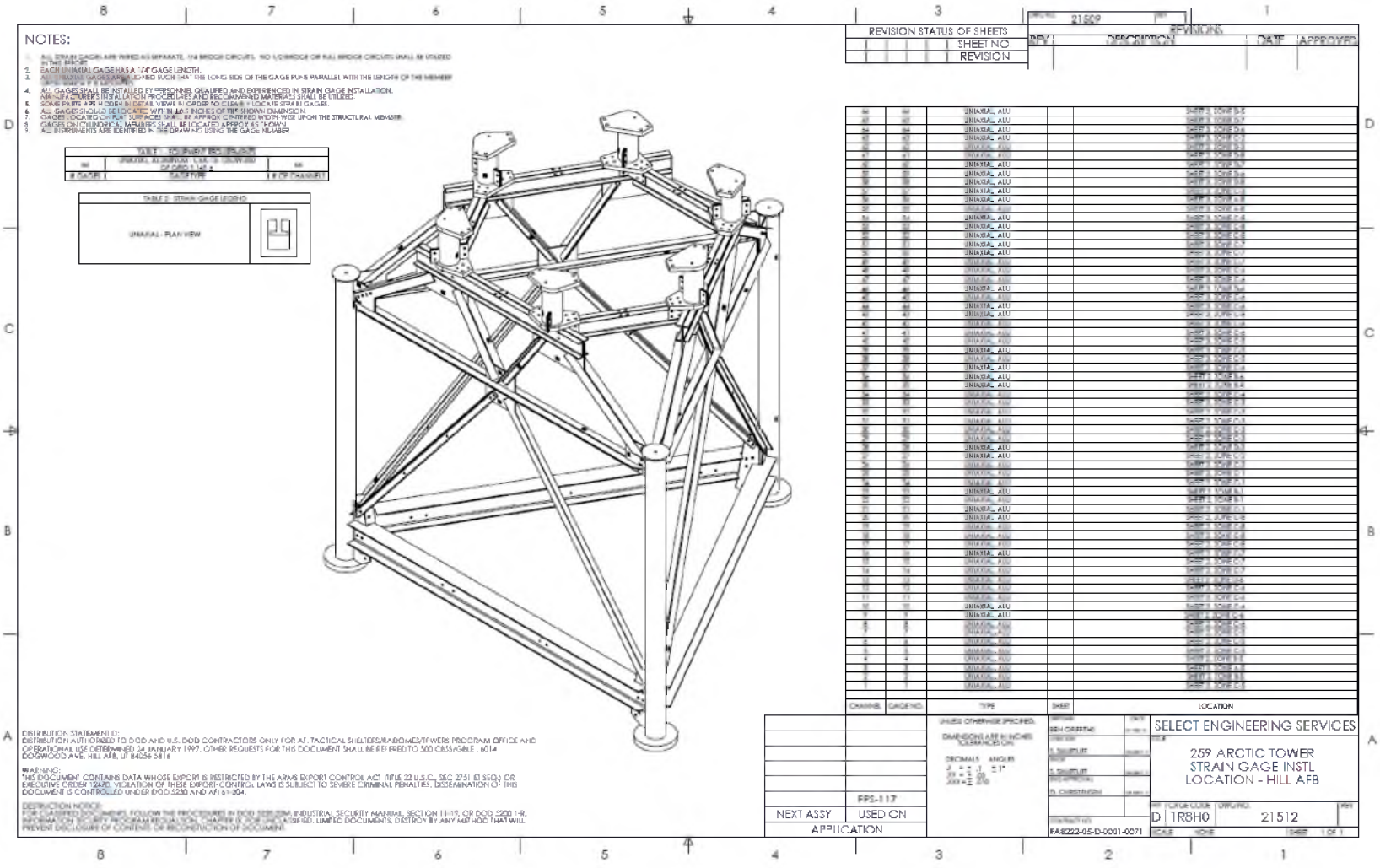

Figure 62 Strain gage mounting locations on the radar tower

APPENDIX C

STRAIN GAGE LEVEL CHANGE RESULTS

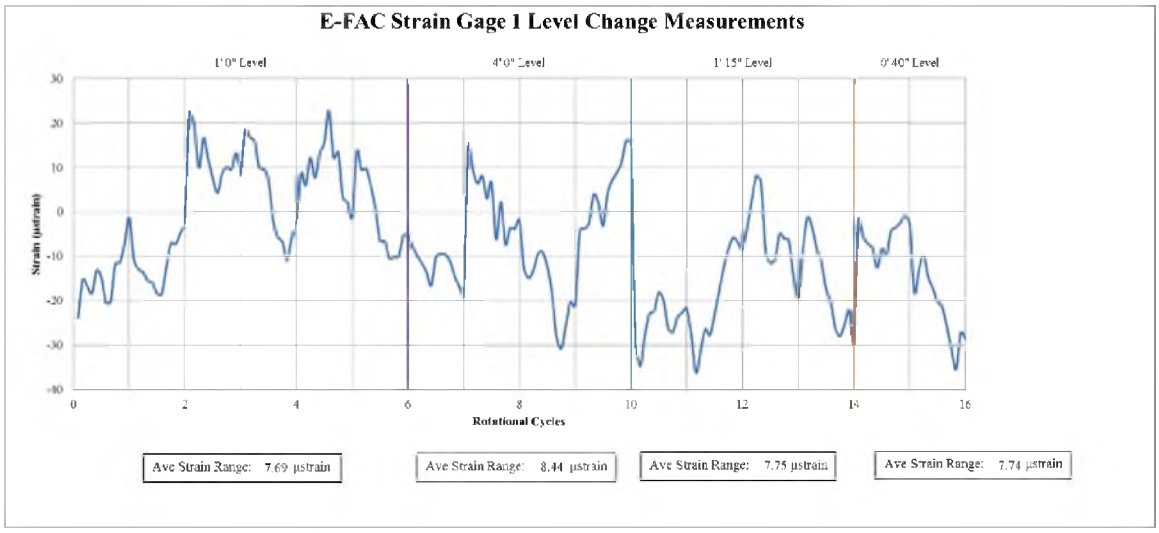

Figure 63 Plot of microstrain versus cycle for the E-FAC Strain Gage 1

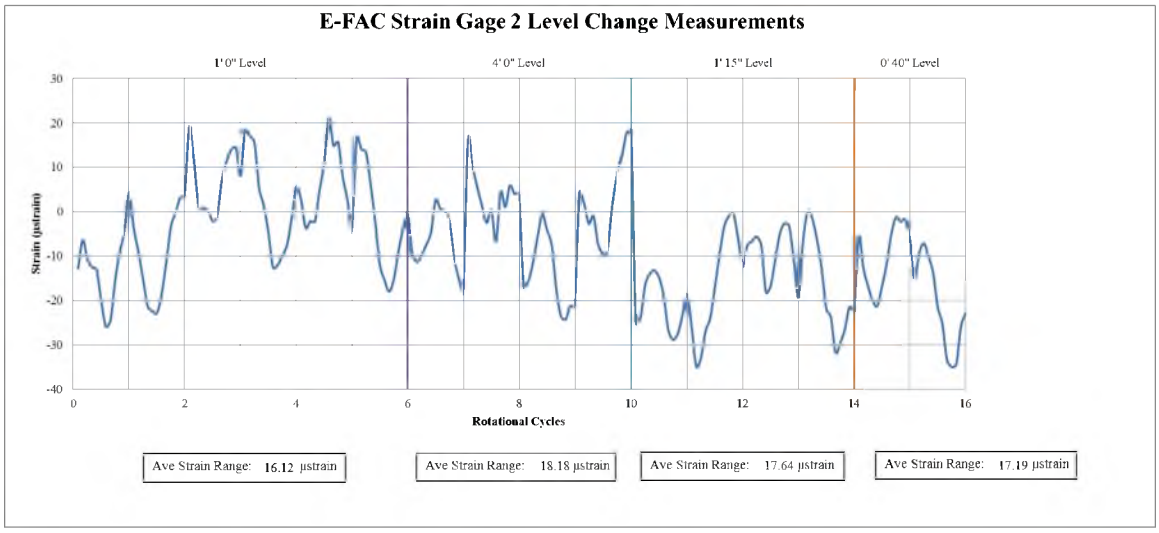

Figure 64 Plot of microstrain versus cycle for the E-FAC Strain Gage 2

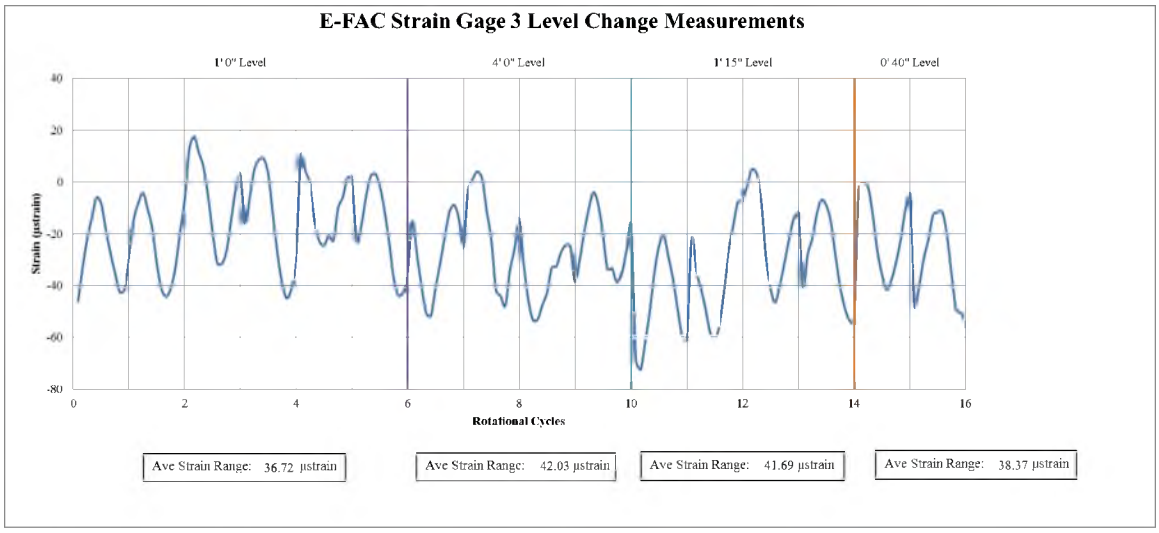

Figure 65 Plot of microstrain versus cycle for the E-FAC Strain Gage 3

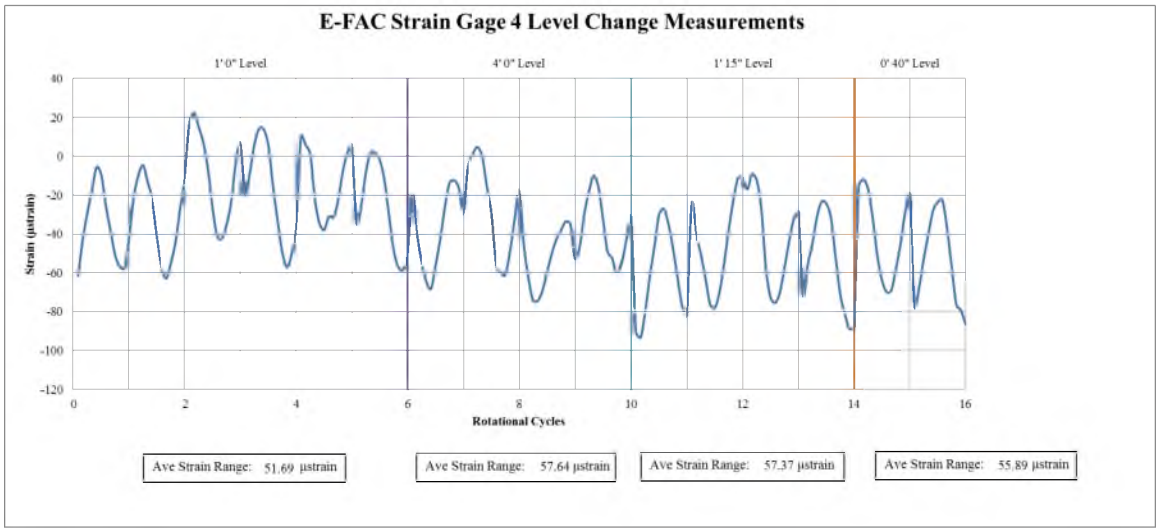

Figure 66 Plot of microstrain versus cycle for the E-FAC Strain Gage 4

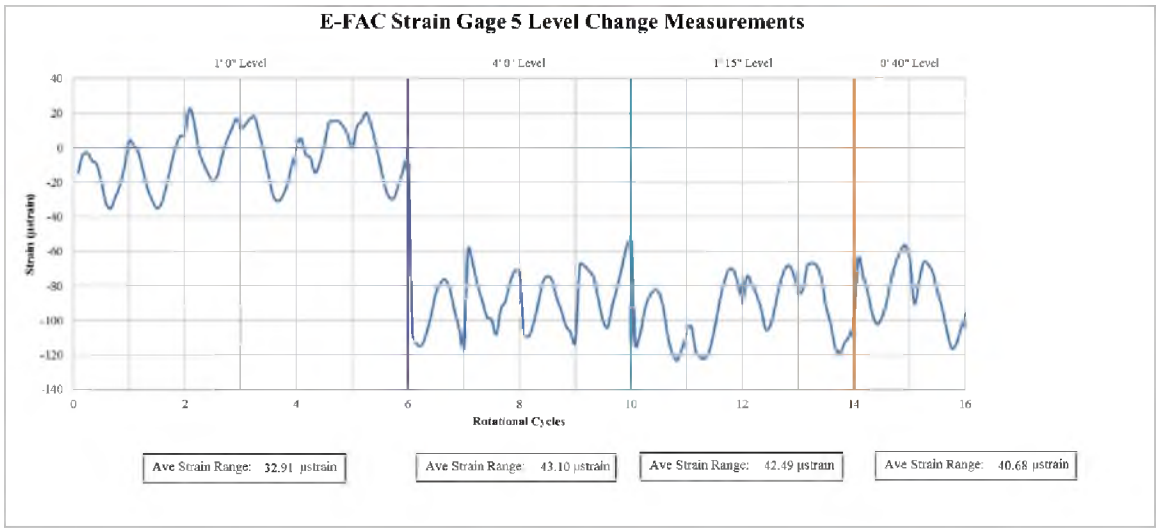

Figure 67 Plot of microstrain versus cycle for the E-FAC Strain Gage 5

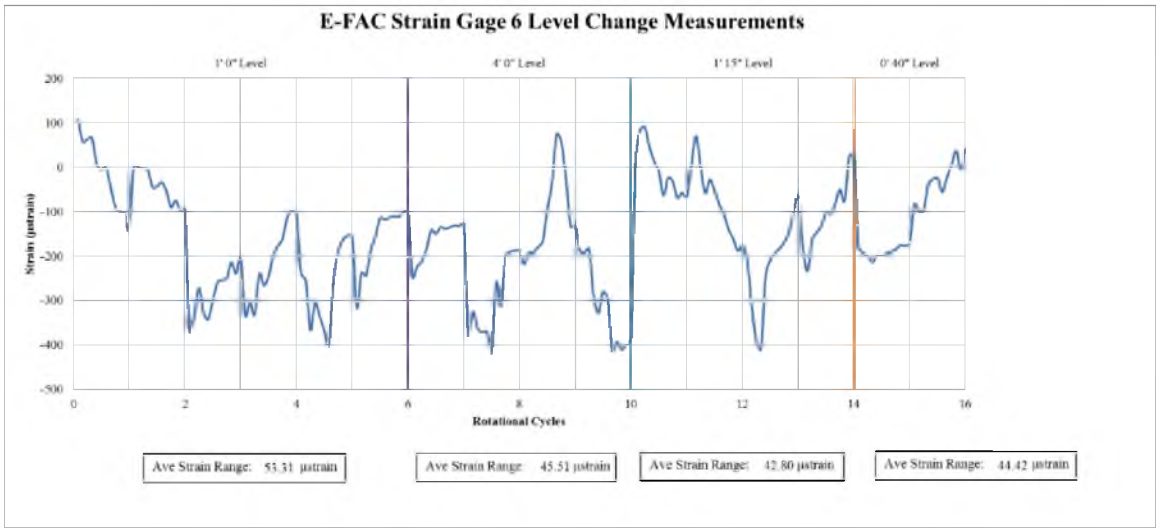

Figure 68 Plot of microstrain versus cycle for the E-FAC Strain Gage 6

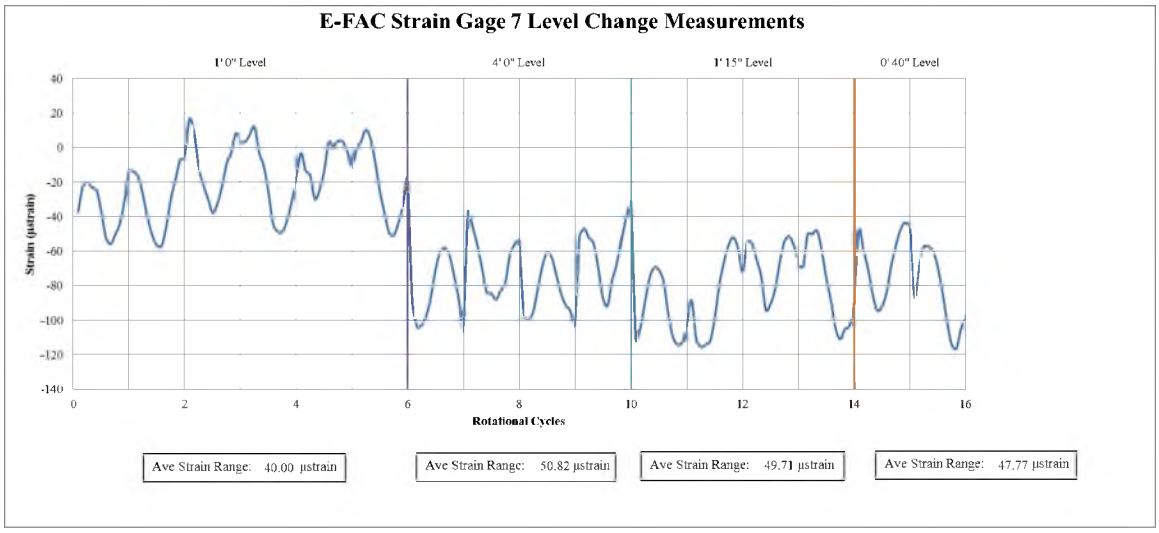

Figure 69 Plot of microstrain versus cycle for the E-FAC Strain Gage 7

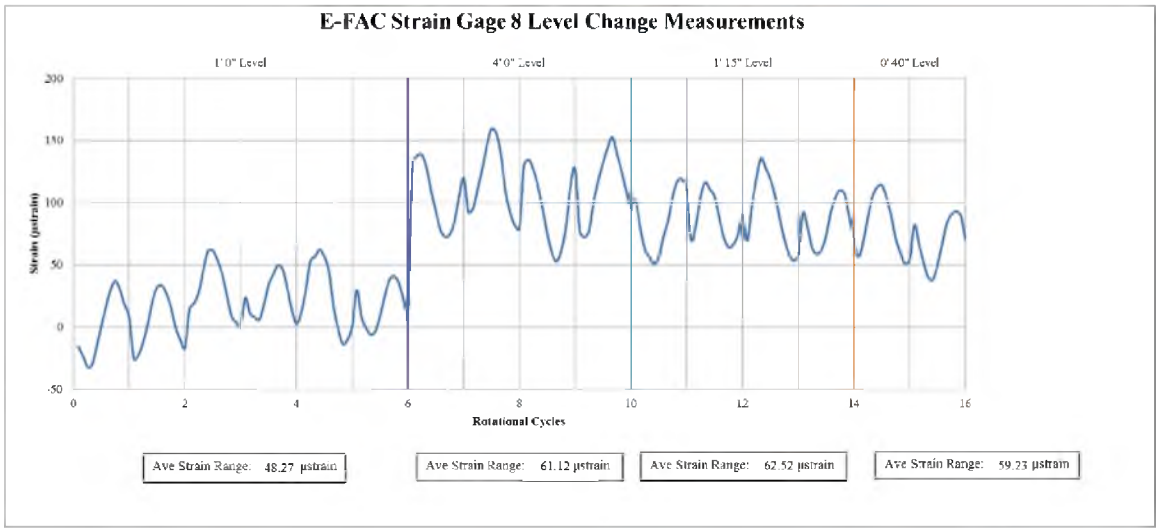

Figure 70 Plot of microstrain versus cycle for the E-FAC Strain Gage 8

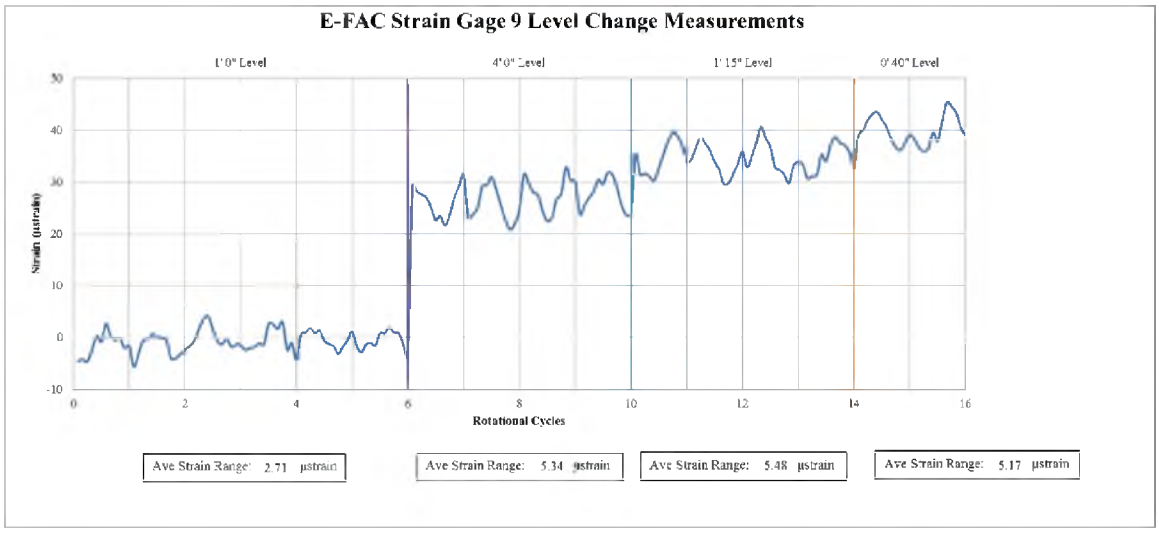

Figure 71 Plot of microstrain versus cycle for the E-FAC Strain Gage 9

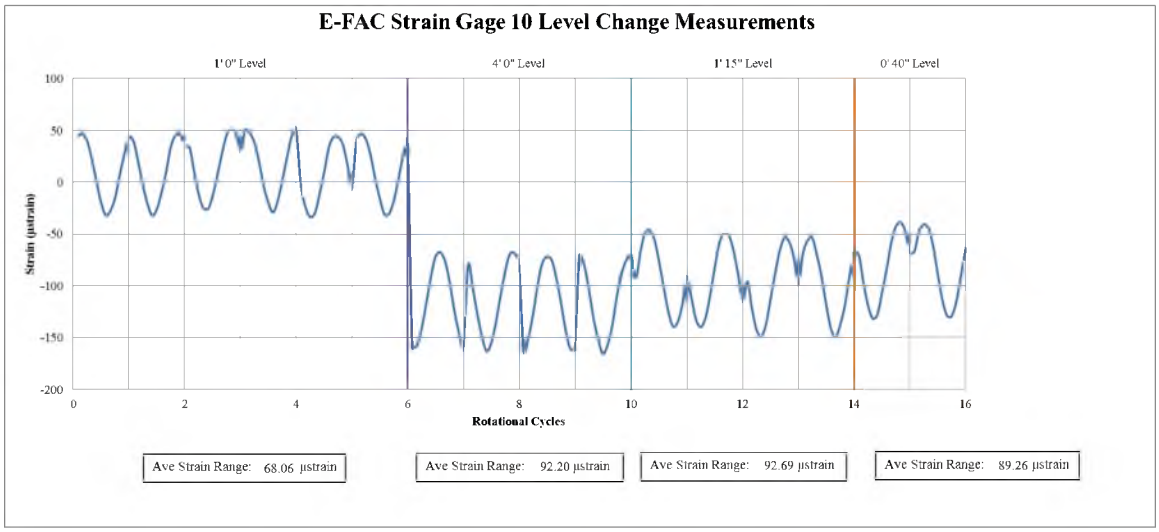

Figure 72 Plot of microstrain versus cycle for the E-FAC Strain Gage 10

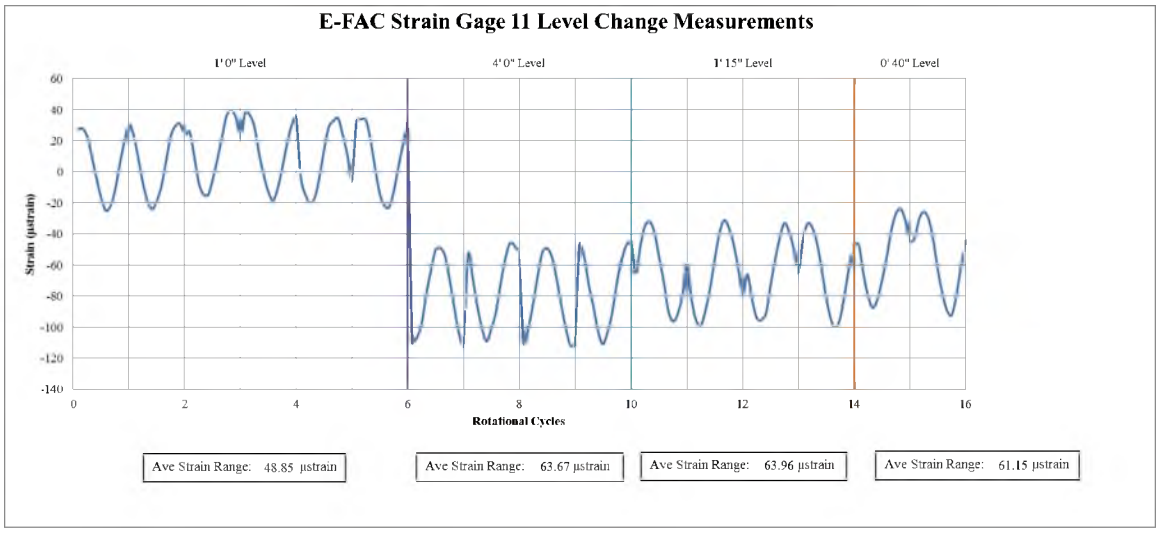

Figure 73 Plot of microstrain versus cycle for the E-FAC Strain Gage 11

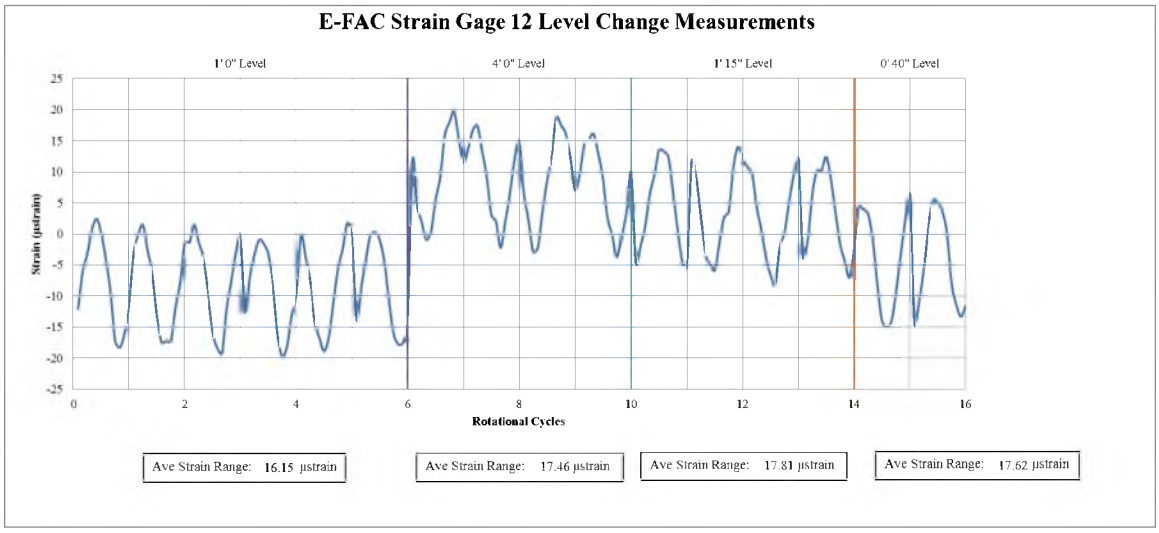

Figure 74 Plot of microstrain versus cycle for the E-FAC Strain Gage 12

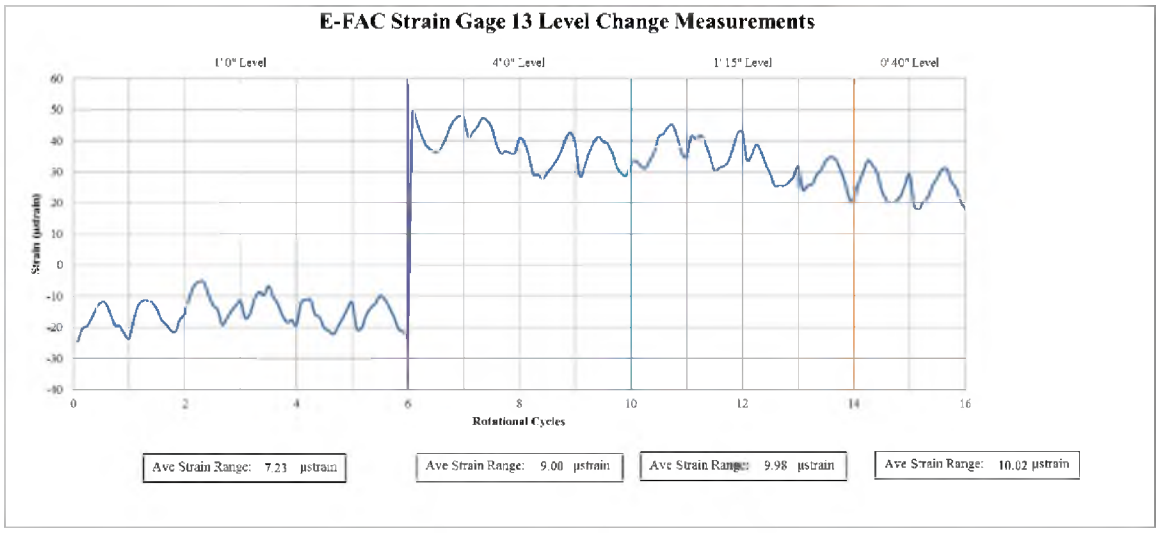

Figure 75 Plot of microstrain versus cycle for the E-FAC Strain Gage 13

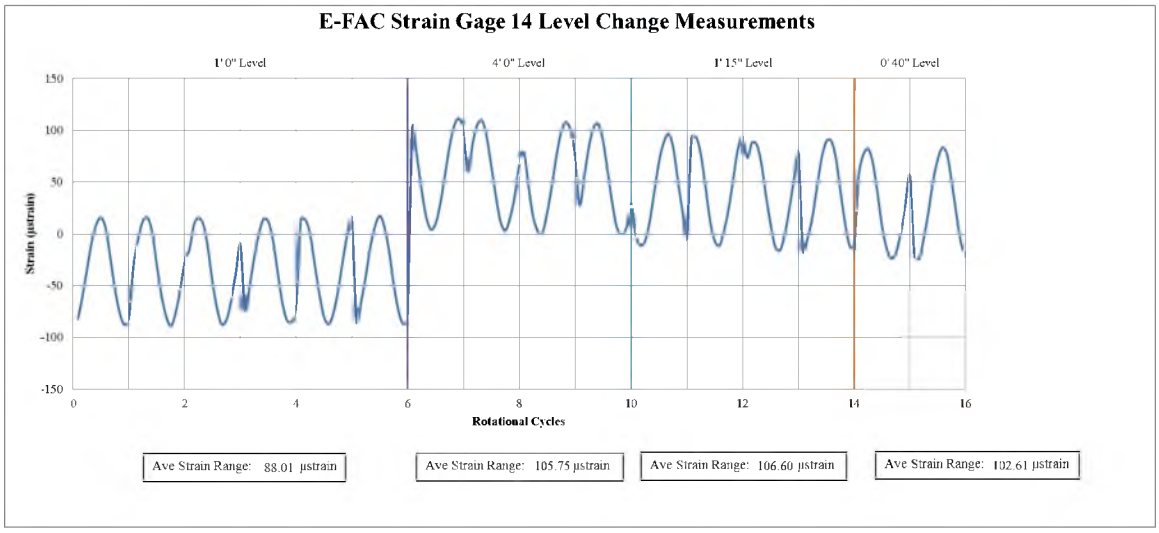

Figure 76 Plot of microstrain versus cycle for the E-FAC Strain Gage 14

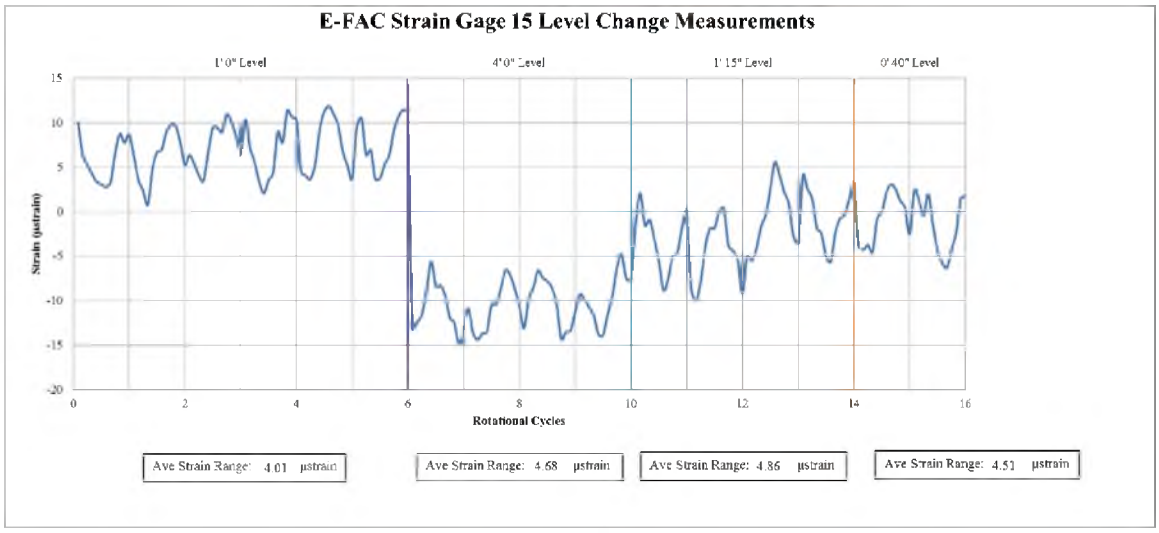

Figure 77 Plot of microstrain versus cycle for the E-FAC Strain Gage 15

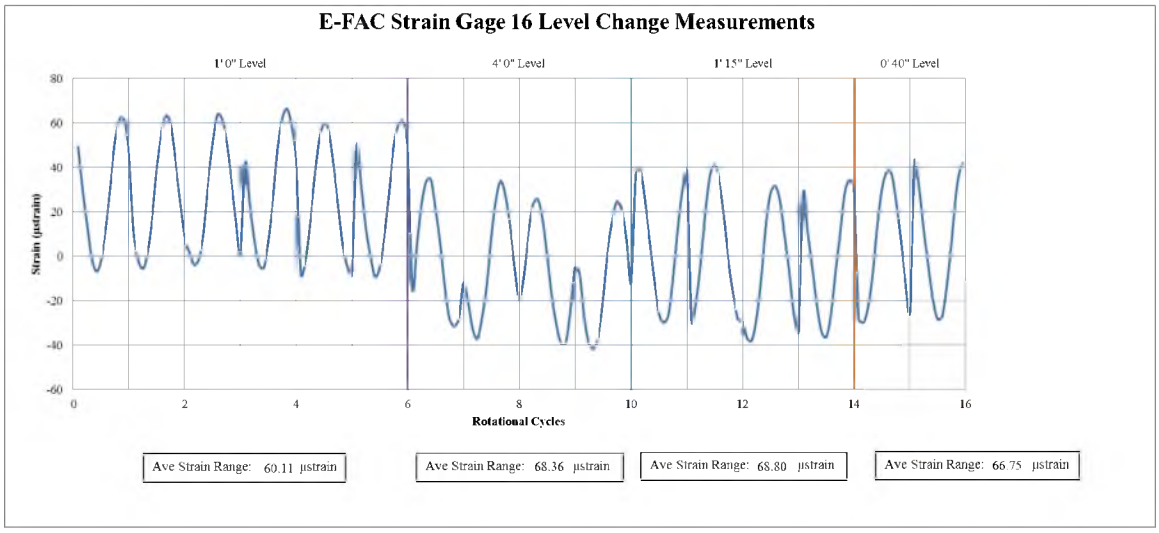

Figure 78 Plot of microstrain versus cycle for the E-FAC Strain Gage 16

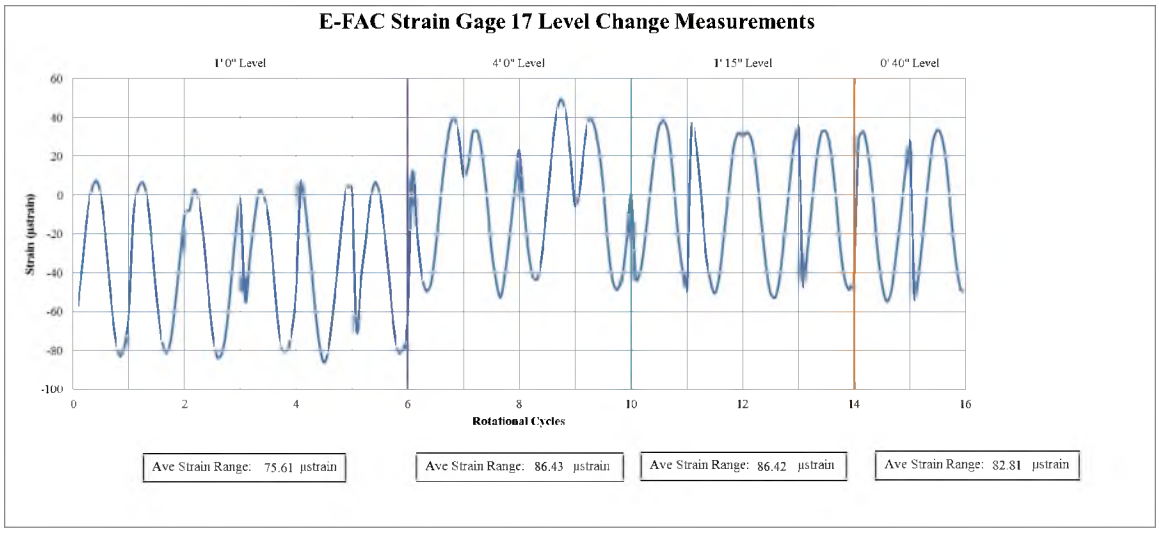

Figure 79 Plot of microstrain versus cycle for the E-FAC Strain Gage 17

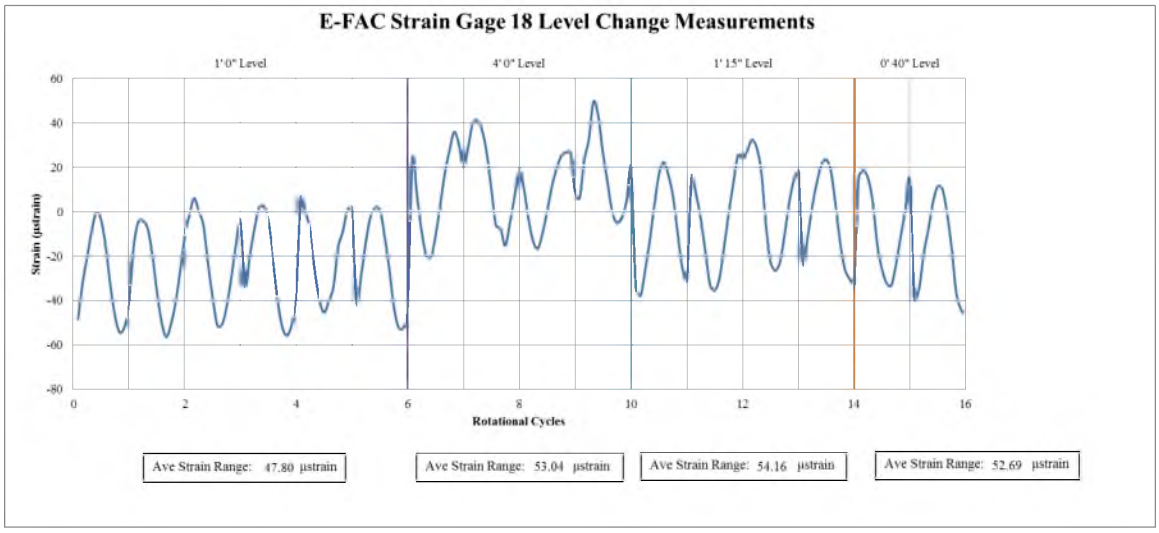

Figure 80 Plot of microstrain versus cycle for the E-FAC Strain Gage 18

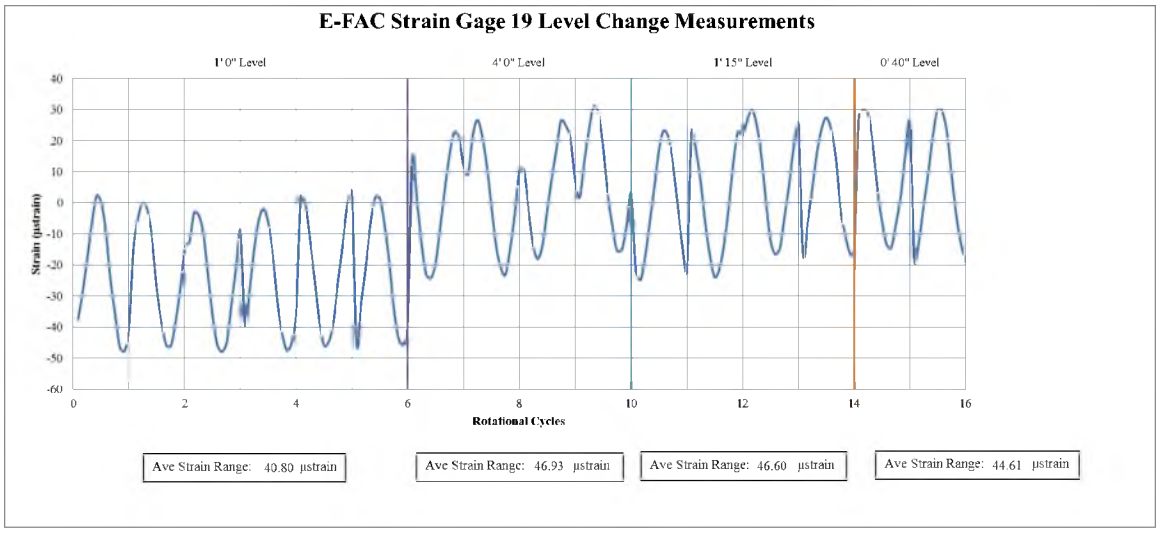

Figure 81 Plot of microstrain versus cycle for the E-FAC Strain Gage 19

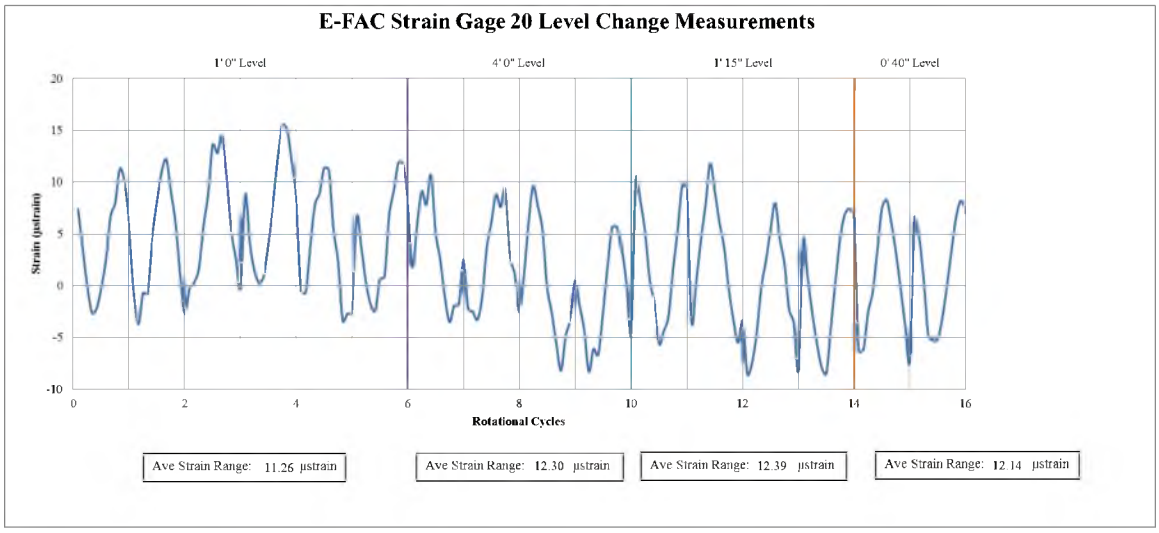

Figure 82 Plot of microstrain versus cycle for the E-FAC Strain Gage 20

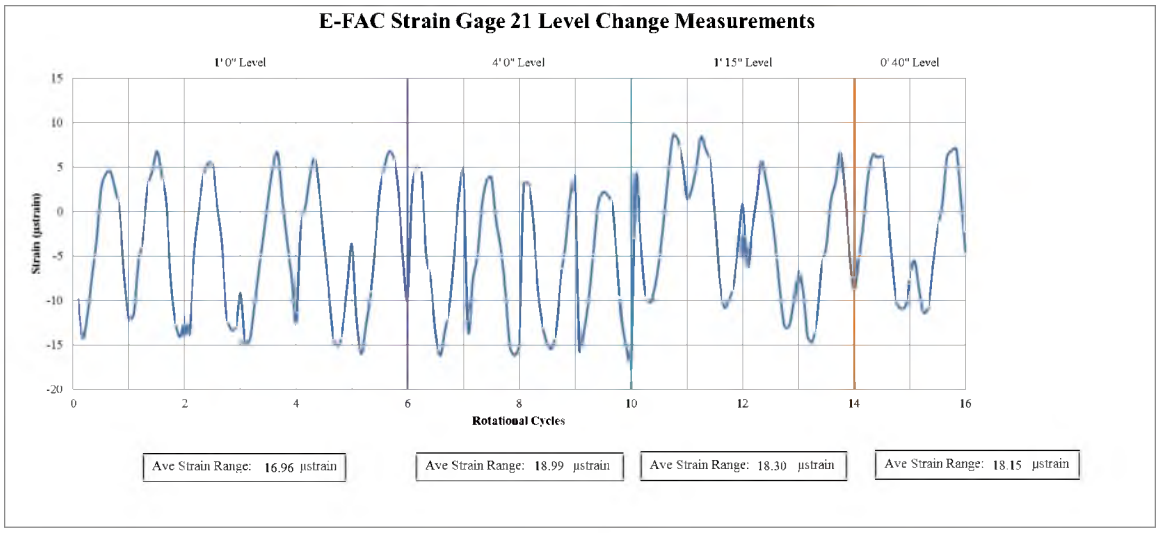

Figure 83 Plot of microstrain versus cycle for the E-FAC Strain Gage 21

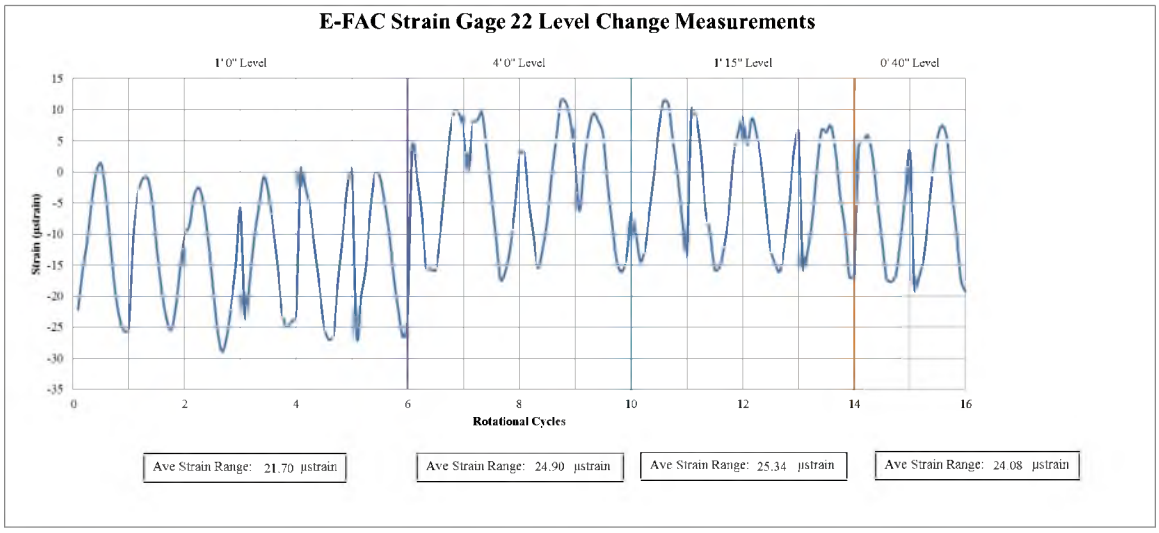

Figure 84 Plot of microstrain versus cycle for the E-FAC Strain Gage 22

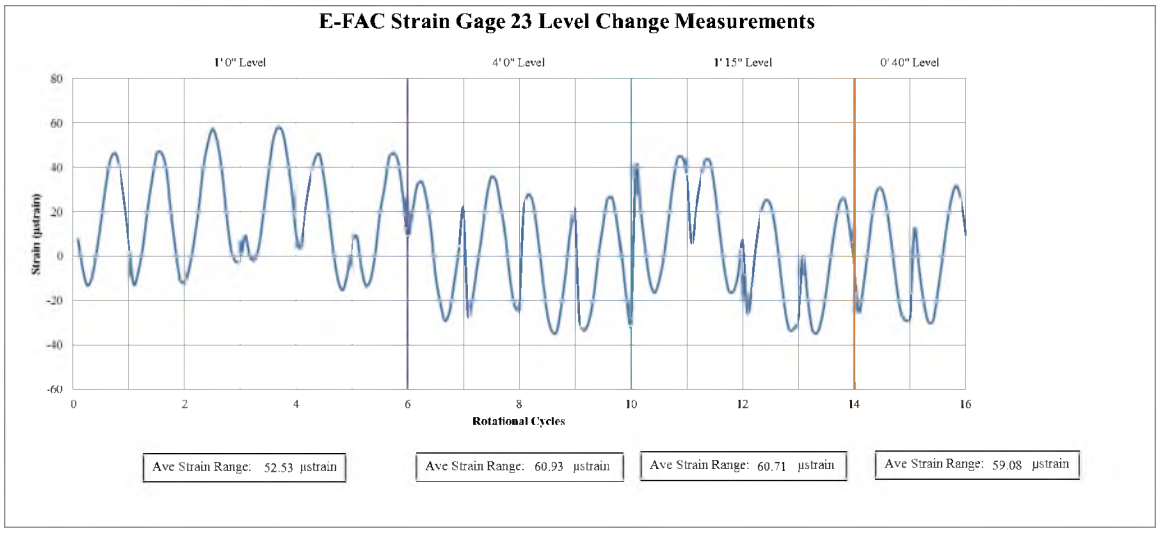

Figure 85 Plot of microstrain versus cycle for the E-FAC Strain Gage 23

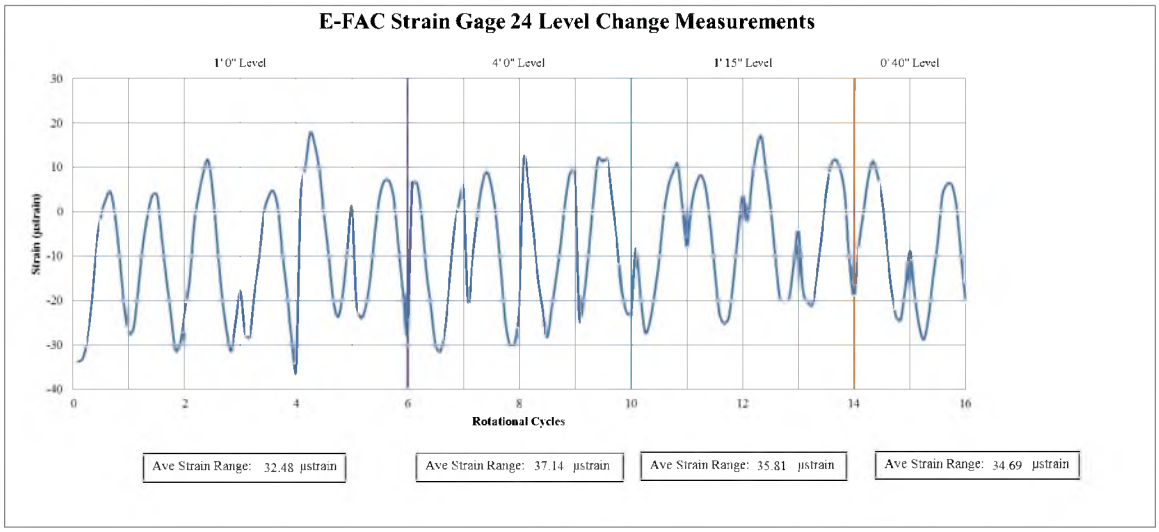

Figure 86 Plot of microstrain versus cycle for the E-FAC Strain Gage 24

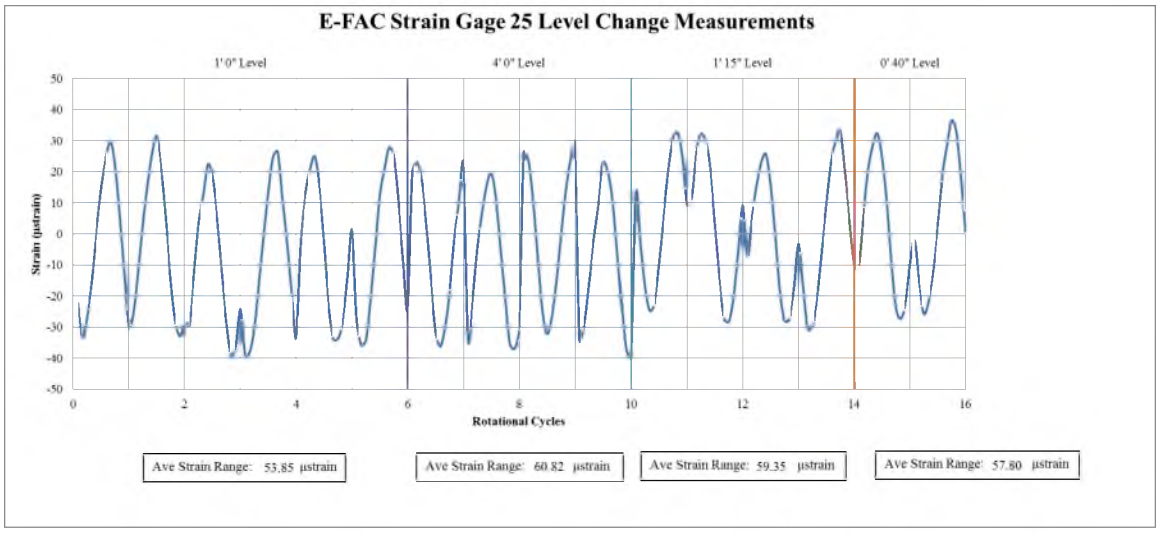

Figure 87 Plot of microstrain versus cycle for the E-FAC Strain Gage 25

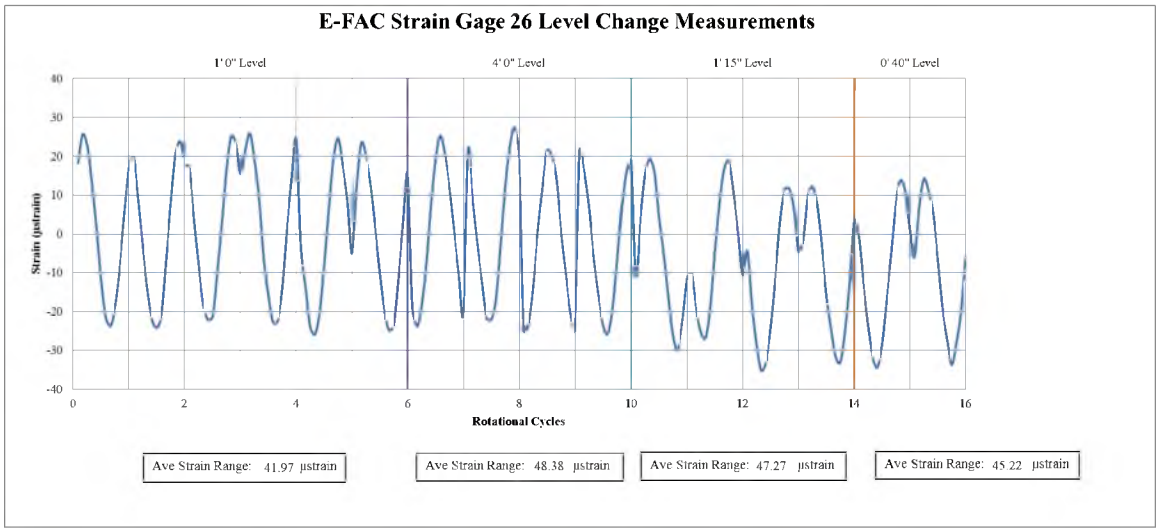

Figure 88 Plot of microstrain versus cycle for the E-FAC Strain Gage 26

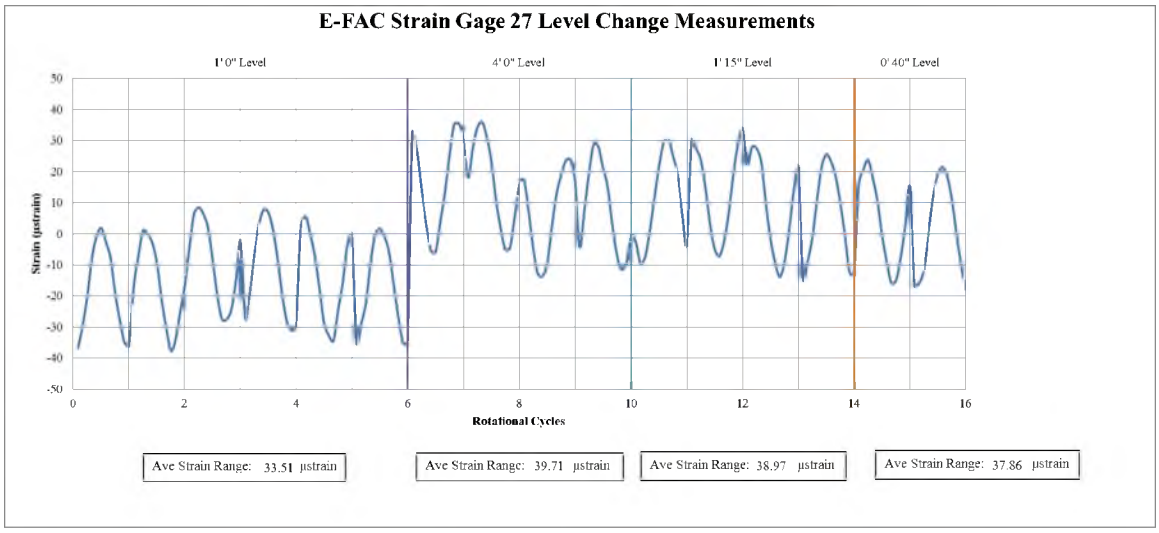

Figure 89 Plot of microstrain versus cycle for the E-FAC Strain Gage 27

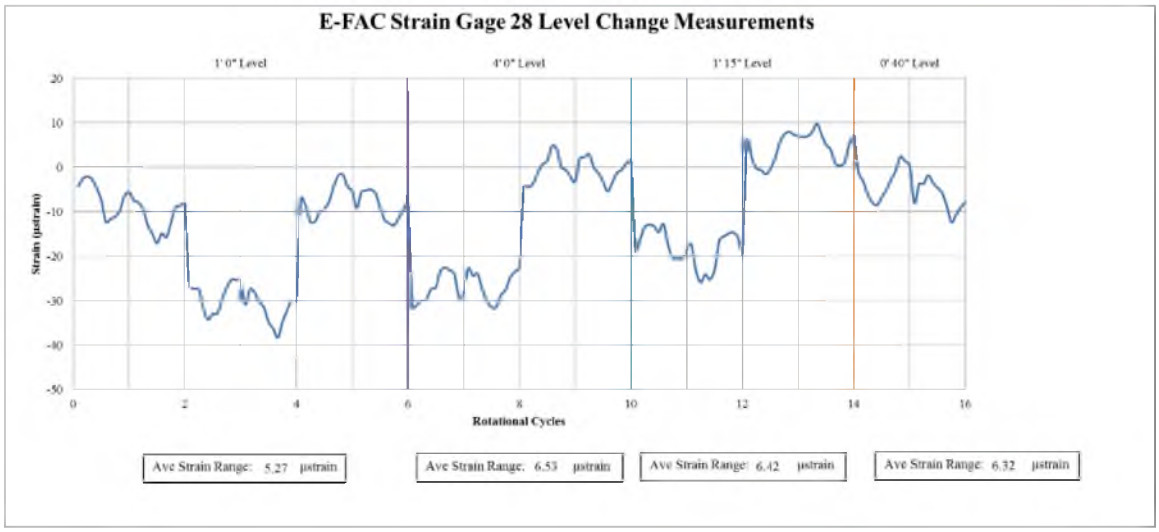

Figure 90 Plot of microstrain versus cycle for the E-FAC Strain Gage 28

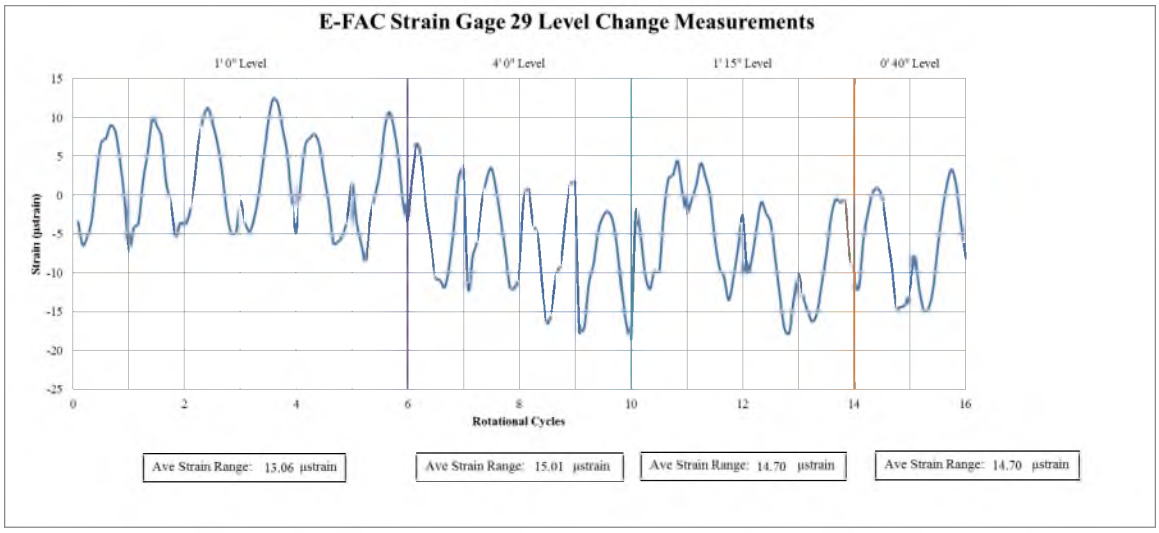

Figure 91 Plot of microstrain versus cycle for the E-FAC Strain Gage 29

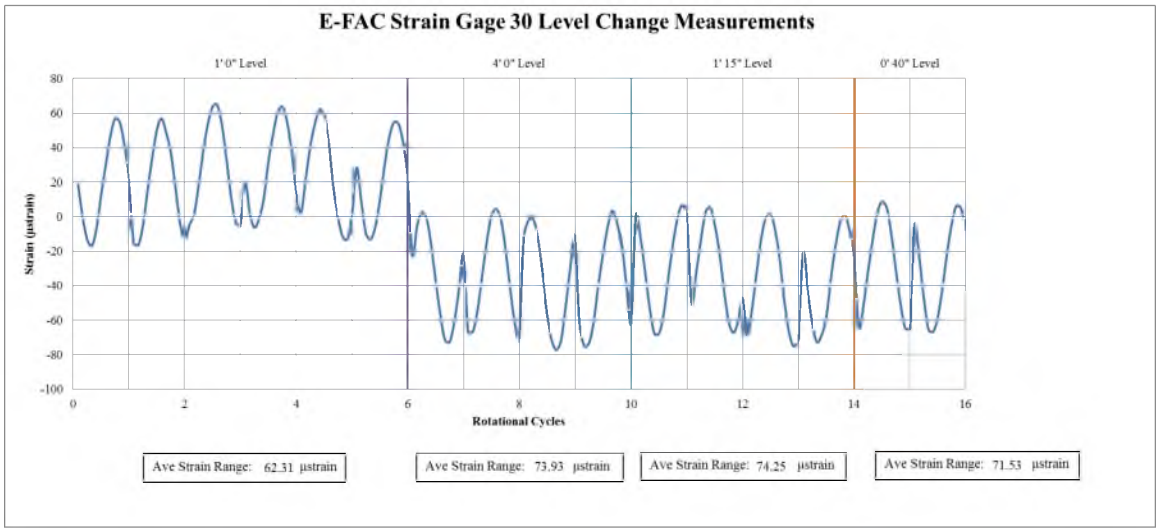

Figure 92 Plot of microstrain versus cycle for the E-FAC Strain Gage 30

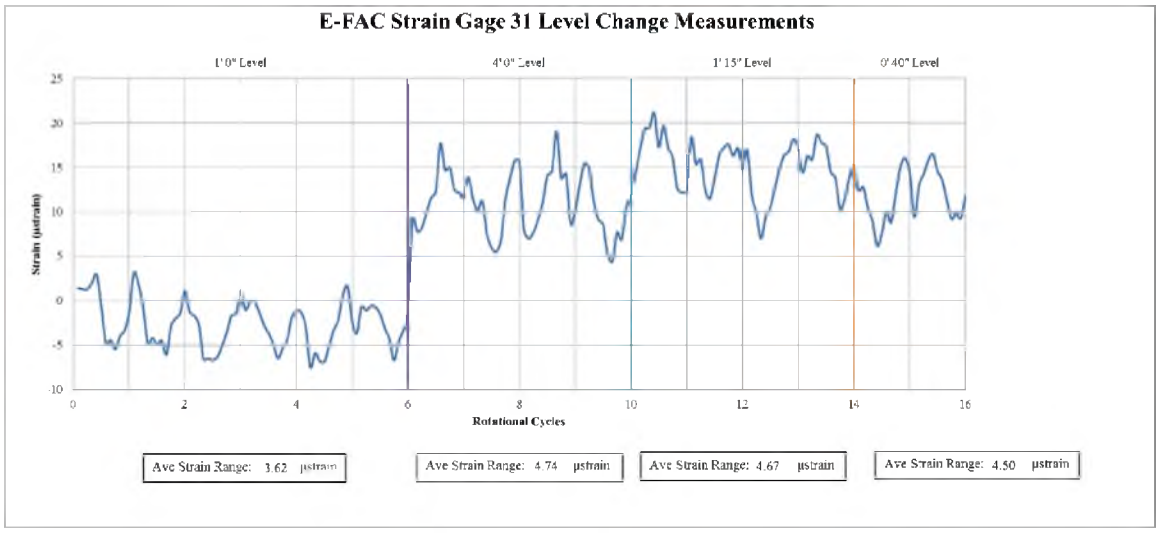

Figure 93 Plot of microstrain versus cycle for the E-FAC Strain Gage 31

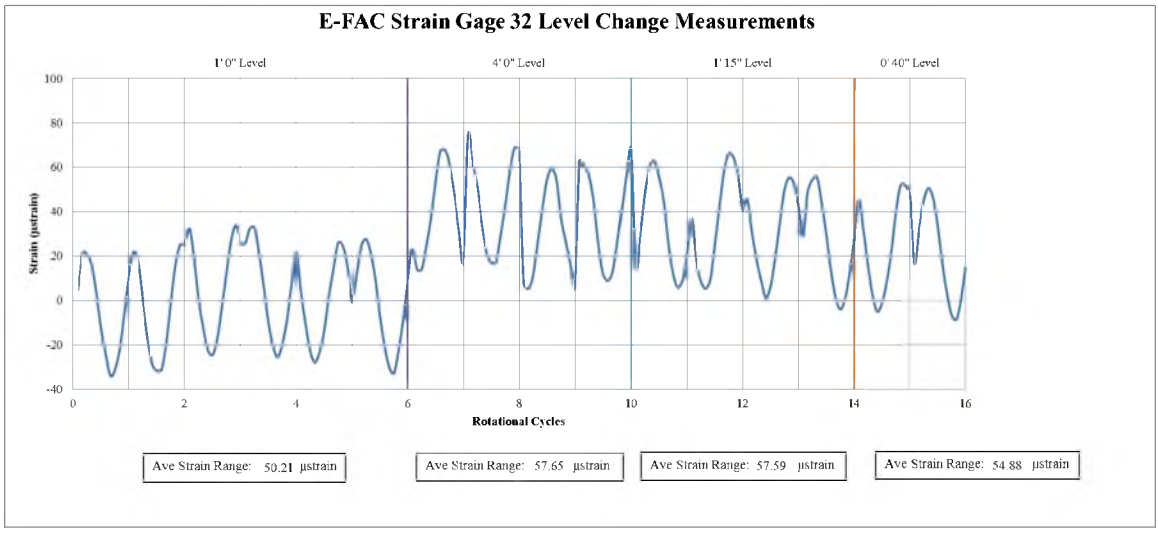

Figure 94 Plot of microstrain versus cycle for the E-FAC Strain Gage 32

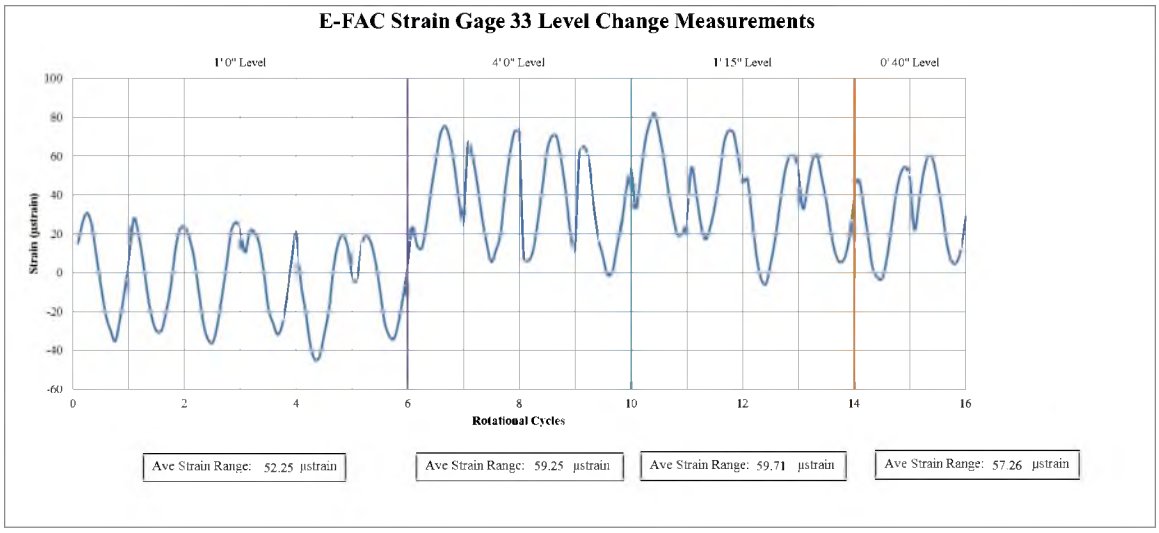

Figure 95 Plot of microstrain versus cycle for the E-FAC Strain Gage 33

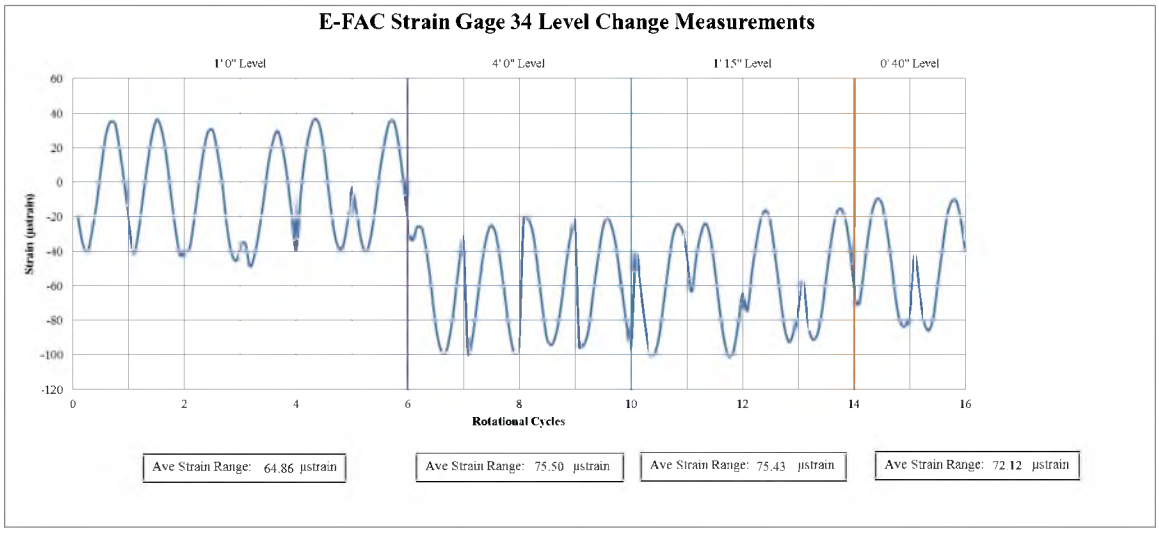

Figure 96 Plot of microstrain versus cycle for the E-FAC Strain Gage 34

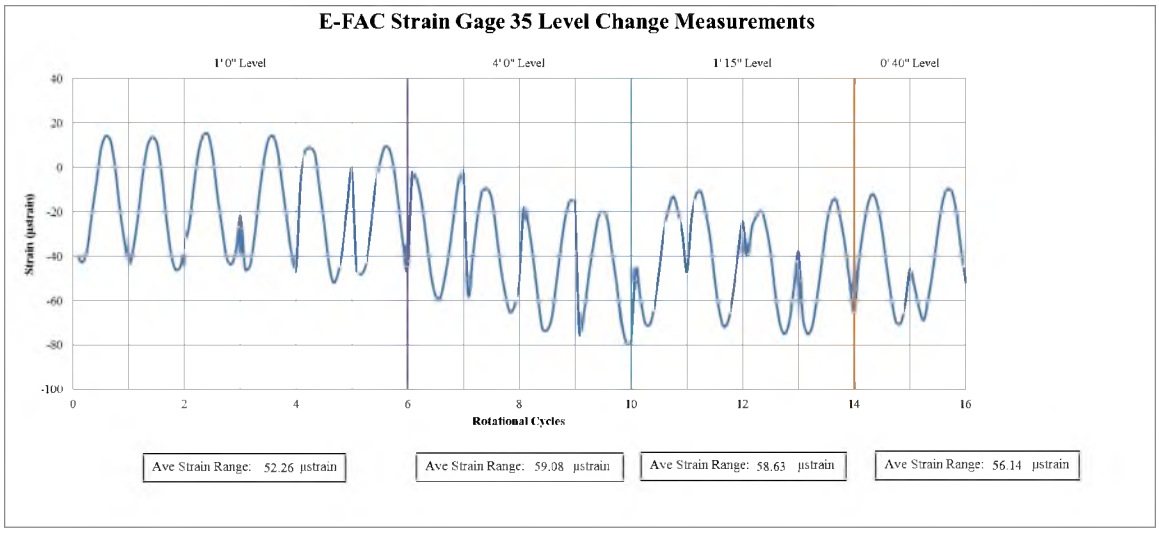

Figure 97 Plot of microstrain versus cycle for the E-FAC Strain Gage 35

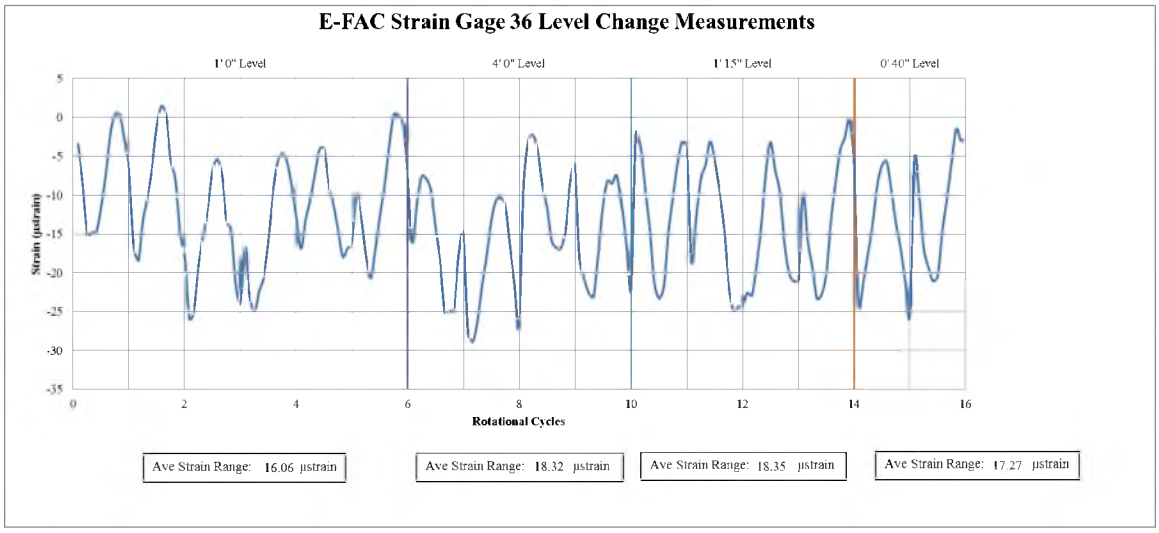

Figure 98 Plot of microstrain versus cycle for the E-FAC Strain Gage 36

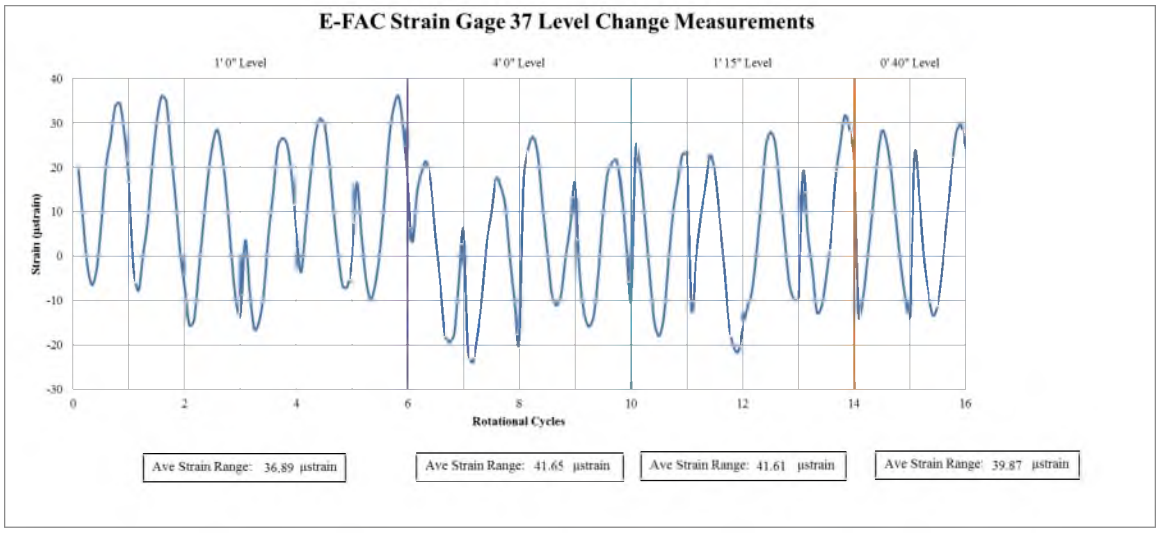

Figure 99 Plot of microstrain versus cycle for the E-FAC Strain Gage 37

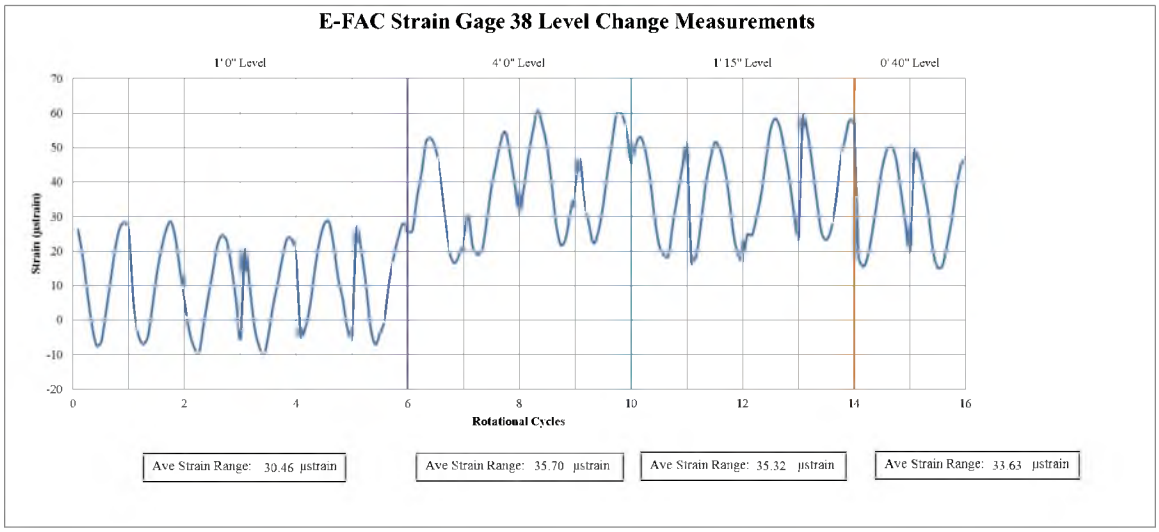

Figure 100 Plot of microstrain versus cycle for the E-FAC Strain Gage 38

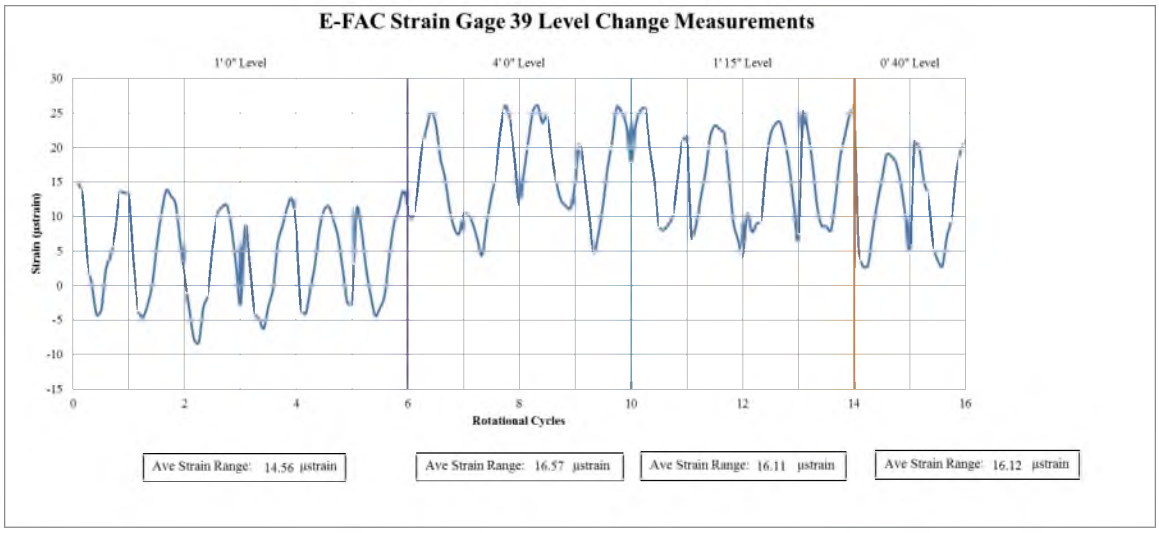

Figure 101 Plot of microstrain versus cycle for the E-FAC Strain Gage 39

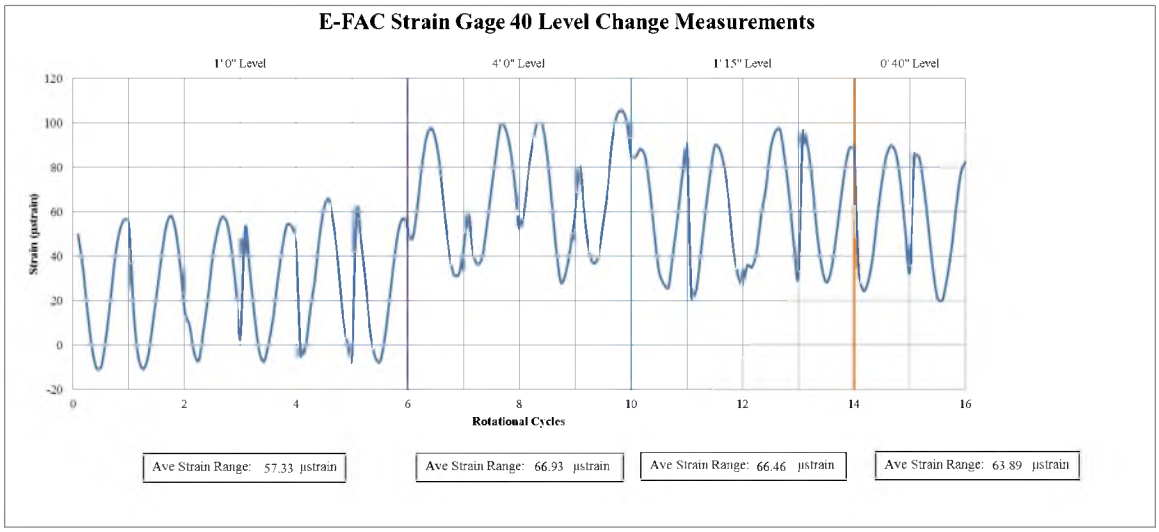

Figure 102 Plot of microstrain versus cycle for the E-FAC Strain Gage 40

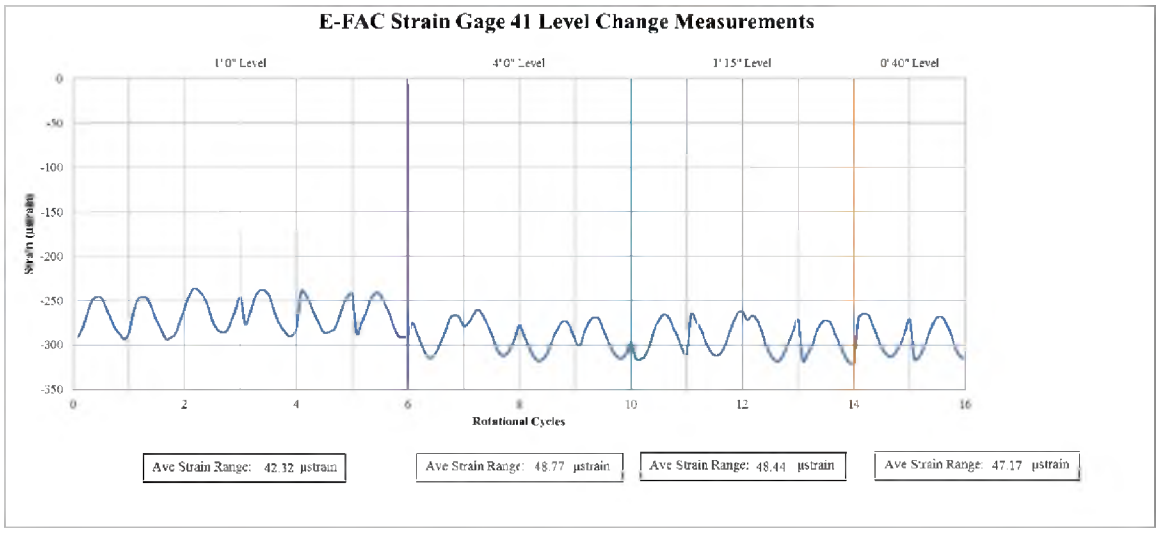

Figure 103 Plot of microstrain versus cycle for the E-FAC Strain Gage 41

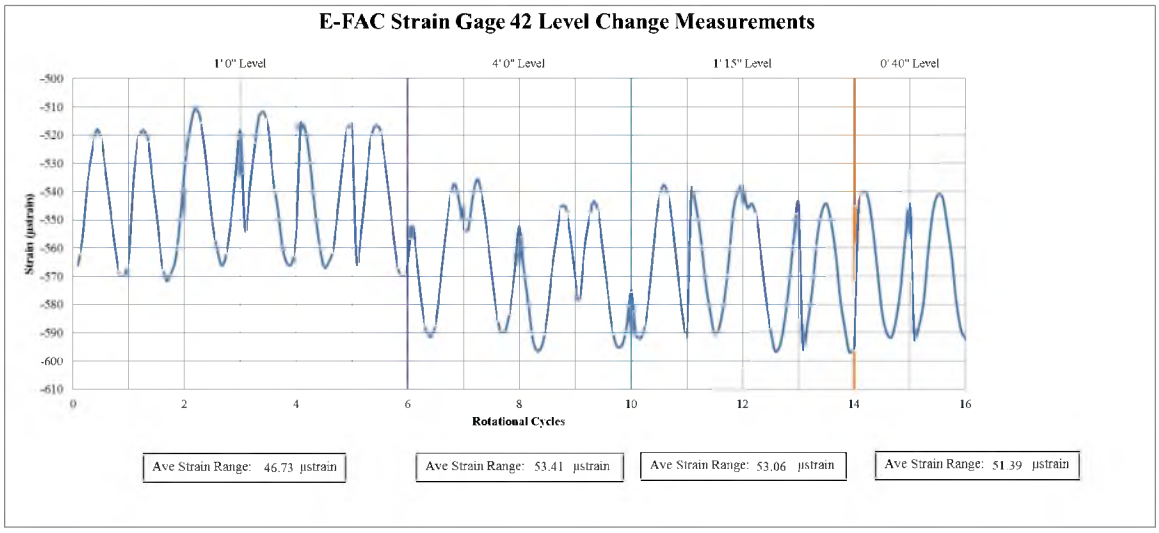

Figure 104 Plot of microstrain versus cycle for the E-FAC Strain Gage 42

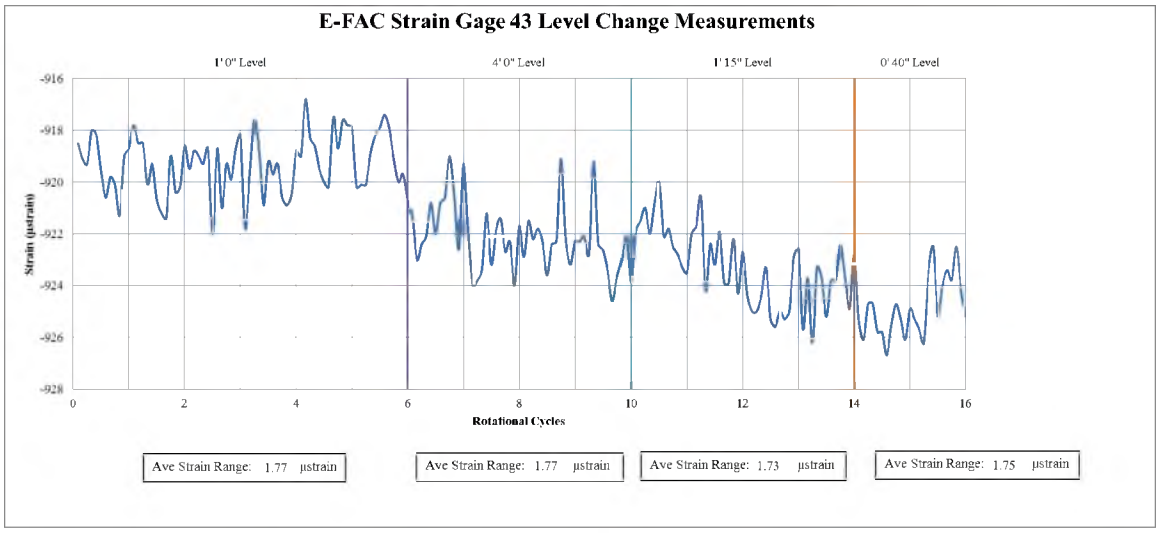

Figure 105 Plot of microstrain versus cycle for the E-FAC Strain Gage 43

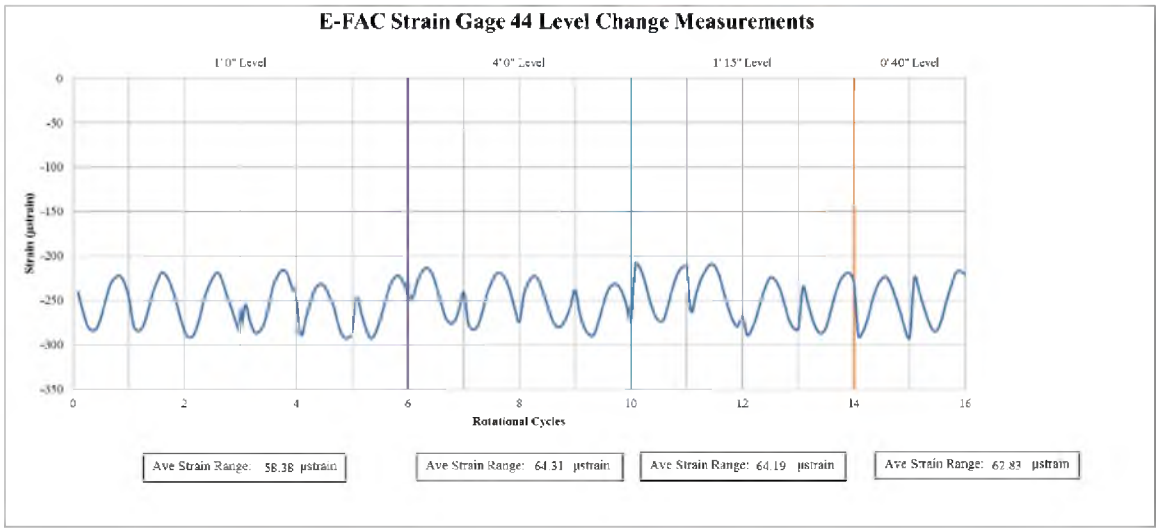

Figure 106 Plot of microstrain versus cycle for the E-FAC Strain Gage 44

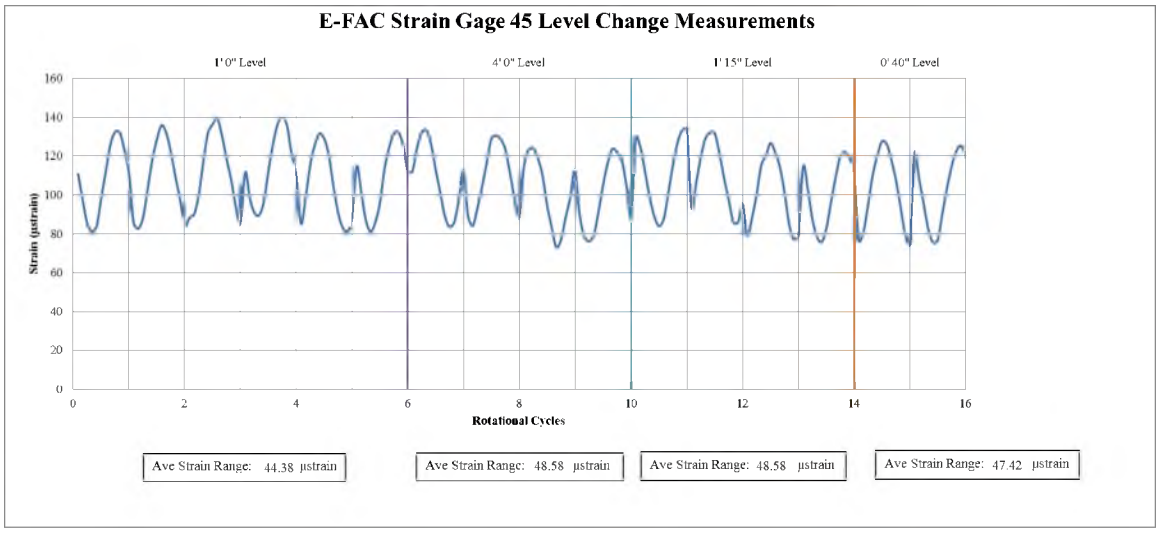

Figure 107 Plot of microstrain versus cycle for the E-FAC Strain Gage 45

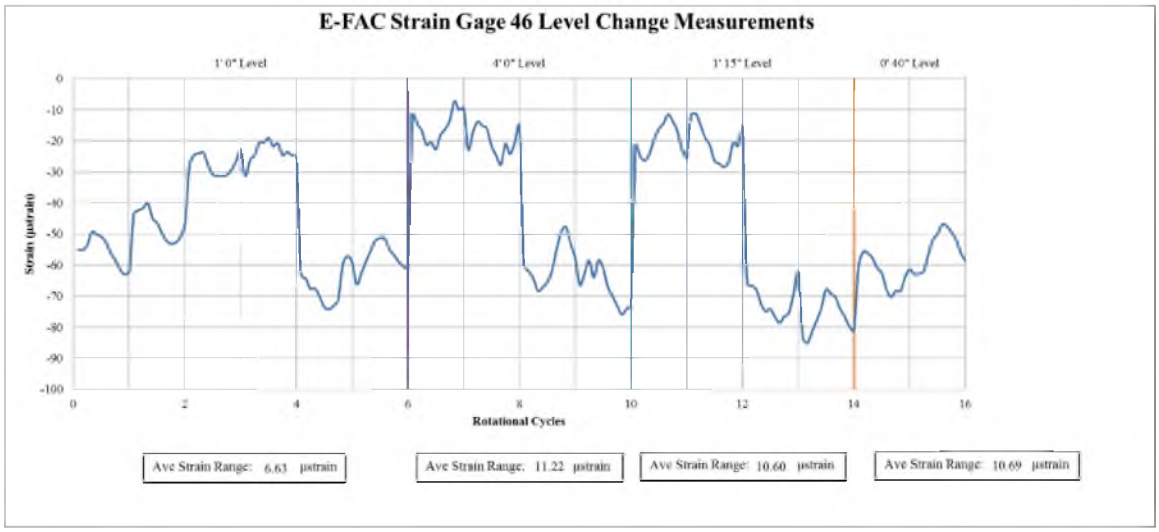

Figure 108 Plot of microstrain versus cycle for the E-FAC Strain Gage 46

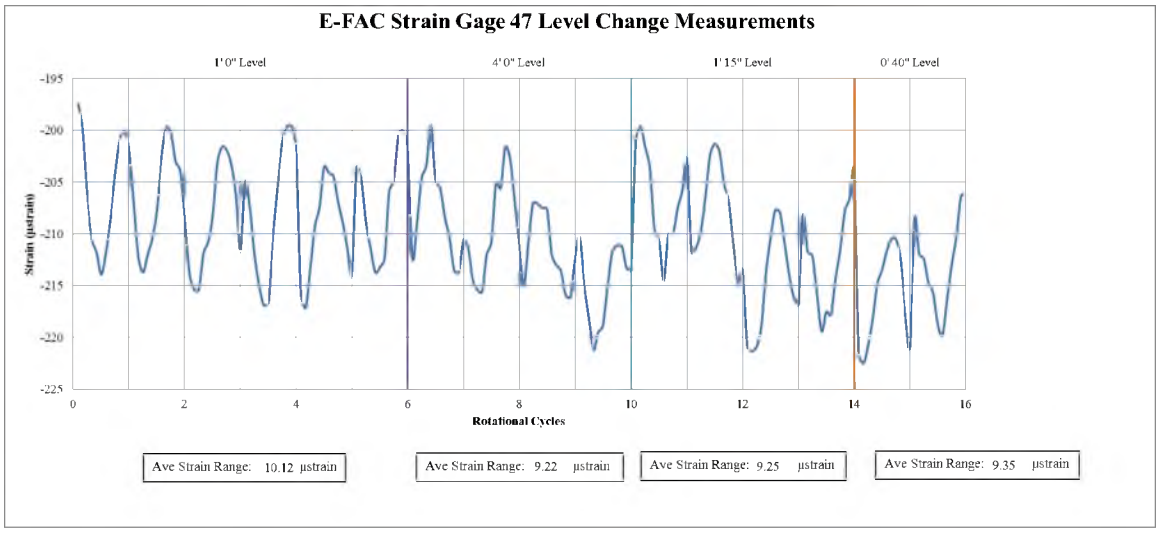

Figure 109 Plot of microstrain versus cycle for the E-FAC Strain Gage 47

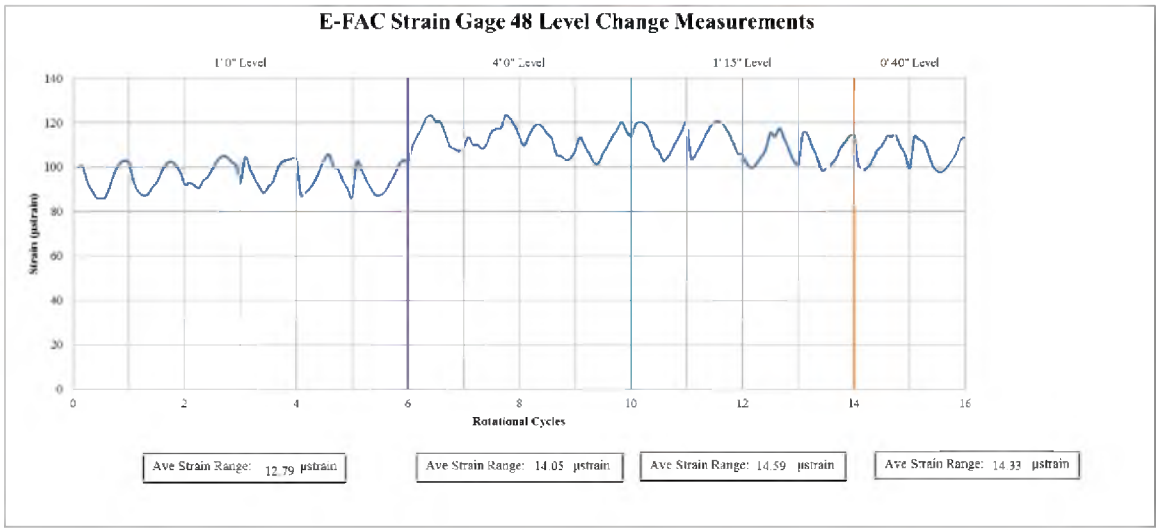

Figure 110 Plot of microstrain versus cycle for the E-FAC Strain Gage 48

Table 12 Strain gage average microstrain range values based on change in level

Strain Gage Number	1' 0"	4' 0"	1' 15"	0' 40"	Deviation 1' 0" to 4' 0"	Deviation 4' 0' to 0' 40"
SG01	2.71	5.34	5.48	5.17	2.64	0.18
SG02	68.06	92.20	92.69	89.26	24.13	2.94
SG03	48.85	63.67	63.96	61.15	14.83	2.53
SG04	16.15	17.46	17.81	17.62	1.31	-0.16
SG05	7.23	9.00	9.98	10.02	1.77	-1.01
SG06	88.01	105.75	106.60	102.61	17.74	3.14
SG07	4.01	4.68	4.86	4.51	0.66	0.16
SG08	60.11	68.36	68.80	66.75	8.24	1.61
SG09	75.61	86.43	86.42	82.81	10.82	3.62
SG10	47.80	53.04	54.16	52.69	5.24	0.35
SG11	40.80	46.93	46.60	44.61	6.13	2.32
SG12	11.26	12.30	12.39	12.14	1.04	0.16
SG13	16.96	18.99	18.30	18.15	2.04	0.85
SG14	21.70	24.90	25.34	24.08	3.20	0.81
SG15	52.53	60.93	60.71	59.08	8.40	1.85
SG16	32.48	37.14	35.81	34.69	4.66	2.45
SG17	53.85	60.82	59.35	57.80	6.98	3.02
SG18	41.97	48.38	47.27	45.22	6.41	3.15
SG19	33.51	39.71	38.97	37.86	6.20	1.85
SG20	5.27	6.53	6.42	6.32	1.26	0.21
SG21	13.06	15.01	14.70	14.70	1.95	0.30
SG22	62.31	73.93	74.25	71.53	11.62	2.41
SG23	3.62	4.74	4.67	4.50	1.12	0.24
SG24	50.21	57.65	57.59	54.88	7.44	2.77
SG25	53.85	60.82	59.35	57.80	6.98	3.02
SG26	41.97	48.38	47.27	45.22	6.41	3.15
SG27	33.51	39.71	38.97	37.86	6.20	1.85
SG28	5.27	6.53	6.42	6.32	1.26	0.21
SG29	13.06	15.01	14.70	14.70	1.95	0.30
SG30	62.31	73.93	74.25	71.53	11.62	2.41
SG31	3.62	4.74	4.67	4.50	1.12	0.24
SG32	50.21	57.65	57.59	54.88	7.44	2.77
SG33	52.25	59.25	59.71	57.26	7.00	1.99
SG34	64.86	75.50	75.43	72.12	10.65	3.38
SG35	52.26	59.08	58.63	56.14	6.83	2.95
SG36	16.06	18.32	18.35	17.27	2.26	1.04

Table 12 Continued

Strain Gage Number	1' 0"	4' 0"	1' 15"	0' 40"	Deviation 1' 0" to 4' 0"	Deviation 4' 0' to 0' 40"
SG37	36.89	41.65	41.61	39.87	4.77	1.78
SG38	30.46	35.70	35.32	33.63	5.24	2.07
SG39	14.56	16.57	16.11	16.12	2.01	0.45
SG40	57.33	66.93	66.46	63.89	9.60	3.04
SG41	42.32	48.77	48.44	47.17	6.44	1.60
SG42	46.73	53.41	53.06	51.39	6.68	2.02
SG43	1.77	1.77	1.73	1.75	0.00	0.02
SG44	58.38	64.31	64.19	62.83	5.93	1.48
SG45	44.38	48.58	48.58	47.42	4.21	1.16
SG46	6.63	11.22	10.60	10.69	4.59	0.53
SG47	10.12	9.22	9.25	9.35	-0.90	-0.13
SG48	12.79	14.05	14.59	14.33	1.27	-0.28
Maximum	**88.01**	**105.75**	**106.60**	**102.61**	**24.13**	**3.62**
Minimum	**1.77**	**1.77**	**1.73**	**1.75**	**-0.90**	**-1.01**

APPENDIX D

STRAIN-LIFE CALCULATIONS

Thesis Calculations

- Radar Geometry from Figure 2

$Ls = 206.68;$ (*inches*)
$Lb = 97.25;$ (*inches*)
$\beta = 80\left(\frac{\pi}{180}\right);$ (*radians*)

Law of Cosines

$La = Lb\,Cos[\beta] + \sqrt{Ls^2 - Lb^2\,Sin[\beta]^2}$ (*inches*)

200.038

The array is 24 feet square

$Le = 288 - La$ (*inches*)

87.9618

$\alpha = ArcSin\left[\frac{La}{Ls}\,Sin[\beta]\right];$ (*radians*)

$\alpha degrees = \alpha\left(\frac{180}{\pi}\right)$ (*degrees*)

72.3942

$\gamma = \pi - \alpha - \beta;$ (*radians*)

$\gamma degrees = \gamma\left(\frac{180}{\pi}\right)$ (*degrees*)

27.6058

- Statics Assuming the Pedestal is Level

Weight (w) of the radar as a distributed load in lbs per inch:

$w = \frac{27\,000}{(La + Le)}$ (*pounds/in*)

93.75

Sum of the Forces in the x direction equal zero:

$Eq1 = Rx - F\,Cos[\alpha]$

$-0.302466\,F + Rx$

Sum of the Forces in the y direction equal zero:

$Eq2 = Ry - w\,(La + Le) + F\,Sin[\alpha]$

$-27\,000. + 0.95316\,F + Ry$

Sum of the Moments about the pillow block equal zero:

$$Eq3 = F\,Lb\,Sin[\alpha] - w\,(La + Le)\,\frac{(La + Le)\,Cos[\beta]}{2}$$

$$-675144. + 92.6948\,F$$

Solving for the reactions at the pillow block and the Force (F) that allows for equilibrium is shown:

$$Res = Solve[\{Eq1 == 0, Eq2 == 0, Eq3 == 0\}, \{Rx, Ry, F\}] // Flatten$$

$$\{Rx \to 2203.02, Ry \to 20057.6, F \to 7283.52\}$$

Because there are two pillow blocks and two back stays supporting the antenna, the reactions and the forces are all divided by two. The following is the reaction on a single pillow block and back stay:

$$Rx = \frac{Rx}{2} /. Res \quad (*pounds*)$$

$$Ry = \frac{Ry}{2} /. Res \quad (*pounds*)$$

$$F = \frac{F}{2} /. Res \quad (*pounds*)$$

1101.51

10028.8

3641.76

The magnitude and angle (measured counterclockwise from horizontal) of the resultant of the reactions at the pillow block is shown below:

$$Rt = \sqrt{Rx^2 + Ry^2} \quad (*pounds*)$$

$$\theta Res = 90 - ArcTan\left[\frac{Rx}{Ry}\right]\left(\frac{180}{\pi}\right) \quad (*degrees*)$$

10089.1

83.7321

- Strain-Life Fatigue Failure Model Based on Tensile Test Results

This is going to have multiple sections (3) 1 is the book numbers for properties, 2 is the static tensile test numbers, and 3 is the universal slope method [ref shigley pg 367]. Using the properties for each of the methods, the strain-life calculations are made. Look at which ones are most conservative or representative of the actual situation.

The following material properties are estimated by using the results from the tensile tests performed at Hill Air Force Base.

maxload = 9911.7;

$$\text{area} = \frac{7874.5}{54.97096\ 10^3};$$

$$\text{Su} = \frac{\text{maxload}}{\text{area}}$$

$\sigma y = 57.85527\ 10^3$;

$$E = \frac{\sigma y}{0.002}$$

$\sigma f = 54.97096\ 10^3$

$\epsilon f = 0.350859$

69 192.4

2.89276×10^7

54 971.

0.350859

$\sigma fprime = \sigma f$

$\epsilon fprime = \epsilon f$

$c = -0.6$

$b = -0.16\ \text{Log}[10, 2\ \sigma f\ Su]$

54 971.

0.350859

−0.6

−1.581

$$\text{strainrangetensile} = \frac{\sigma fprime}{E} (2\ Nf)^b + \epsilon fprime\ (2\ Nf)^c$$

$$\frac{0.000635175}{Nf^{1.581}} + \frac{0.231481}{Nf^{0.6}}$$

```
LogLogPlot[{strainrangetensile}, {Nf, 0.25, 10^9},
  AxesLabel → {"Log of Reversals (2 Nf)", "Log of Strain Amplitude (Δϵ/2)"}, PlotRange → {0, 1}]
```

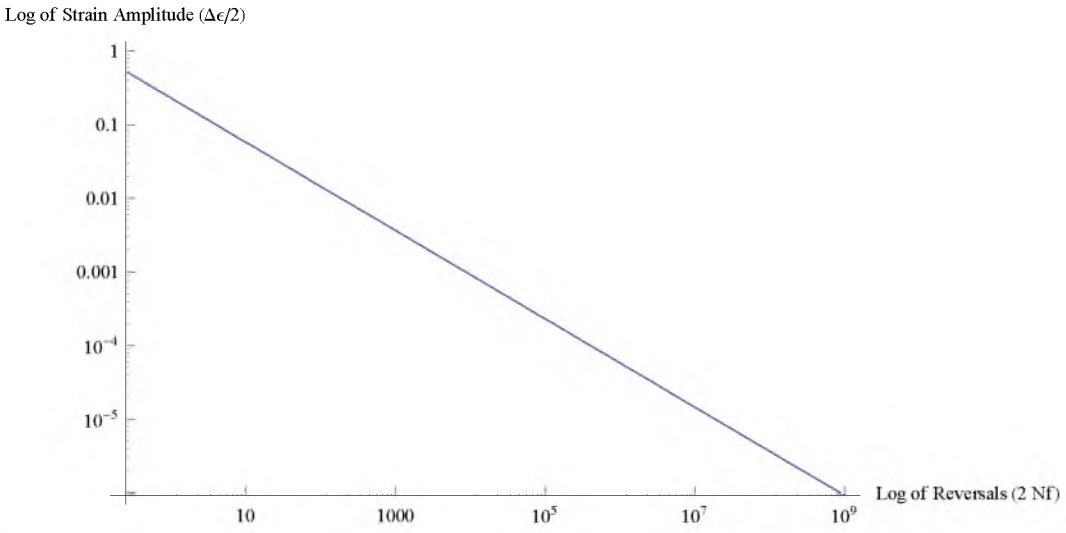

For 10^7cycles the strain amplitude would be the following:

$$\text{Solve}\left[\text{strainrangetensileeval} == \frac{\sigma\text{fprime}}{E}\left(2\,10^7\right)^b + \epsilon\text{fprime}\left(2\,10^7\right)^0,\ \text{strainrangetensileeval}\right]$$

$$\{\{\text{strainrangetensileeval} \to 0.0000146054\}\}$$

As shown above, the fatigue strength exponent (b) is outside of the normal range. This tends to dominate the strain life curve and does not allow to account for the ductility components of the curve. For this reason, this method of determining the fatigue life is omitted. The following methods are employed instead.

- Strain-Life Fatigue Failure Model Based on Published Material Property Data

This is going to have multiple sections (3) 1 is the book numbers for properties, 2 is the static tensile test numbers, and 3 is the universal slope method [ref shigley pg 367]. Using the properties for each of the methods, the strain-life calculations are made. Look at which ones are most conservative or representative of the actual situation.

The following material properties are estimated by using the results from the tensile tests performed at Hill Air Force Base.

σfprime = 130 000
ϵfprime = 0.41
c = −0.51
b = −0.12

130 000

0.41

−0.51

−0.12

$$\text{strainrangeASM} = \frac{\sigma\text{fprime}}{E}(2\,Nf)^{b} + \epsilon\text{fprime}\,(2\,Nf)^{c}$$

$$\frac{0.287911}{Nf^{0.51}} + \frac{0.0041353}{Nf^{0.12}}$$

LogLogPlot[{strainrangeASM}, {Nf, 0.25, 10^9},
AxesLabel → {"Log of Reversals (2 Nf)", "Log of Strain Amplitude (Δϵ/2)"}, PlotRange → {0, 1}]

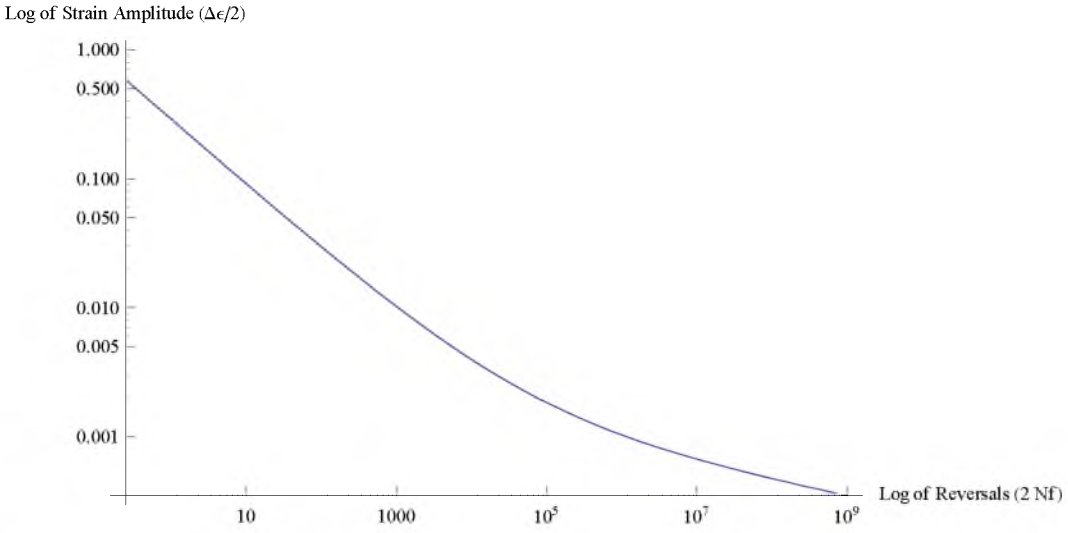

For 10^7cycles the strain amplitude would be the following:

$$\text{Solve}\left[\text{strainrangeASMeval} == \frac{\sigma\text{fprime}}{E}\left(2\,10^{7}\right)^{b} + \epsilon\text{fprime}\left(2\,10^{7}\right)^{c},\ \text{strainrangeASMeval}\right]$$

{{strainrangeASMeval → 0.000675225}}

- Strain-Life Fatigue Failure Model Based on the Modified Universal Slopes Method

The following material properties are estimated by using the Universal Slope Method. This is another approximation based on knowing S_{ut}, ϵ_f, and E, setting b = -0.12 and c = -0.6 and evaluating for the total strain amplitude.

Su
ϵfprime = 0.41
c = −0.56
b = −0.09

69 192.4

0.41

−0.56

−0.09

$$\text{strainrangeMUSM} = 0.623\left(\frac{Su}{E}\right)^{0.832}(2\,Nf)^{b} + 0.0196\,\epsilon f^{0.155}\left(\frac{Su}{E}\right)^{-0.53}(2\,Nf)^{c}$$

$$\frac{0.276974}{Nf^{0.56}} + \frac{0.00385933}{Nf^{0.09}}$$

```
LogLogPlot[{strainrangeMUSM}, {Nf, 0.25, 10^9},
  AxesLabel → {"Log of Reversals (2 Nf)", "Log of Strain Amplitude (Δϵ/2)"}, PlotRange → {0, 1}]
```

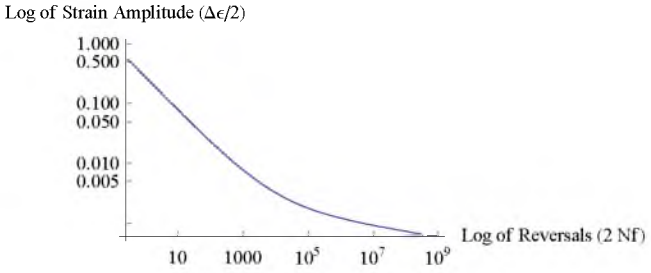

For 10^7 cycles the strain amplitude would be the following:

```
Solve[strainrangeMUSMeval == 0.623(Su/E)^0.832 (2 10^7)^b + 0.0196 ϵf^0.155 (Su/E)^-0.53 (2 10^7)^c, strainrangeMUSMeval]
```

```
{{strainrangeMUSMeval → 0.000938014}}
```

- Log-Log Plot Showing the Three Derived Strain Amplitude and Fatigue Life Relationships

```
LogLogPlot[{strainrangetensile, strainrangeASM, strainrangeMUSM}, {Nf, 0.25, 10^9},
  AxesLabel → {"Log of Reversals (2 Nf)", "Log of Strain Amplitude (Δϵ/2)"},
  PlotRange → {0, 1}, PlotStyle → {Thick, Dashed, Orange}]
```

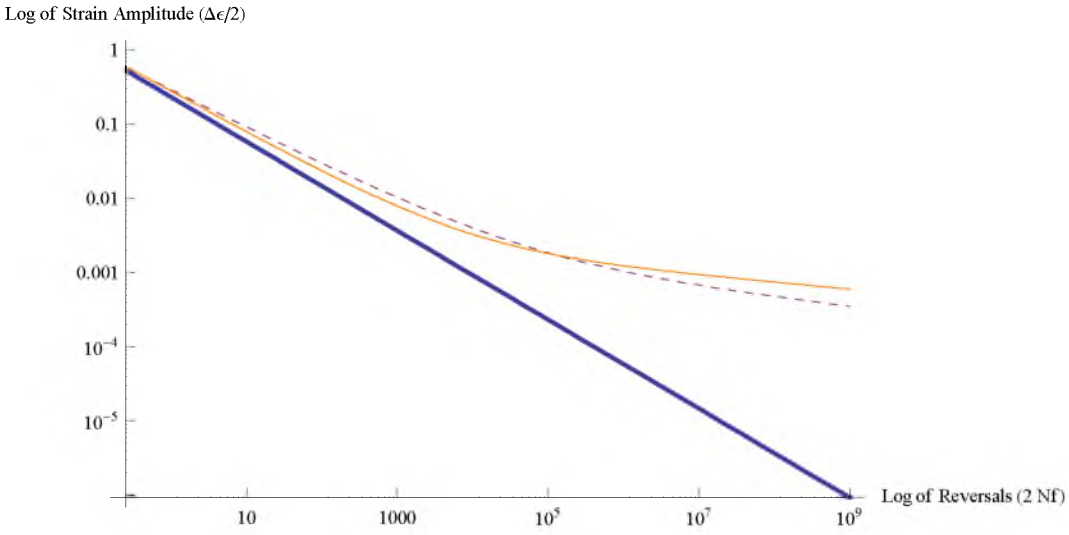

- Strain Data Based on EFAC Tower Strain Gage Measurements

The values for the following strain amplitudes are from the readings on the six posts at the E-FAC.

$$\epsilon max1 = -4.7*\text{^}-6;\ \epsilon min1 = -41.0*\text{^}-6;\ \Delta\epsilon SG1 = \epsilon max1 - \epsilon min1;$$

$$strainampSG1 = \frac{\Delta\epsilon SG1}{2}$$

$$\epsilon max2 = 50.6*\text{^}-6;\ \epsilon min2 = -18.7*\text{^}-6;\ \Delta\epsilon SG2 = \epsilon max2 - \epsilon min2;$$

$$strainampSG2 = \frac{\Delta\epsilon SG2}{2}$$

$$\epsilon max3 = 11.1*\text{^}-6;\ \epsilon min3 = -22.1*\text{^}-6;\ \Delta\epsilon SG3 = \epsilon max3 - \epsilon min3;$$

$$strainampSG3 = \frac{\Delta\epsilon SG3}{2}$$

$$\epsilon max4 = 11*\text{^}-6;\ \epsilon min4 = -51.8*\text{^}-6;\ \Delta\epsilon SG4 = \epsilon max4 - \epsilon min4;$$

$$strainampSG4 = \frac{\Delta\epsilon SG4}{2}$$

$$\epsilon max5 = 32.5*\text{^}-6;\ \epsilon min5 = -59.5*\text{^}-6;\ \Delta\epsilon SG5 = \epsilon max5 - \epsilon min5;$$

$$strainampSG5 = \frac{\Delta\epsilon SG5}{2}$$

$$\epsilon max6 = 34.8*\text{^}-6;\ \epsilon min6 = -31.9*\text{^}-6;\ \Delta\epsilon SG6 = \epsilon max6 - \epsilon min6;$$

$$strainampSG6 = \frac{\Delta\epsilon SG6}{2}$$

0.00001815

0.00003465

0.0000166

0.0000314

0.000046

0.00003335

- Strain Data Based on Finite Element Analysis

The values for the following strain amplitudes are from the readings on the six posts at the E-FAC.

$\epsilon max1 = 24.9*^{-6};\ \epsilon min1 = 19.6*^{-6};\ \Delta\epsilon 1 = \epsilon max1 - \epsilon min1;$

$$strainampFEA1 = \frac{\Delta\epsilon 1}{2}$$

$\epsilon max2 = 26.6*^{-6};\ \epsilon min2 = 18.5*^{-6};\ \Delta\epsilon 2 = \epsilon max2 - \epsilon min2;$

$$strainampFEA2 = \frac{\Delta\epsilon 2}{2}$$

$\epsilon max3 = 33.6*^{-6};\ \epsilon min3 = 0.2*^{-6};\ \Delta\epsilon 3 = \epsilon max3 - \epsilon min3;$

$$strainampFEA3 = \frac{\Delta\epsilon 3}{2}$$

$\epsilon max4 = 27.3*^{-6};\ \epsilon min4 = 25.7*^{-6};\ \Delta\epsilon 4 = \epsilon max4 - \epsilon min4;$

$$strainampFEA4 = \frac{\Delta\epsilon 4}{2}$$

$\epsilon max5 = 30.5*^{-6};\ \epsilon min5 = 2.94*^{-6};\ \Delta\epsilon 5 = \epsilon max5 - \epsilon min5;$

$$strainampFEA5 = \frac{\Delta\epsilon 5}{2}$$

$\epsilon max6 = 21.9*^{-6};\ \epsilon min6 = 20.8*^{-6};\ \Delta\epsilon 6 = \epsilon max6 - \epsilon min6;$

$$strainampFEA6 = \frac{\Delta\epsilon 6}{2}$$

2.65×10^{-6}

4.05×10^{-6}

0.0000167

$8. \times 10^{-7}$

0.00001378

5.5×10^{-7}

- Plot of the Measured and Calculated Strain Amplitudes Relative to the Strain-Life Curve for the Tower Posts

```
LogLogPlot[{strainrangeASM, strainrangeMUSM, strainampSG5, strainampFEA3},
  {Nf, 0.25, 10^9}, AxesLabel → {"Log of Reversals (2 Nf)", "Log of Strain Amplitude (Δϵ/2)"},
  PlotRange → {0, 1}, PlotStyle → {Thick, Dashed, Orange}, GridLines → {{7.6 10^7}, {}}]
```

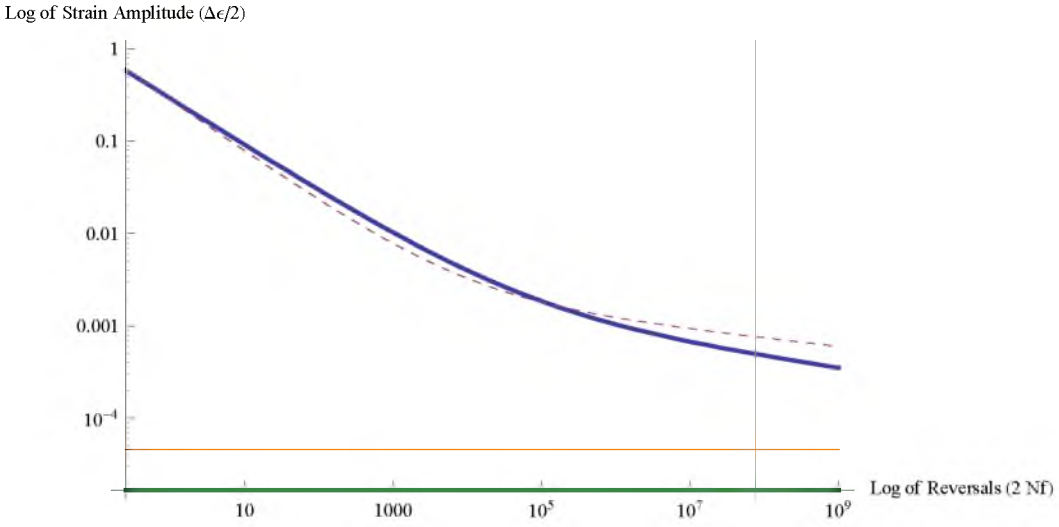

Strain Data Based on LAB-6 Pedestal Strain Gage Measurements

The values for the following strain amplitudes are from the strain gage measurements at the LAB-6 radar site.

$\Delta\epsilon LAB1 = 11.46$; $\Delta\epsilon LAB2 = 21.35$; $\Delta\epsilon LAB3 = 24.97$; $\Delta\epsilon LAB4 = 24.29$; $\Delta\epsilon LAB5 = 16.21$; $\Delta\epsilon LAB6 = 7.94$;
$\Delta\epsilon LAB7 = 17.95$; $\Delta\epsilon LAB8 = 30.4$; $\Delta\epsilon LAB9 = 20.26$; $\Delta\epsilon LAB10 = 11.48$; $\Delta\epsilon LAB11 = 5.26$;
$\Delta\epsilon LAB12 = 16.61$; $\Delta\epsilon LAB13 = 6.89$; $\Delta\epsilon LAB14 = 17.43$; $\Delta\epsilon LAB15 = 15.46$; $\Delta\epsilon LAB16 = 17.3$;

The max and min values are shown below:

$$\Delta\epsilon LAB8Amp = \frac{\Delta\epsilon LAB8}{2} * 10^{-6}$$

$$\Delta\epsilon LAB11Amp = \frac{\Delta\epsilon LAB11}{2} * 10^{-6}$$

0.0000152

2.63×10^{-6}

```
LogLogPlot[{strainrangeASM, strainrangeMUSM, ΔϵLAB8Amp, ΔϵLAB11Amp},
  {Nf, 0.25, 10^9}, AxesLabel → {"Log of Reversals (2 Nf)", "Log of Strain Amplitude (Δϵ/2)"},
  PlotRange → {0, 1}, PlotStyle → {Thick, Dashed, Orange}]
```

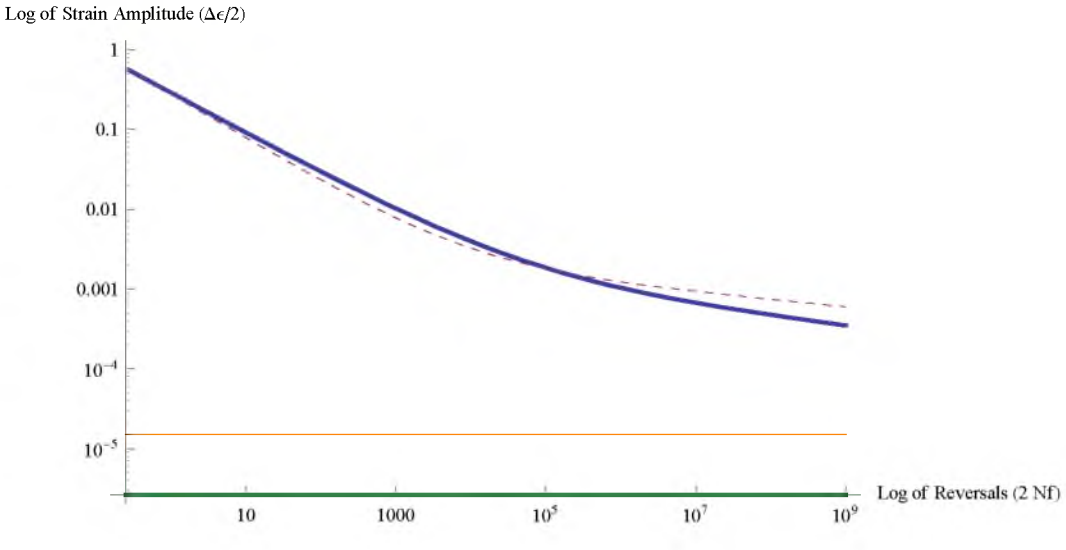

- Maximum Strains Calculated in Finite Element Analysis

The above results show the strains that are found at the strain gage locations. However, the strain gages were not placed at the maximum stress or strain locations. The maximum and minimum strains from the Finite Element Analysis are plotted on the strain-life curve below.

```
max1 = 1.133*^-4; min1 = 1.395*^-9; max2 = 1.231*^-4; min2 = 8.024*^-10; max3 = 1.091*^-4;
min3 = 1.556*^-9; max4 = 1.053*^-4; min4 = 1.347*^-9; max5 = 1.133*^-4; min5 = 1.442*^-9;
max6 = 1.813*^-4; min6 = 1.236*^-9; max7 = 1.269*^-4; min7 = 3.183*^-9; max8 = 1.595*^-4;
min8 = 1.737*^-9; max9 = 1.068*^-4; min9 = 1.860*^-9; max10 = 1.284*^-4; min10 = 2.578*^-9;
max11 = 2.769*^-4; min11 = 2.569*^-9; max12 = 1.080*^-4; min12 = 1.236*^-9;

ΔϵFEAamp1 = (max1 - min1)/2; ΔϵFEAamp2 = (max2 - min2)/2; ΔϵFEAamp3 = (max3 - min3)/2;
ΔϵFEAamp4 = (max4 - min4)/2; ΔϵFEAamp5 = (max5 - min5)/2; ΔϵFEAamp6 = (max6 - min6)/2;
ΔϵFEAamp7 = (max7 - min7)/2; ΔϵFEAamp8 = (max8 - min8)/2; ΔϵFEAamp9 = (max9 - min9)/2;
ΔϵFEAamp10 = (max10 - min10)/2; ΔϵFEAamp11 = (max11 - min11)/2
ΔϵFEAamp12 = (max12 - min12)/2;


0.000138449
```

The maximum value for the strain amplitude is shown above which occurs at ΔϵFEAamp11. This corresponds to the 300 degree rotation.

```
LogLogPlot[{strainrangeASM, strainrangeMUSM, (*ΔϵFEAamp1,
   ΔϵFEAamp2,ΔϵFEAamp3,ΔϵFEAamp4,ΔϵFEAamp5,*)ΔϵFEAamp6, ΔϵFEAamp7,
   ΔϵFEAamp8, ΔϵFEAamp9, ΔϵFEAamp10, ΔϵFEAamp11, ΔϵFEAamp12}, {Nf, 0.25, 10^9},
  AxesLabel → {"Log of Reversals (2 Nf)", "Log of Strain Amplitude (Δϵ/2)"}, PlotRange → {0, 1},
  GridLines → {{8.9 10^7}, {}}, PlotStyle → {Thick, Dashed, Thick, Thick, Thick, Thick, Thick, Thick, Thick}]
```

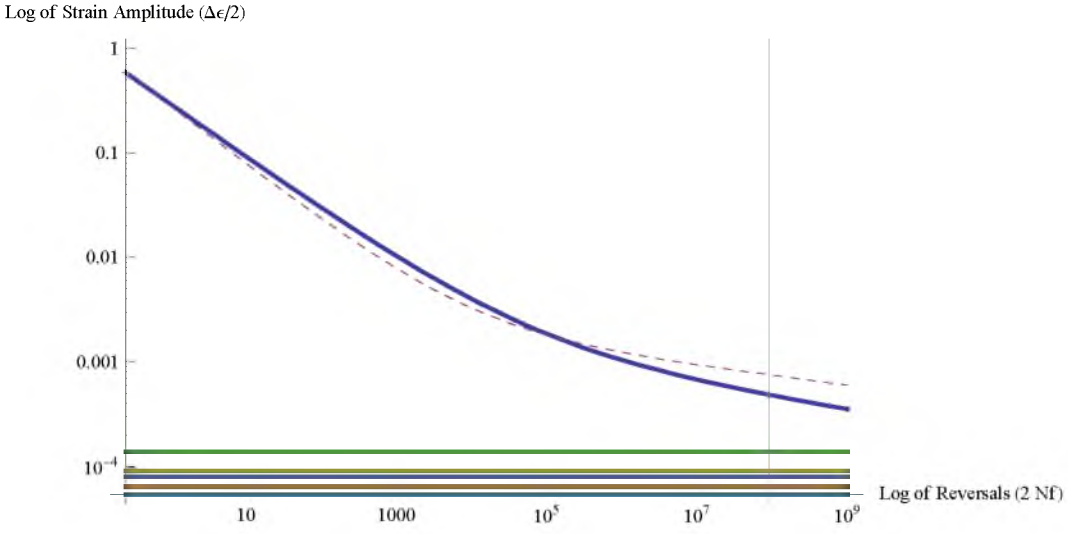

```
LogLogPlot[{strainrangeASM, strainrangeMUSM, (*ΔϵFEAamp1,
    ΔϵFEAamp2,ΔϵFEAamp3,ΔϵFEAamp4,ΔϵFEAamp5,*)ΔϵFEAamp6, ΔϵFEAamp7,
    ΔϵFEAamp8, ΔϵFEAamp9, ΔϵFEAamp10, ΔϵFEAamp11, ΔϵFEAamp12},
  {Nf, 0.25, 10^13}, AxesLabel → {"Log of Reversals (2 Nf)", "Log of Strain Amplitude (Δϵ/2)"},
  PlotRange → {0, 1}, GridLines → {{8.9 10^7, 2 * 10^12}, {}},
  PlotStyle → {Thick, Dashed, Thick, Thick, Thick, Thick, Thick, Thick, Thick}]
```

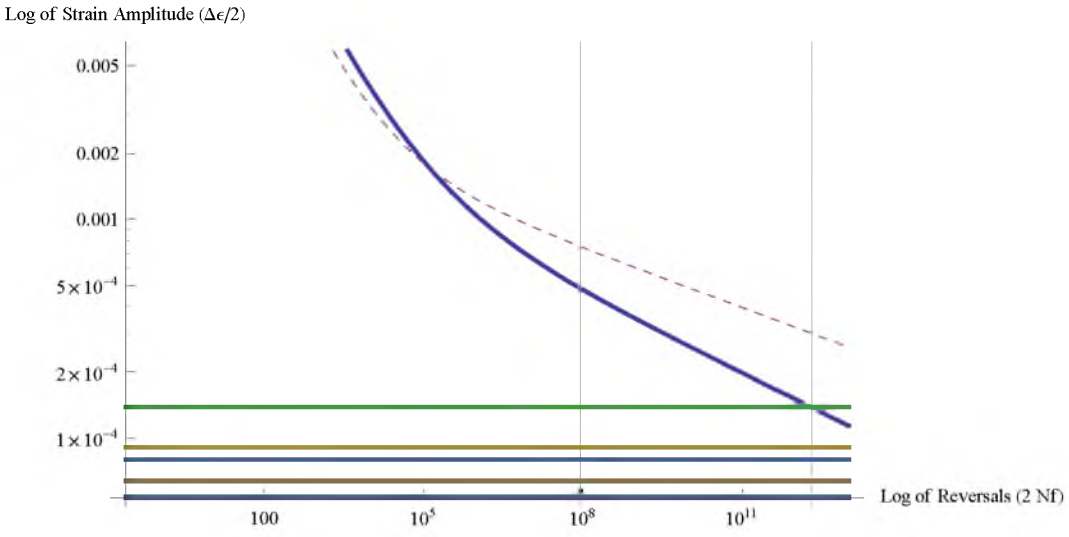

- Estimated Remaining Life

```
NSolve[ΔϵFEAamp11 == strainrangeASM, Nf]
```

$$\{\{Nf \to 1.98386 \times 10^{12}\}\}$$

```
(*NSolve[ΔϵFEAamp11==strainrangeMUSM,Nf]*)
```

$$\text{CyclesRemaining} = \left(1.98386 * 10^{12}\right) - \left(8.9 * 10^{7}\right)$$

$$\text{CyclesPerYear} = 5 * 60 * 24 * 365 * 99.6$$

$$\text{YearsRemaining} = \frac{\text{CyclesRemaining}}{\text{CyclesPerYear}}$$

$$1.98377 \times 10^{12}$$

$$2.61749 \times 10^{8}$$

$$7578.91$$

- Combination of Finite Element Strains and Actual Measured Strains

The strain gages show the cyclic strains that are induced by the rotation of the radar. As discussed in Section 3.1, the weight of the radar is not directly measured by the strain gages because the gages were applied to the structure much later. The total amount of strain calculated by the finite element analysis is added to the strain measured by the strain gages. This is then plotted against the fatigue curve.

```
Δϵcomb1 = Δϵ FEAamp1 + Δϵ LAB1 * 10^-6; Δϵcomb2 = Δϵ FEAamp2 + Δϵ LAB2 * 10^-6;
Δϵcomb3 = Δϵ FEAamp3 + Δϵ LAB3 * 10^-6; Δϵcomb4 = Δϵ FEAamp4 + Δϵ LAB4 * 10^-6;
Δϵcomb5 = Δϵ FEAamp5 + Δϵ LAB5 * 10^-6; Δϵcomb6 = Δϵ FEAamp6 + Δϵ LAB6 * 10^-6;
Δϵcomb7 = Δϵ FEAamp7 + Δϵ LAB7 * 10^-6; Δϵcomb8 = Δϵ FEAamp8 + Δϵ LAB8 * 10^-6;
Δϵcomb9 = Δϵ FEAamp9 + Δϵ LAB9 * 10^-6; Δϵcomb10 = Δϵ FEAamp10 + Δϵ LAB10 * 10^-6;
Δϵcomb11 = Δϵ FEAamp11 + Δϵ LAB11 * 10^-6
Δϵcomb12 = Δϵ FEAamp12 + Δϵ LAB12 * 10^-6;

0.000143709
```

The maximum value for the strain amplitude is shown above which occurs at ΔϵFEAamp11. This corresponds to the 300 degree rotation.

```
LogLogPlot[{strainrangeASM, strainrangeMUSM, (*Δϵcomb1,Δϵcomb2,Δϵcomb3,Δϵcomb4,Δϵcomb5,*)
    Δϵcomb6, Δϵcomb7, Δϵcomb8, Δϵcomb9, Δϵcomb10, Δϵcomb11, Δϵcomb12}, {Nf, 0.25, 10^9},
  AxesLabel → {"Log of Reversals (2 Nf)", "Log of Strain Amplitude (Δϵ/2)"}, PlotRange → {0, 1},
  GridLines → {{8.9 10^7}, {}}, PlotStyle → {Thick, Dashed, Thick, Thick, Thick, Thick, Thick, Thick, Thick}]
```

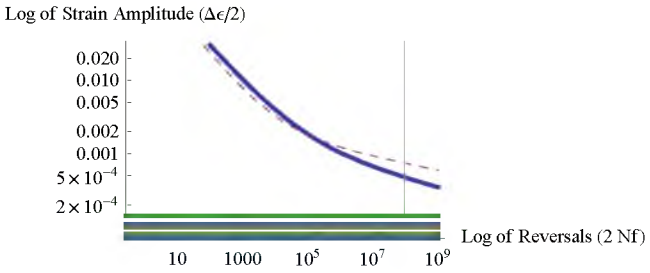

Log of Strain Amplitude ($\Delta\epsilon/2$)

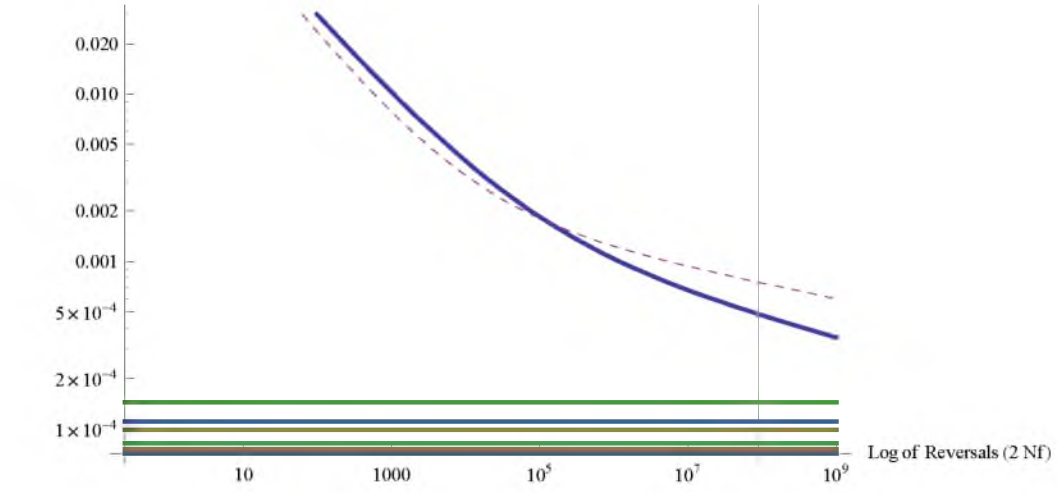

Log of Strain Amplitude ($\Delta\epsilon/2$)

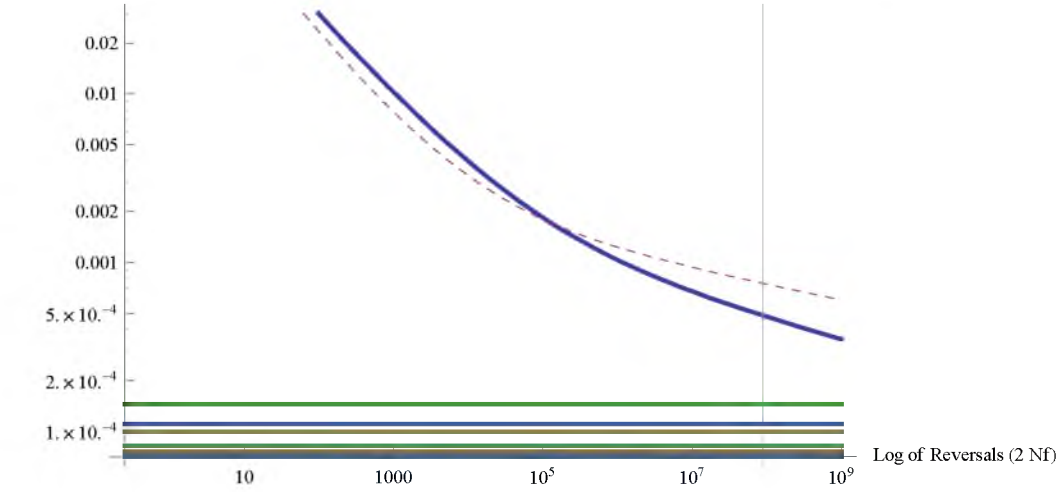

```
LogLogPlot[{strainrangeASM, strainrangeMUSM, (*ΔϵFEAamp1,
    ΔϵFEAamp2,ΔϵFEAamp3,ΔϵFEAamp4,ΔϵFEAamp5,*)ΔϵFEAamp6, ΔϵFEAamp7,
    ΔϵFEAamp8, ΔϵFEAamp9, ΔϵFEAamp10, ΔϵFEAamp11, ΔϵFEAamp12},
  {Nf, 0.25, 10^13}, AxesLabel → {"Log of Reversals (2 Nf)", "Log of Strain Amplitude (Δϵ/2)"},
  PlotRange → {0, 1}, GridLines → {{8.9 10^7, 2 * 10^12}, {}},
  PlotStyle → {Thick, Dashed, Thick, Thick, Thick, Thick, Thick, Thick, Thick}]
```

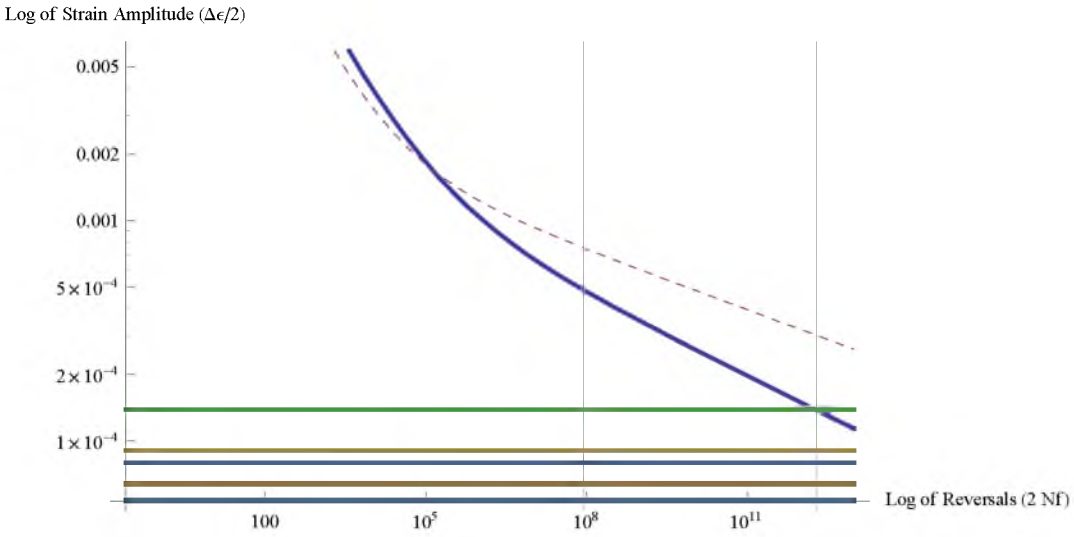

- Strain Amplitude At Current Life

The number of cycles the radar has seen to date are 8.9 x 10^7. The strain amplitude at this value is calculated below.

```
criticalstrainampASM = strainrangeASM /. Nf → 8.9 * 10^7
criticalstrainampMUSM = strainrangeMUSM /. Nf → 8.9 * 10^7
```

0.000485226

0.000752923

$$\frac{\Delta\epsilon Comb11}{criticalstrainampASM}$$

$$\frac{\Delta\epsilon Comb11}{criticalstrainampMUSM}$$

0.296169

0.190868

REFERENCES

[1] United States Air Force. 2003. *What is AEWS*. Atmospheric Early Warning System Mission and Description.

[2] United States Department of Defense. August 2005. *DOD Guide for Achieving Reliability, Availability, and Maintainability.*

[3] Hoeppner, David W. September 1, 2009. Class Lecture: *Fatigue and Creep Considerations in Engineering Design*. University of Utah, Salt Lake City, UT.

[4] United States Department of Defense. 2005. Aircraft Structural Integrity Program (MIL STD 1530C). Department of Defense Standard Practice. United States Air Force.

[5] Thomsen, Mark L. January 10, 2011. Class Lecture: *Chapter 1*. University of Utah, Salt Lake City, UT.

[6] Air Force Technical Manual 31P6-2FPS117-21-5. 2013. *Operation and Maintenance Instructions, Chapter 6, Radar System AN/FPS-117.*

[7] Air Force Technical Manual 31P6-2FPS117-24. 2013. *Illustrated Parts Breakdown, Radar System AN/FPS-117.*

[8] Hill Air Force Base Science and Testing Laboratory. November 17, 2012. *Radome and Towers Tensile Strength Analysis Report.*

[9] Dassault Systèmes. 2013. "Static-Adaptive Simulation Analysis Options." Accessed December 27, 2013. http://help.solidworks.com/2012/English/SolidWorks/cworks/IDC_HELP_PRESTATIC_P_ADAPTIVE.htm.

[10] Cleland Jardine Engineering LTD. August 2, 2013. *Structural Health Monitoring Implementation Plan*. Ottawa, Ontario, Canada.

[11] Select Engineering Services. January 23, 2014. *Structural Analysis Arctic Tower*. Final Technical Report for TSRT Task Order 0004.

[12] Cameron, D.W., and Hoeppner, David. 1996. "Fatigue Properties in Engineering." *ASM Handbook*. Volume 19 Fatigue and Fracture. ASM International Handbook Committee.

[13] American Society for Testing and Materials. August, 1981. *Statistical Analysis of Fatigue Data*. ASTM STP 744. Philadelphia, PA.

[14] Collins, J.A. 1981. *Failure of Materials in Mechanical Design*. New York, NY.

[15] American Society for Metals. 1983. *American Society for Metals Reference Book*. Second Edition. Metals Park, Ohio.

[16] Ellyn, Fernand. 1997. *Fatigue Damage, Crack Growth, and Life Prediction*. Springer, Netherlands.

[17] Shigley, Joseph, and Mischke, Charles. 2001. *Mechanical Engineering Design*. Sixth Edition. New York, NY.

[18] Roessle M.L., and Fatemi, A. 2000. "Strain-Controlled Fatigue Properties of Steels and Some Simple Approximations." *International Journal of Fatigue*, 22.

[19] Hoeppner, David. November 3, 2009. Class Lecture: *Fracture Mechanics*. University of Utah, Salt Lake City, UT.

[20] Thomsen, Mark. February 16, 2011. Class Lecture: *Chapter 11*. University of Utah, Salt Lake City, UT.

[21] Thomsen, Mark. January 19, 2011. Class Lecture: *Chapter 2*. University of Utah, Salt Lake City, UT.

[22] ASM Handbooks Online. 1997. *Nondestructive Evaluation and Quality Control*. Volume 17.

[23] United States Air Force, AFLCMC/HBZCC, and 809 MXSS/MXDEA. August 10, 2012. *AN/FPS-117 Radar Tower Inspection Report*.

[24] Cleland Jardine Engineering LTD. October 4, 2012. *East Coast Long Range Radar Tower/Pedestal Interface Analysis, Phase 2 - NDT Inspection Summary Report*. Ottawa, Ontario, Canada.

[25] Hill Air Force Base Science and Testing Laboratory. February 12, 2014. *Failure Analysis of AN/FPS-117 Radar Support Plate*.

[26] Hoeppner, David. November 24, 2009 Class Lecture: *Fretting Fatigue Design Considerations in Holistic Structural Integrity Based Design*. University of Utah, Salt Lake City, UT.

[27] Suresh, Subra. 1998. *Fatigue of Materials*. New York, NY.

[28] Yildirim, Halid C. and Marquis, Gary. November 2012. "Fatigue Strength Improvement Factors for High Strength Steel Welded Joints Treated by High Frequency Mechanical Impact." *International Journal of Fatigue*, 44, 168-176.